AN ABSTRACT OF THE THESIS OF

Wenchun Zhu for the degree of Doctor of Philosophy in Electrical & Computer Engineering presented on June 13, 1994 .

Title: Analysis of Subsynchronous Resonance in Power Systems

Redacted for Privacy

Abstract approved: _____
R. Spee

Three aspects of Subsynchronous Resonance (SSR) related problems in power systems are addressed in this dissertation which aims at contributing to a better understanding of these problems.

Subsynchronous Resonance (SSR) problems in series compensated steam-turbine power systems co-exist with the beneficial effects provided by the series capacitors. Since the early 1930s, numerous researchers have addressed issues relating to these problems.

The development of a generalized frequency scan method for analyzing SSR in a Single-Machine Infinite-Bus (SMIB) power system equipped with fixed series capacitor compensation is presented. This method overcomes shortcomings present in the traditional frequency scan technique which is widely used in power system analysis.

It has been noticed that there are nonlinear dynamic phenomena in power systems which can not be explained by linear system theory. This includes limited oscillations in a power system when it experiences SSR at a frequency close to one of the system modes. The phenomenon can be explained by Hopf bifurcations. This dissertation presents an analysis for a high dimensional model of a SMIB power system equipped with fixed series capacitor compensation. The results obtained can lead to a more precise

understanding of this phenomenon than those available to date which use perturbation methods and highly simplified second-order power system models.

Compared with fixed series capacitor compensation in power systems, the newly developed Thyristor Controlled Series Compensation (TCSC) scheme has some well known advantages with regard to flexible power system control. It has been noted that vernier mode TCSC operation can provide for SSR mitigation. In this thesis, such beneficial effect is demonstrated and analyzed for a simplified North-Western American Power System (NWAPS) model, based on EMTP simulations. Issues relating to modelling and simulation of power system and TCSC are addressed.

Analysis of Subsynchronous Resonance in Power Systems

by

Wenchun Zhu

A THESIS

submitted to

Oregon State University

in partial fulfillment of the requirements for the degree of

Doctor of Philosophy

Completed June 13, 1994

Commencement June 1995

APPROVED:

Redacted for Privacy

Associate Professor of Electrical & Computer Engineering in charge of major

Redacted for Privacy

Head of department of Electrical & Computer Engineering

Redacted for Privacy

Dean of Graduate School

Date thesis is presented June 13, 1994

Typed by Wenchun Zhu for Wenchun Zhu

ACKNOWLEDGEMENT

Time silently passes by. Most at the moment of closing, memories of the starting days are fresh - a rainy spring of 1991, which I am used to, but which added so much to my confusion in those beginning days. Hardly did I believe I knew anything. Then the day came when I learned to lead my life instead of being pushed by. The hardship was balanced by the joy. Finally, the reward is the work itself.

I am thankful to the FACTS (Flexible AC Transmission Systems) project in the ECE department of OSU, which has been funded by BPA, EPRI, and NSF, and by which my research work has been supported for the past more than three years.

I would like to thank my major professor R. Spee in the ECE department for correcting this dissertation patiently, without whose effort the presentation of the dissertation would have been much less clear. Also, I would like to thank him for correcting my reports and papers many times for the past three years. I would like to thank Prof. R. R. Mohler in the ECE department for giving this dissertation corrections and comments out of his years' research experience, and for encouraging a rather flexible atmosphere in our FACTS research group, which gave me a chance to work on the problems I am interested in. I would like to thank Prof. W. J. Kolodziej in the ECE department for giving comments and corrections for this dissertation. From his lecture I have learned the subject of linear systems quite solidly, which has been helpful to my research through out these three years. I would like to thank Prof. G. C. Alexander in the ECE department for being kind and helpful and for teaching me the subject of EMTP which is a very useful tool for power system analysis. I would like to thank Mr. W.A. Mittelstadt in BPA for his listening and supporting. Mostly owing to his efforts, my summer internship in BPA, 1993, was possible and successful. I would like to thank

Professor Joel Davis in the MATH department whose humorous lectures on numerical analysis I have attended lightened even the exam days. I would like to thank Prof. D. V. Finch in the MATH department, from whose lectures on nonlinear dynamics and differential equations I have learned a lot.

I am very grateful to my parents who care their children very much, and with whom I have learned so much since my childhood. Their influence to me by their discipline, persistence and intelligence is far beyond what I can express. I am also grateful to them for giving me two wonderful friends - sisters.

I would like to thank my friend and colleague Radek for reading through this dissertation and picking out mistakes, and for being understanding and kind. I would like to thank Yu Wang, who was a visiting scholar in our FACTS project, for his helpful discussions on power systems when I started newly in Corvallis. Especially, I would like to thank my friend and colleague Rajkumar, who has given me inspiring ideas and suggestions, with whom I have had many discussions on different research topics, whose once upon a time line "When are you going to start your own research topic, Wen?" upset me very much and for which I am thankful, who shared his music, and from whom I have learned the song "I got by with a little help from friend".

I would like to thank all my friends who have helped me and eased my difficult days.

TABLE OF CONTENTS

TABLE OF CONTENTS (continued)

LIST OF FIGURES

LIST OF FIGURES (continued)

LIST OF TABLES

ANALYSIS OF SUBSYNCHRONOUS RESONANCE IN POWER SYSTEMS

Chapter I
Introduction

1.1 Problem Definition

It is well known that series capacitor compensation in AC transmission systems is an economical means to increase load capability, control load sharing among parallel lines and enhance transient stability. However, capacitors in series with transmission lines may cause Subsynchronous Resonance (SSR) that can lead to severe problems, e.g., shaft failure. Therefore, the effects of SSR should be fully analyzed and understood for the series compensated power systems, and appropriate SSR countermeasures should be applied [1].

SSR is a power system condition where the series compensated electric network exchanges significant energy with a turbine-generator following disturbances. This energy exchange is lightly damped, undamped, or even negatively damped [2], and, as indicated by the name, occurs at frequencies below line frequency (i.e., 50 or 60 Hz).

Technically, SSR problems are divided into three categories: induction generator effect, torsional interaction, and torque amplification[1, 2].

For explanation, we consider a simple Single-Machine Infinite-Bus(SMIB) power system shown in Fig1.1, which consists of electrical and mechanical sub-systems. The

mechanical sub-system has several natural frequencies corresponding to the mechanical shaft natural modes. The electric sub-system has a natural frequency f_{er}, where

$$f_{er} = f_0 (X_c/(X'' + X_t))^{1/2}$$

in which f_0 is the synchronous frequency of 60 Hz. X_c, X_t, X'' are capacitor reactance, line reactance, and generator subtransient reactance. Since the series compensation level is normally less than 100%, it is seen that f_{er} is subsynchronous.

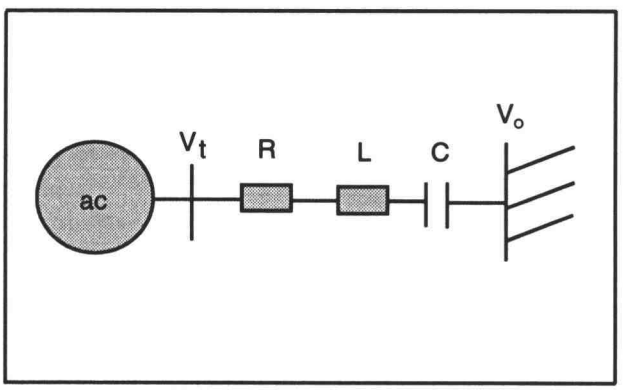

Fig.1.1 A SMIB power system with series capacitor compensation

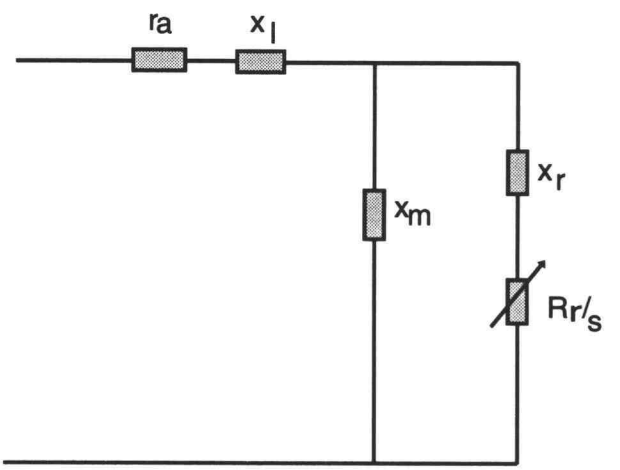

Fig.1.2 Equivalent circuit of a synchronous generator with respect to subsynchronous armature currents
X_i, r_a- stator reactance and resistance, X_r, R_r - effective rotor reactance and resistance
X_m - magnetizing reactance, s - slip

Three phase armature currents at frequency f_{er} will flow for any small electrical disturbance. The positive sequence component of these currents will produce a rotating magnetic field at an electrical frequency of f_{er}. The currents induced in the rotor windings by this magnetic field are governed by the relative speed of the field and the rotor speed[1].

Considering the resonance in the electrical sub-system alone, and assume constant rotor speed at synchronous frequency. Since the rotor circuits are turning faster than the rotating magnetic field produced by the subsynchronous armature currents, the effect can be explained by the familiar induction generator circuit[1,3]. Viewed from the generator armature terminals, the equivalent circuit of the generator with respect to the subsynchronous frequency f_{er} is as shown in Fig 1.2 . Since slip $s = (f_{er}-60) / f_{er}$ in Fig 1.2, it is seen that s is negative, i.e., the rotor resistance to subsynchronous currents viewed from the armature terminals is negative. When this negative resistance exceeds the sum of the armature and the network resistance, the electrical sub-system is self excited. The phenomenon is called ***Induction Generator Effect***. A rigorous derivation of the equivalent circuit for explaining an induction generator effect can be found in [4]. When the system is subject to the induction generator effect, the electric sub-system undergoes growing oscillations under the slightest disturbance. Since the armature currents affect the mechanical sub-system through the electrical torque applied to the shaft, the mechanical sub-system will go unstable with a delay.

Small power system disturbances result in simultaneous excitation of all natural modes of the electrical and mechanical sub-systems. Oscillations of the generator rotor at one of its mechanical natural frequencies, f_m, result in modulation of the generator voltage. The resulting subsynchronous three phase voltage component is at frequency $f_e = f_0 - f_m$. When this frequency is close to the natural frequency of the electrical sub-

system f_{er}, the resulting armature currents produce a magnetic field which is phased to produce a torque which reinforces the aforementioned generator rotor oscillations. This phenomenon can result in sustained or growing oscillations, and is referred to as ***torsional interaction*** [1].

The interplay between the electrical and the mechanical sub-systems can result in shaft torques which are much larger under disturbances than those produced by similar disturbances in a system without series compensation. The effect is referred to as shaft ***torque amplification*** [1].

The three categories can also be explained from a small signal stability point of view.

For explanation, consider the SMIB power system shown in Fig 1.1. The series compensation level can be considered as a changing parameter in the system. Linearization of the system yields the eigenvalues with one complex pair of corresponding to the electrical mode, and several complex pairs corresponding to the mechanical shaft modes. It is noticed that with changing compensation level, the electrical mode can become unstable at some series compensation levels, while all the mechanical modes remain stable. This indicates ***induction generator effect***.

It is noticed that one (or possibly more) of the mechanical modes is prone to becoming unstable when the series compensation level is such that the electrical mode (in the d-q domain) is close to the mechanical mode. When this happens, the system is vulnerable to ***torsional interaction***. Since the two modes are close to each other, there will be a "beat" effect [5] in the system response to disturbances. This effect aggravates the unstable oscillations, since the amplitudes of the oscillations are larger due to the

"beat" effect. This explains why torsional interaction is of most concern among the three categories of SSR problem.

Due to the "beat" effect, the electric torques can become much larger under disturbances than in the system without torsional interaction. This occurs when the electrical mode is close to one of the shaft modes, as mentioned above, and the shaft mode is not necessarily unstable. This explains shaft ***torque amplification***.

From the above arguments, it is clear that the phenomena of induction generator effect and torsional interaction can be considered equilibrium stability problems, while shaft torque amplification can be considered a transient stability problem in power systems. In general, SSR is recognized as a power system dynamical problem, along with other dynamical problems, e.g., transient stability, dynamic stability, dynamic voltage stability.

1.2 Literature Survey

Investigations and reports of SSR problems started in the 1930s [6,7]. Early studies were centered around the induction generator effect. In 1971, two shaft failures caused by SSR occurred at the Mohave Generating Station in Southern Nevada[8]. Since then, many studies have been directed towards a complete understanding of the three SSR categories, with an emphasis on the understanding of torsional interactions [9-12]. In the literature, analysis and mitigation of SSR are two of the main topics, and most studies are based on linear system theory.

1.2.1 Analysis of SSR

The main linear SSR analysis methods include frequency domain methods [3, 4, 13-20] and eigen-based methods [21-23]. Eigenvalue analysis is direct and accurate, but the results are not intuitive, and for multi-machine systems, the analysis is complicated and not cost effective. On the other hand, frequency domain methods give approximate, yet intuitive results. Also, frequency domain methods are easier to implement than eigen-based approaches. Linear analysis contributes to the clarification of the problem and the prediction of certain system parameters and operating conditions, such as series capacitor compensation levels, transmission line and armature resistances, steady-state operating conditions etc., which are critical to the excitation of SSR.

One category of popular frequency domain techniques derives equivalent induction generator circuits for analyzing the induction generator effect [3, 4, 13, 14, 17, 18]. To indicate the occurrence of torsional interaction, the techniques analyze the electrical damping torque coefficient, which is widely used in the analysis of dynamic stability problems in power systems [22]. The analysis investigates electrical torque frequency response to a small oscillation of generator rotor angle and speed at one of its shaft natural modes. The electrical damping torque coefficient is defined as the imaginary part of the ratio of the resulting electrical torque and the original rotor angle oscillation. A negative coefficient indicates torsional interaction at the shaft mode under consideration.

Another important frequency domain technique is summarized in [19, 20], and addresses torsional interaction only. Both the electrical damping and synchronizing torque coefficients are involved in the process of analysis. A detailed explanation is presented in Chapter II.

Each of the frequency domain approaches discussed above has distinct advantages. The first approach strictly follows the principles of analyzing electrical damping torque coefficients, which is a well accepted concept in power systems [22]. For analyzing torsional interaction, the approach results in individual electrical damping torque coefficients at shaft natural modes. The second technique yields results over a range of frequencies (including the vicinity of shaft modes), which enables a closer study of the danger of torsional interactions [20]. Since both the electrical damping and synchronizing torque coefficients are involved in the analysis, the second technique is not strictly based on analyzing the electrical damping torque coefficient, and implicitly assumes the decoupling of electrical and mechanical sub-systems. This has not been theoretically justified, though the process involved in the analysis appears to be intuitive. Also, the second technique can not explain induction generator effect.

Both frequency domain approaches have been widely used for analyzing SSR problems. However, the problems associated with the second technique as discussed above seem to be neglected. In addition, there has not been an extensive discussion in the literature comparing eigen-based results to those based on frequency domain methods.

In [24], a generalized frequency scan method has been developed based on the second frequency domain technique discussed above. This new method no longer assumes the decoupling of electrical and the mechanical sub-systems, and is also applicable to the analysis of induction generator effects. A close match of the results from this method with the eigen-based results is shown in [24] and discussed in Chapter II.

Discussion of nonlinear analysis of SSR in the literature started in the late 1980s. Perturbation techniques have been used as a mathematical tool for conducting local

nonlinear analysis [25-27]. Certain nonlinear phenomena have been studied, such as Hopf-Bifurcation, multivalueness, etc.. The dynamic models used in these analyses are highly simplified second-order models of power systems.

Power systems involve a high degree of nonlinearity. Many phenomena can not be analyzed to a sufficient degree by relying on linear theory exclusively. A Hopf bifurcation phenomenon has been observed in the operation of the North-Western American Power System(NWAPS). While the phenomenon can not be explained by linear theory, it is not unexpected, since SSR defines a condition where with changing series compensation level, one or more of the system modes become unstable. If the analysis is confined to the instability of a single system mode, it addresses the most important condition for the occurrence of Hopf bifurcation in a system [28-30]. Since mathematical results of Hopf bifurcation analysis for high dimensional systems are available, applying the results for the analysis of SSR may result in much more precise understanding of the Hopf bifurcation phenomenon accompanying SSR than the previous studies. In [31], this phenomenon has been analyzed by applying the Hopf bifurcation theorem illustrated in [28] to a 15th-order model of a SMIB power system. This work will be discussed in detail in Chapter III.

1.2.2 SSR Countermeasures

SSR countermeasures discussed in the literature may be grouped as open-loop countermeasures, closed-loop countermeasures, and capacitor based countermeasures.

Open-loop countermeasures include filtering (e.g., static blocking), system switching and generator tripping, as well as generator and system modification [1]. Static

blocking filters [32] block transmission line currents at resonant frequencies from entering the generator and interacting with the torsional modes.

Closed-loop countermeasures include dynamic stabilizers, excitation system damping, phase shift damping, etc.. Yu [22] suggests the use of the excitation control along with linear optimal control. Linear pole placement based excitation control is proposed to dampen the SSR modes of unidentical multimachine systems in [33]. The dynamic stabilizer [4, 32, 34] consists of thyristor modulated shunt reactors which are connected to the isolated phase bus of the protected turbine-generator unit. Control of subsynchronous oscillations is achieved by modulation of the thyristor switch firing angles around a normal operating point in response to measured oscillation of the turbine-generator units' rotor. In the absence of rotor oscillation, the normal operation of the stabilizer has a continuous reactive load. Reference [35] proposes the use of static phase shifters in conjunction with rotor deviation measurements to damp SSR oscillations.

Capacitor based SSR countermeasures are most attractive. Since the series capacitor directly influences SSR, countermeasures at the capacitor site are favored by the power industry over those at generating station sites. Reference [36] summarizes SSR countermeasures which make use of the protection schemes associated with series capacitors. The protection scheme for a series capacitor aims at limiting the voltage across the capacitor, and also can be used to limit transient torques caused by SSR by adapting settings and/or control schemes of the protection system. For example, the dual-gap protection scheme can limit transient torque effectively and allow the capacitor to be reinserted successfully after being bypassed. One notable capacitor based SSR countermeasure is the NGH scheme, named after N.G. Hingorani. In its basic design [37-39], the NGH device consists of a resistor and an antiparallel thyristor across a series

capacitor segment with appropriate instrumentations and controls. The NGH device checks the capacitor voltage continuously. Subsynchronous currents are detected and the control system controls the firing of the thyristors to dissipate subsynchronous energy in the resistor [37].

TCSC (Thyristor Controlled Series Capacitor) based SSR countermeasures deserve mention. Due to the advances in power electronic components, thyristor controlled series compensation is replacing traditional mechanically controlled series compensators. TCSC benefits power systems in many ways, e.g., increasing dynamic and transient stability limits to higher levels, controlling load flows more flexibly and controlling loop flows. Also, when operated in a vernier mode, the TCSC can mitigate SSR [40-43]. This effect has been demonstrated by simulation studies[43], as well as by power system simulator tests[42]. Reference [43] demonstrates TCSC SSR mitigation in a simplified NWAPS model, via EMTP simulation studies, and explains the effect by interpreting the TCSC equivalent impedance with respect to different frequencies. A detailed discussion of these studies is presented in chapter IV. To date, no satisfactory theoretical results have been documented explaining the TCSC SSR performance.

1.3 Dissertation Overview

The preceding sections provide some background information on SSR in power systems, and introduce several of the main topics of this thesis. It should be emphasized that the thesis concentrates on several aspects of SSR analysis, aimed to an improved understanding of SSR in power systems, and its corrections with series capacitor compensation.

Chapter II summarizes the development of a generalized frequency scan method for SSR analysis, which overcomes some short-comings of the traditional method on which it is based. Also, an evaluation of eigen-based results serves as a benchmark comparison for the newly developed method.

Chapter III is devoted to Hopf bifurcation analysis for a SMIB power system experiencing SSR. The bifurcation phenomenon is predicted and the stability of the bifurcated periodic orbits is analyzed by applying the analytical results in the Hopf - Bifurcation theorem [28]. The stability of the bifurcated periodic orbits also is analyzed by numerically solving two-point boundary value problems. Compared with the analytical study of applying the Hopf bifurcation theorem, the numerical study has several advantages which are shown in chapter III. It is shown that the analytical and the numerical results match well, and both results match those of simulations.

Chapter IV discusses the modelling and simulation-based analysis of SSR mitigation effect provided by the TCSC operated in vernier mode in a simplified NWAPS, using EMTP.

Chapter V concludes the contributions of the thesis.

Chapter II
A Generalized Frequency Scan Method for the Analysis of Subsynchronous Resonance

2.1 Introduction

In chapter I, two important frequency scan techniques have been introduced. The first technique [3, 4] can be used to analyze both induction generator effect and torsional interaction. For indicating the occurrence of torsional interaction, the technique is strictly based on analyzing the electrical damping torque coefficient, which is an important tool for understanding a variety of dynamic power system problems. Negative damping torque coefficients at individual shaft natural frequencies indicate torsional interactions at these frequencies. The second technique [19, 20] is for analyzing torsional interaction. This frequency scan technique provides for the analysis over a range of frequencies (including the vicinity of shaft modes), which enables a closer study of the danger of torsional interactions [19]. Since the analysis involves both electrical damping and synchronizing torque coefficients, the technique is not based strictly on analyzing the electrical damping torque coefficient and implicitly assumes the decoupling of mechanical and electrical sub-systems, which has not been theoretically supported, although the process appears to be intuitive.

For a more detailed explanation of the frequency scan technique, consider a SMIB power system as shown in Fig 2.1 . Neglecting dynamics of the Automatic Voltage Regulator (AVR), and the turbine-governor, the coupling between the electrical and mechanical sub-systems is shown in Fig 2.2.

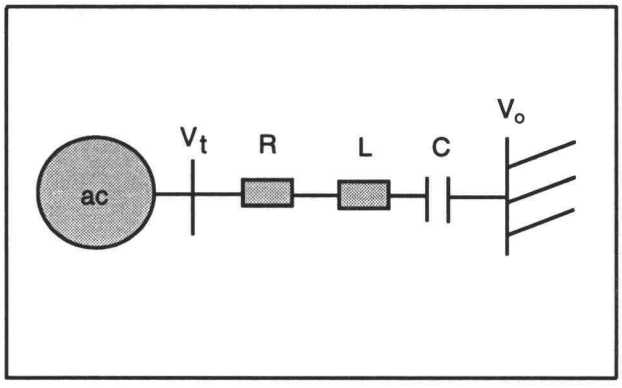

Fig.2.1 A SMIB power system with series capacitor compensation

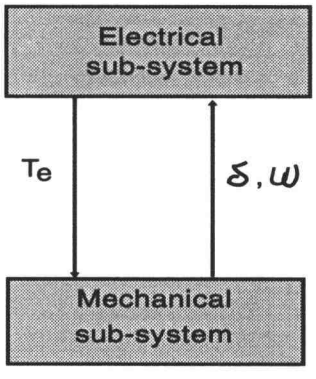

Fig.2.2 Coupling between the electrical and mechanical sub-systems

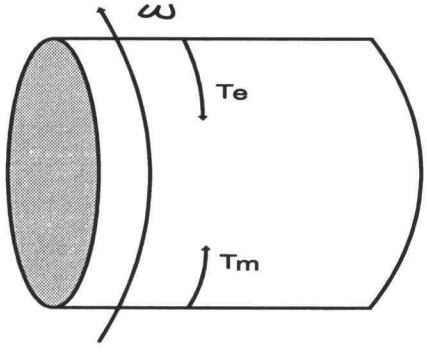

Fig.2.3 Motion of generator mass

Assume that the mechanical shaft of the generator consists of several masses, one of which represents the generator. Motion of the generator mass is governed by the balances between the electrical and mechanical torques applied, as shown in Fig 2.3 . This can be modelled by the familiar second-order differential equation as follows:

$$M\, d^2\delta/dt^2 + D\, d\delta/dt = -T_e + T_m$$

which can be rewritten as

$$T_m - M\, d^2\delta/dt^2 - D\, d\delta/dt = T_e \qquad (2.1)$$

In the above equations, T_e and T_m represent electrical and mechanical torques. δ represents the relative generator rotor angle. M and D represent inertial and damping constants.

Defining the left hand side of (2.1) as T_s, the frequency scan technique is based on analyzing the balances between the mechanical quantity T_s and the electrical torque T_e.

Assuming small sustained oscillations in the generator rotor angle of the form

$$\Delta \cos \omega t$$

the frequency scan technique calculates the frequency responses of T_e and T_s to the disturbance, from the decoupled mechanical and electrical sub-system, respectively. The resulting T_e and T_s are of the form:

$$T_e = T_{ec}\, e^{j\omega t} + cc_1, \text{ and } T_s = T_{sc}\, e^{j\omega t} + cc_2$$

where T_{ec} and T_{sc} are complex coefficients, and are functions of ω. cc_1 and cc_2 are complex conjugate of $T_{ec}\, e^{j\omega t} + cc_1$ and $T_{sc}\, e^{j\omega t} + cc_2$, respectively. Via a frequency scan, it may be found that at a given series compensation level and in the vicinity of one (or more) shaft natural frequency, the real parts of T_{ec} and T_{sc} are equal to each other, while the imaginary part of T_{ec} is less than that of T_{sc}. This indicates torsional interaction at the shaft frequency at which the equality holds.

It can be seen that the idea of the technique closely resembles the concept of analyzing the electrical damping torque coefficient. However, it is not strictly based on this concept, since both electrical damping and synchronizing torque coefficients are involved. Rather, the process searches for torsionally unstable solutions for the system. Since no feedback is involved in the process, the technique implicitly assumes decoupling of the electrical and mechanical sub-systems while searching for torsionally unstable solutions for the coupled system as shown in Fig 2.2 .

In this chapter, the development of a generalized frequency scan method based on the traditional frequency scan technique is discussed. In the developed method, the assumption of sustained oscillations in generator rotor angle is replaced by that of oscillations with an exponential coefficient, i.e., $\Delta\, e^{\sigma t} \cos \omega t$. A trial and error process (which can be recognized as a feedback process) is included for searching for a proper σ, such that at a certain series compensation level σ_0, and at certain torsional frequencies, there are matches between both the real parts of T_{ec} and T_{sc} and the imaginary parts of T_{ec} and T_{sc}. If $\sigma_0 > 0$, torsional interactions are indicated at the frequencies where the equalities hold. The assumption of decoupling electrical and mechanical sub-systems is no longer involved in the developed method. Thus, the method can predict torsional interactions more precisely than the traditional frequency scan technique. Following the same process, induction generator effects can also be predicted.

A comparative analysis of SSR in a SMIB power system using the developed method, the traditional frequency scan technique, and an eigen-based method is presented to verify the proposed technique.

2.2 System Description

The system used for the study is a SMIB power system, as shown in Fig 2.1, which is modelled by a set of 18th-order differential equations (2.2), (2.3), (2.4) [22], as shown in the following. Dynamics of the AVR and turbine-governor are neglected. For the SMIB power system, the electrical sub-system is expressed as

$$
\begin{cases}
(-x_l-x_d)\, di_d/dt + x_{ad}\, di_f/dt = & \omega_b\,[(r_a+r)\, i_d - (x_l+x_q)\, i_q + x_{aq}\, i_Q + e_{cd} \\
 & - x_q\, i_{qe}\, \omega + v_o \cos\delta_e\, \delta] \\
-x_{ad}\, di_d/dt + x_f\, di_f/dt = & \omega_b\,(-r_f\, i_f) \\
(-x_l-x_q)\, di_q/dt + x_{aq}\, di_Q/dt = & \omega_b[(x_l + x_d)\, i_d + (r_a+r)\, i_q - x_{ad}\, i_f + e_{cq} \\
 & + (x_d i_{de} - x_{ad} i_{fe})\, \omega - v_o \sin\delta_e\, \delta] \\
x_{aq}\, di_q/dt + x_Q\, di_Q/dt = & \omega_b\,(-r_Q\, i_Q) \\
de_{cd}/dt = & \omega_b\, x_c\, i_d + \omega_b\, e_{cq} \\
de_{cq}/dt = & \omega_b\, x_c\, i_q - \omega_b\, e_{cd}
\end{cases}
\tag{2.2}
$$

$$
T_e = [(x_q-x_d) i_{qe}]\, i_d + [(x_q-x_d) i_{de} + x_{ad} i_{fe}]\, i_q + x_{ad}\, i_{qe}\, i_f - x_{aq}\, i_{de}\, i_Q \tag{2.3}
$$

in which $\omega_b = 377$ rad/sec .

The mechanical sub-system is described by

$$
\mathbf{M}\, d^2\theta/dt^2 + \mathbf{D}\, d\theta/dt + \mathbf{K}\, \theta = [0\ 0\ 0\ 0\ -T_e\ 0]^T \tag{2.4}
$$

where

$\theta = [\theta_1\ \theta_2\ \theta_3\ \theta_4\ \delta\ \theta_6]^T$, and superscript "T" indicates vector transpose,

and

$$
\mathbf{M} = \begin{bmatrix} M_1 & & & & & \\ & M_2 & & & & \\ & & M_3 & & & \\ & & & M_4 & & \\ & & & & M_5 & \\ & & & & & M_6 \end{bmatrix}
\qquad
\mathbf{D} = \begin{bmatrix} D_{m1} & & & & & \\ & D_{m2} & & & & \\ & & D_{m3} & & & \\ & & & D_{m4} & & \\ & & & & D_{m5} & \\ & & & & & D_{m6} \end{bmatrix}
$$

$$\mathbf{K} = \begin{bmatrix} K_{12} & -K_{12} & & & & \\ -K_{12} & K_{12}+K_{23} & -K_{23} & & & \\ & -K_{23} & K_{23}+K_{34} & -K_{34} & & \\ & & -K_{34} & K_{34}+K_{45} & -K_{45} & \\ & & & -K_{45} & K_{45}+K_{56} & -K_{56} \\ & & & & -K_{56} & K_{56} \end{bmatrix}.$$

Parameter values are taken from the First Bench Mark Model recommended by an IEEE committee for SSR analysis [22].

Parameters in per unit for the synchronous generator and the line are:

$x_{ad} = 1.660$, $x_d = 1.790$, $x_f = 1.700$

$x_{aq} = 1.580$, $x_q = 1.710$, $x_Q = 1.695$

$r_f = 0.001$, $r_Q = 0.0053$, $r_a = 0.0015$,

$x_l = 0.7$, $r = 0.001$,

where subscript "e" indicates the equilibrium operation condition, which is as follows in our study (the values are in p.u.):

$P_e = 0.9$, $Q_e = 0.43$, $v_t = 1.05$, $v_o = 1.0$

The mechanical damping, inertia and stiffness constants in p.u. are:

$D_{m1} = 0.25/\omega_b$ $M_1 = 0.1858/\omega_b$

$D_{m2} = 0.25/\omega_b$ $M_2 = 0.3112/\omega_b$ $K_{12} = 19.303$

$D_{m3} = 0.10/\omega_b$ $M_3 = 1.7173/\omega_b$ $K_{23} = 34.929$

$D_{m4} = 0.10/\omega_b$ $M_4 = 1.7684/\omega_b$ $K_{34} = 52.038$

$D_{m5} = 0.10/\omega_b$ $M_5 = 1.7370/\omega_b$ $K_{45} = 70.858$

$D_{m6} = 0.25/\omega_b$ $M_6 = 0.0684/\omega_b$ $K_{56} = 2.822$.

Subscripts 1, 2, 3, 4, 5 and 6 indicate HP (high-pressure turbine), IP (medium-pressure turbine), LAP (low-A-pressure turbine), LBP (low-B-pressure turbine), GEN (generator) and EX (exciter), respectively.

The mechanical shaft natural modes in rad/sec are obtained approximately from the imaginary part of the eigenvalues of the system:

mode 0 (or GEN mode): 9.469,

mode 1 (or LAP mode): 99.35,

mode 2 (or EX mode): 127.1,

mode 3 (or LBP mode): 161.4,

mode 4 (or IP mode): 202.9,

mode 5 (or HP mode): 298.2 .

2.3 Development of a Generalized Frequency Scan Method

Assume that under small disturbances the generator rotor angle response is of the following form:

$$\delta = a\, e^{\sigma t} \cos(\Omega t) + b\, e^{\sigma t} \sin(\Omega t) + G_\delta(t)$$

or,

$$\delta = F_\delta\, e^{\sigma t}\, e^{j\Omega t} + cc_1 + G_\delta(t) \qquad (2.5)$$

where cc_1 indicates the complex conjugate of the first term in (2.5), F_δ is a complex constant, a, b, σ and Ω are real constants, and $G_\delta(t)$ is a function of time. Since $d\delta/dt = \omega_b\omega$, the corresponding generator rotor speed response is expressed as

$$\omega = (d\delta/dt)/\omega_b$$

or,

$$\omega = (\sigma+j\Omega)\, F_\delta\, e^{\sigma t}\, e^{j\Omega t} / \omega_b + cc_2 + [dG_\delta(t)/dt] / \omega_b \qquad (2.6)$$

where cc_2 indicates the complex conjugate of the first term in (2.6).

If $\rho=(\sigma+j\Omega) / \omega_b$, then

$$\omega = \rho\, F_\delta\, e^{\sigma t}\, e^{j\Omega t} + cc_2 + [dG_\delta(t)/dt] / \omega_b \qquad (2.7)$$

Since superposition holds for linear systems, the following two parts of the generator rotor angle and speed responses under small disturbances can be analyzed separately:

$$\begin{cases} \delta^{(1)} = F_\delta e^{\sigma t} e^{j\Omega t} + cc_1 \\ \omega^{(1)} = \rho F_\delta e^{\sigma t} e^{j\Omega t} + cc_2 \end{cases} \tag{2.8}$$

and

$$\begin{cases} \delta^{(2)} = G_\delta(t) \\ \omega^{(2)} = [dG_\delta(t)/dt] / \omega_b \end{cases}$$

where $\delta = \delta^{(1)} + \delta^{(2)}$, and $\omega = \omega^{(1)} + \omega^{(2)}$.

Of interest are the assumed oscillation components (2.8) of the generator rotor angle and speed responses under small disturbances.

The traditional frequency scan method assumes generator rotor angle oscillations of the form

$$F_\delta e^{j\Omega t} + cc$$

where F_δ is a complex constant, and cc indicates the complex conjugate of the first term. The distinguishing point of the generalized frequency scan method is the inclusion of the exponential section $e^{\sigma t}$.

Considering (2.8), it can be seen from the system description (2.2), (2.3) and (2.4) that the system is decoupled into electrical and mechanical sub-systems, with time functions (2.8) of the generator rotor angle and speed acting as forcing functions.

Now, consider the second-order differential equation governing the motion of the generator mass:

$$M_5 d^2\delta/dt^2 + D_{m5} d\delta/dt - K_{45} \theta_4 + (K_{45}+K_{56}) \delta - K_{56} \theta_6 = -T_e \tag{2.9}$$

Define the left-hand side of the above equation as T_s, which is a mechanical quantity.

From the decoupled mechanical sub-system, T_s can be calculated as a response to the forcing function (2.8). For this purpose, the mechanical sub-system can be expressed as follows:

$$\mathbf{M'}\, d^2\theta'/dt^2 + \mathbf{D'}\, d\theta'/dt + \mathbf{K'}\, \theta' = [0 \;\; 0 \;\; 0 \;\; K_{45}\delta]^T \tag{2.10}$$

$$M_6\, d^2\theta_6/dt^2 + D_{m6}\, d\theta_6/dt + K_{56}\, \theta_6 = k_{56}\, \delta \tag{2.11}$$

$$T_s = -M_5\, d^2\delta/dt^2 - D_{m5}\, d\delta/dt + K_{45}\, \theta_4 - (K_{45}+K_{56})\, \delta + K_{56}\, \theta_6 \tag{2.12}$$

where

$\theta' = [\theta_1\ \theta_2\ \theta_3\ \theta_4]^T$, with superscript "T" indicating vector transpose,

$$\mathbf{M'} = \begin{bmatrix} M_1 & & & \\ & M_2 & & \\ & & M_3 & \\ & & & M_4 \end{bmatrix}, \qquad \mathbf{D'} = \begin{bmatrix} D_{m1} & & & \\ & D_{m2} & & \\ & & D_{m3} & \\ & & & D_{m4} \end{bmatrix},$$

and

$$\mathbf{K'} = \begin{bmatrix} K_{12} & -K_{12} & & \\ -K_{12} & K_{12}+K_{23} & -K_{23} & \\ & -K_{23} & K_{23}+K_{34} & -K_{34} \\ & & -K_{34} & K_{34}+K_{45} \end{bmatrix}.$$

The problem can be restated as solving for $T_s = T_s[\theta'_p(t),\ \theta_{6p}(t),\ \delta(t),\ \omega(t)]$ from (2.12), where $\theta'_p(t)$ and $\theta_{6p}(t)$ are particular solutions of (2.10) and (2.11) under forcing functions $\delta(t)$ and $\omega(t)$ as in (2.8). There can be obtained

$$T_s = T_{sc}\, F_\delta\, e^{\sigma t}\, e^{j\Omega t} + cc_4 \tag{2.13}$$

where cc_4 indicates the complex conjugate of the first term in (2.13), and T_{sc} is a complex coefficient, the derivation of which is shown in Appendix A.

From the decoupled electrical sub-system, the response of the electrical torque T_e to the forcing function (2.8) can be calculated. Then

$$T_e = T_{ec}\, F_\delta\, e^{\sigma t}\, e^{j\Omega t} + cc_3 \tag{2.14}$$

where cc_3 indicates the complex conjugate of the first term in (2.14), and T_{ec} is a complex coefficient, the derivation of which is shown in Appendix A.

For the existence of the assumed oscillation components (2.8) in generator rotor angle and speed responses under small disturbances, the following condition must be satisfied:

$$T_e = T_s \tag{2.15}$$

The assumption in (2.15) is equivalent to the following condition:

$$T_{ec} = T_{sc} \tag{2.16}$$

or,

$$\begin{cases} \text{Real}[T_{ec}] = \text{Real}[T_{sc}] \\ \text{Imag}[T_{ec}] = \text{Imag}[T_{sc}] \end{cases} \tag{2.17}$$

Further, the complex coefficients T_{ec} and T_{sc} are functions of Ω, σ and the series compensation level. For a given series compensation level, (2.17) can be solved for unique $\sigma = \sigma_0$ and $\Omega = \Omega_0$. As illustrated in (2.8), the system undergoes oscillation at the frequency $\Omega = \Omega_0$ with exponential coefficient $\sigma = \sigma_0$. If $\sigma_0 > 0$, the oscillation is unstable.

Eqn(2.17) can also be solved approximately and directly via a frequency scan of T_{ec} and T_{sc} at different values of σ. For a certain value $\sigma = \sigma_0$ (obtained by a trial and error process), a common intersection of Real[T_{ec}] with Real[T_{sc}] and Imag[T_{ec}] with Imag[T_{sc}] at certain frequency $\Omega = \Omega_0$ can be achieved. Examples will be given in the following section to illustrate the application of the proposed method.

It should be noted that when $\sigma = 0$, the generalized frequency scan method is equivalent to the frequency scan technique. The criterion for the indication of SSR is now

when $\quad \text{Real}[T_{ec}] = \text{Real}[T_{sc}]$,

there is $\quad \text{Imag}[T_{ec}] < \text{Imag}[T_{sc}]$. (2.18)

It is in this sense that the developed method is referred to as the generalized frequency scan method.

2.4 Examples of Comparative Analysis of SSR in the SMIB Power System

In this section, two examples of SSR analysis in the SMIB power system using the frequency scan technique, the generalized frequency scan method, and the eigen-based method are presented.

In the first example, an SSR problem in the SMIB power system with a compensation level of 41% of line reactance is examined. A frequency scanning of T_{ec} and T_{sc} for different σ values has been tried. Final results are shown in Figs 2.4(a) through (d).

Figures 2.4(a) and (b) show the results obtained with the frequency scan technique, which can be recognized as a special case of the generalized frequency scan method with $\sigma = 0$, as mentioned before. It can be observed from Fig 2.4(a) that an unstable oscillation at a frequency of around 202 rad/sec is predicted, which is close to shaft natural mode 4 of the system. Figure 2.4(b) shows an enlarged section of Fig 2.4(a), from which it can be observed that the frequency scan technique also predicts an unstable oscillation at a frequency of around 163 rad/sec, which is close to shaft natural mode 3 of the system. The result indicates that at a series compensation level of 41%, SSR at shaft natural modes 3 and 4 are predicted by the frequency scan technique. Figures 2.4(c) and (d) show the results obtained with the generalized frequency scan method. From

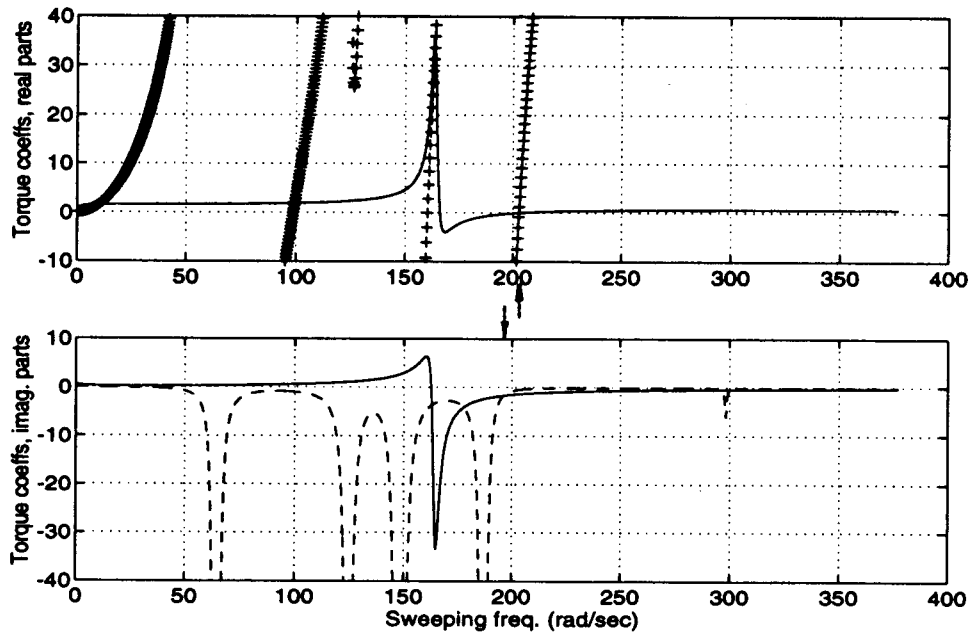

(a) $\sigma = 0$.

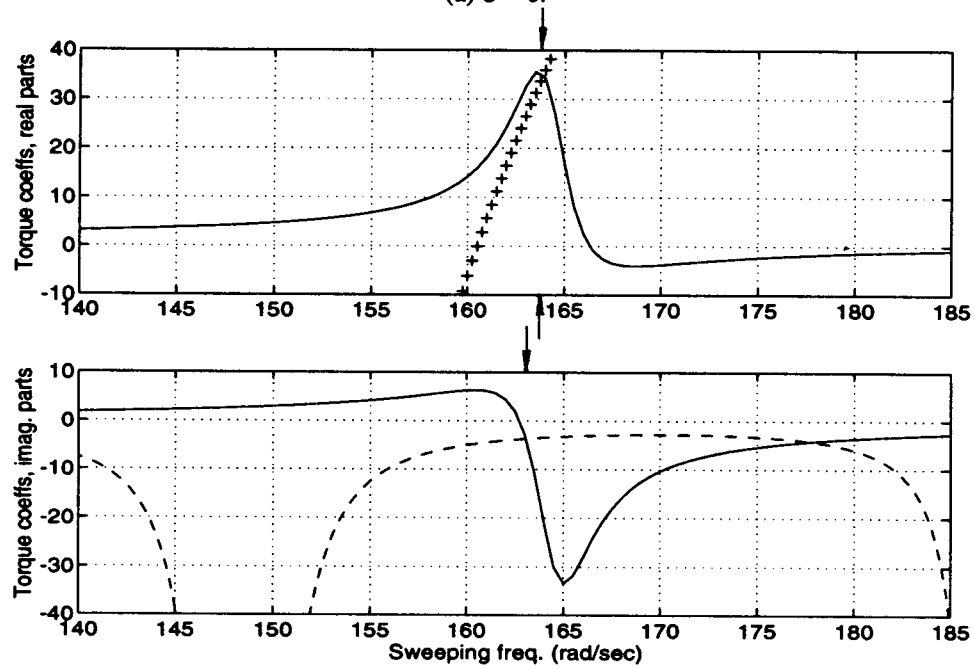

(b) $\sigma = 0$.

Fig.2.4 SSR analysis using the frequency scan technique, at series compensation level of 41% of line reactance

___Real[T_{ec}]; +++Real[T_{sc}]; in upper plot

___Imag[T_{ec}]; ---Imag[T_{sc}] in lower plot

(arrows indicate the intersections of Real[T_{ec}] with Real[T_{sc}] and Imag[T_{ec}] with Imag[T_{sc}])

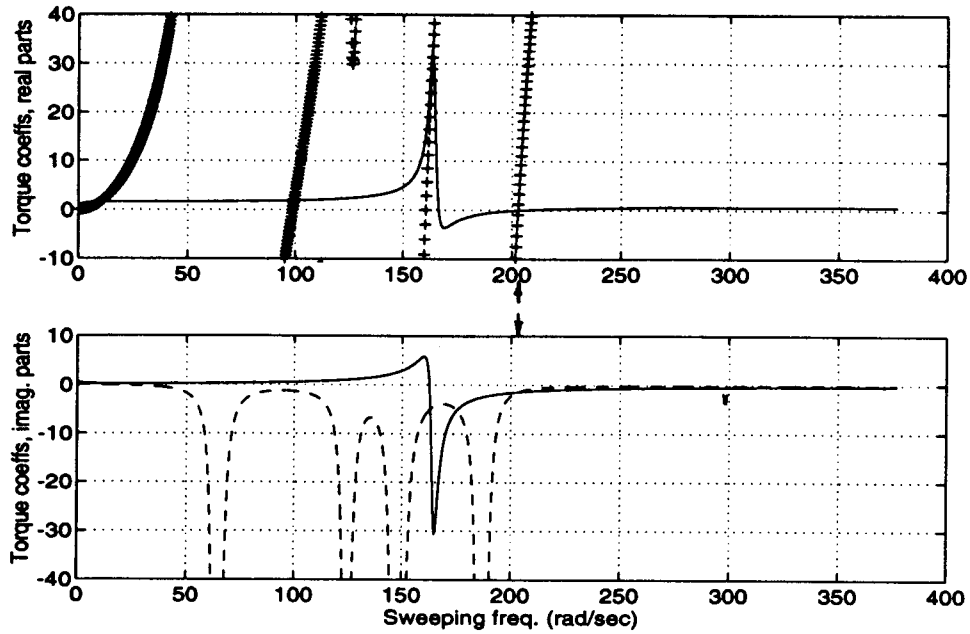

(c) $\sigma = 0.15$

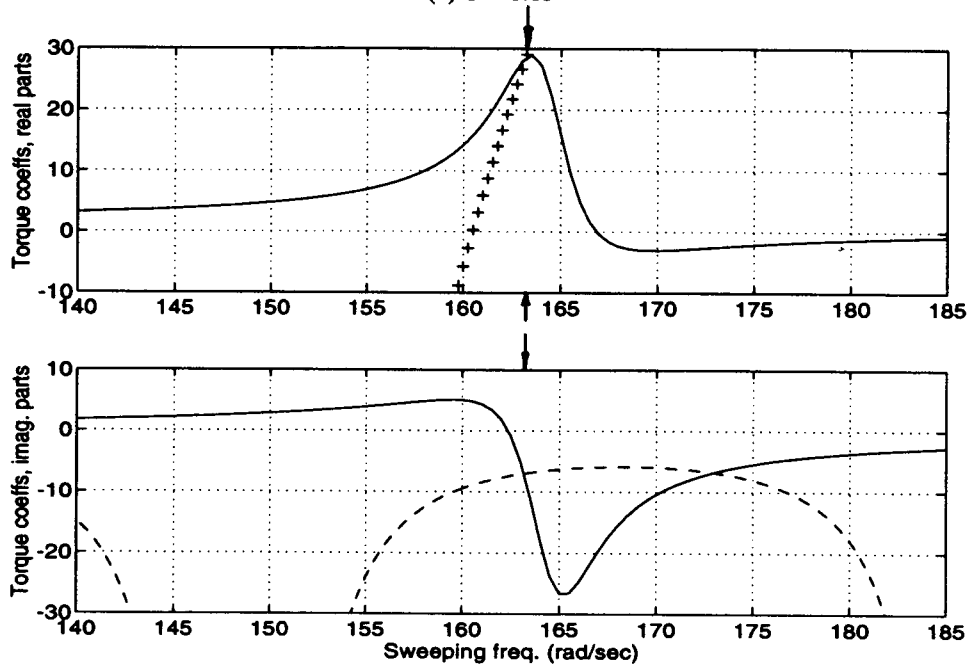

(d) $\sigma = 0.41$

Fig.2.4, Continued. SSR analysis using the generalized frequency scan method, at series compensation level of 41% of line reactance

___ Real[T_{ec}]; +++Real[T_{sc}]; in upper plot

___Imag[T_{ec}]; ---Imag[T_{sc}] in lower plot

(arrows indicate the intersections of Real[T_{ec}] with Real[T_{sc}] and Imag[T_{ec}] with Imag[T_{sc}])

Fig 2.4(c), it can be observed that when $\sigma = 0.15$, Imag[T_{ec}] and Imag[T_{sc}] intersect at the same frequency at which Real[T_{ec}] and Real[T_{sc}] intersect. The frequency is around 202 rad/sec. This indicates an SSR problem at shaft natural mode 4 with an increasing exponential coefficient $\sigma = 0.15$. Figure 2.4(d) shows the frequency scan result at $\sigma = 0.41$, from which it can be seen that the generalized frequency scan method predicts SSR at a frequency of around 163 rad/sec, which is close to shaft natural mode 3, with an increasing exponential coefficient $\sigma = 0.41$.

Table 2.1 shows the result of the eigenvalue analysis which concludes that at series compensation level of 41%, there are SSR problems at both shaft natural mode 3 with increasing exponential coefficient $\sigma = 0.4061$, and shaft natural mode 4 with increasing exponential coefficient $\sigma = 0.1063$.

Table. 2.1 Eigenvalues at 41% series compensation level

-2.5858 ± j 589.7288	-2.3286 ± j 161.5245
-0.4522 ± j 298.1713	-1.6649 ± j 127.0698
0.1063 ± j 202.8489	-0.5614 ± j 99.3975
0.4061 ± j 163.2150	-0.6854 ± j 9.9721
	-0.2842
	-3.4413

It is shown that the results obtained with the generalized frequency scan method and from the eigenvalue analysis match well. It is also shown that the prediction of SSR by the frequency scan technique and the prediction by the eigenvalue analysis match in this case.

It should be mentioned that both the frequency scan technique and the generalized frequency scan method can predict more than one SSR unstable modes at a given series compensation level. This is due to the superposition property of the linearized systems.

It should be noted that a trial and error process is involved for fixing proper values of σ in the generalized frequency scan method, while in the frequency scan technique, σ is always set to be zero. The generalized method involves an iteration of the traditional technique. The assumption of decoupling the electrical and mechanical sub-systems, as implicitly assumed in the traditional technique no longer exists in the generalized method.

In the second example, a series compensation level of 90% is considered. Figure 2.5(a) shows the result obtained with the frequency scan technique. It can be seen that the frequency scan technique does not predict any SSR problem at the given compensation level. Figure 2.5(b) shows the result obtained with the generalized frequency scan method with $\sigma = 0.39$. It is shown that the generalized frequency scan method predicts an SSR problem at a frequency of around 60 rad/sec, with an increasing exponential coefficient $\sigma = 0.39$. Table 2.2 shows the result of the eigenvalue analysis. It can be seen that the eigenvalue analysis predicts an SSR problem at the frequency 61.53 rad/sec, which corresponds to the network mode in the d-q domain, with an increasing exponential coefficient σ=0.3937.

It is shown in this case that the results from the generalized frequency scan method and the eigenvalue analysis match well. It is also shown, however, that the traditional frequency scan technique does not accurately predict the unstable network mode, i.e., the induction generator effect.

Table. 2.2 Eigenvalues at 90% series compensation level

-2.6611 ± j 692.1584	-1.6299 ± j 126.9996
-0.4522 ± j 2.981713	-0.0627 ± j 98.3622
-0.0345 ± j 202.9330	0.3937 ± j 61.5270
-0.3709 ± j 160.5545	-2.0515 ± j 16.3768
	-0.5401
	-4.9786

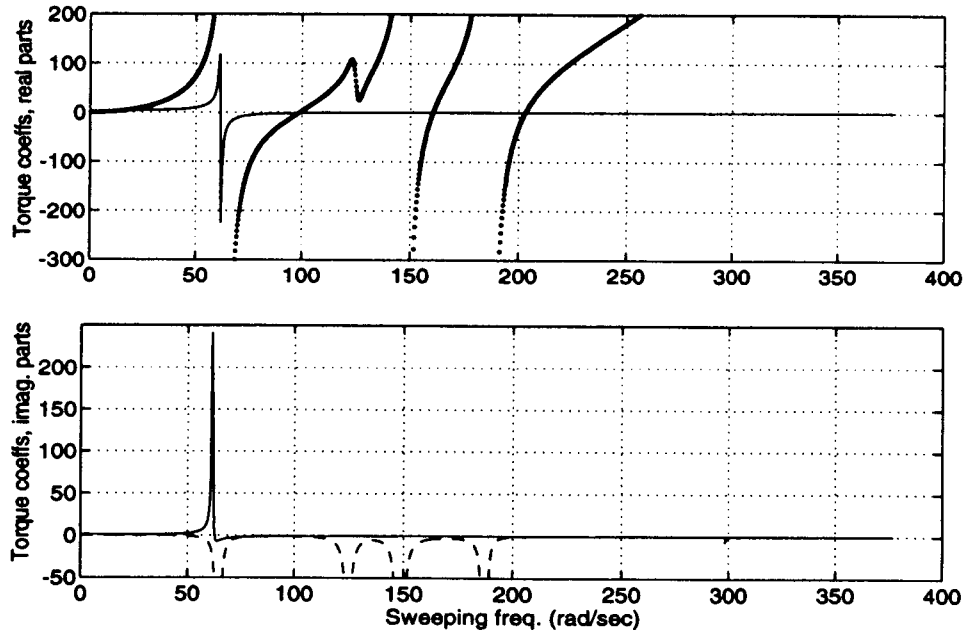

(a) $\sigma = 0$.

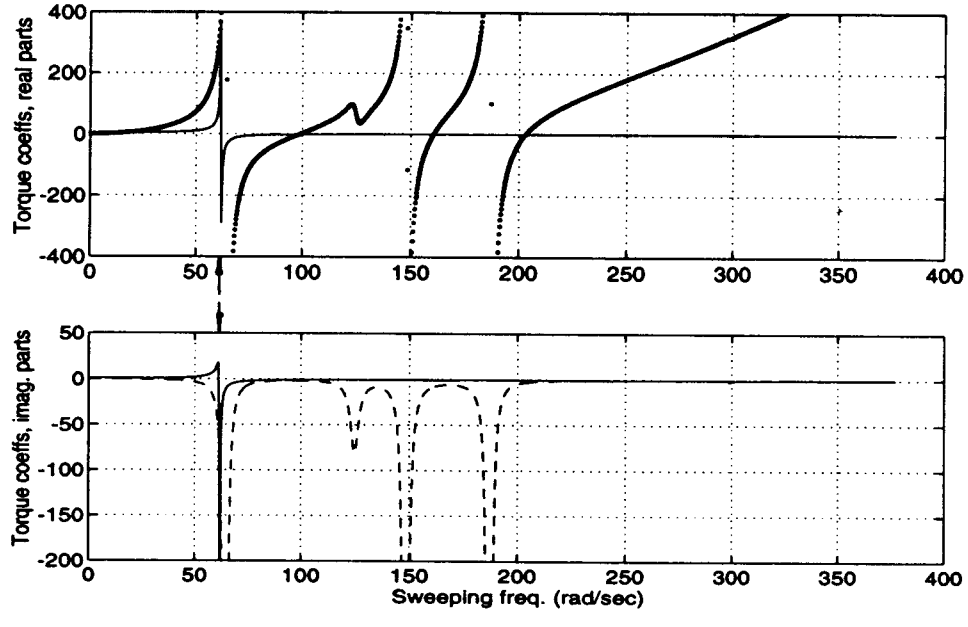

(b) $\sigma = 0.39$

Fig.2.5 SSR analysis using (a) traditional and (b) generalized frequency scan techniques at a series compensation level of 90% of line reactance
___ Real[T_{ec}]; +++Real[T_{sc}]; in upper plot
___Imag[T_{ec}]; ---Imag[T_{sc}] in lower plot
(arrows indicate the intersections of Real[T_{ec}] with Real[T_{sc}] and Imag[T_{ec}] with Imag[T_{sc}])

2.5 Conclusion

The development of a generalized frequency scan method for SSR analysis has been summarized and a comparative SSR analysis in a SMIB power system has been conducted using different analyzing methods. The study shows that the generalized frequency scan method can predict torsional interactions more precisely than the traditional frequency scan technique for the SMIB power system studied. Also, the generalized frequency scan method can predict induction generator effects, whereas the frequency scan technique can only predict torsional interactions. The results obtained with the generalized frequency scan method match well with the results of the eigenvalue analysis for the cases studied. The traditional frequency scan technique matches eigenvalue analysis for some cases, but does not accurately predict the unstable network mode, i.e., the induction generator effect. The usefulness of the developed method can be improved significantly after the application of the method is extended to multimachine power systems successfully.

Chapter III
Hopf Bifurcations in a SMIB Power System Experiencing SSR

3.1 Introduction

Power systems involve a high degree of nonlinearity. Many phenomena can not be analyzed by relying on linear theory exclusively. It has been noticed in the operation of North-Western American Power System (NWAPS) that the SSR oscillations at one of the mechanical shaft modes may be limited instead of increasing exponentially. This phenomenon can not be explained by linear system theory. Such behavior seems to be explained naturally by Hopf bifurcations.

Limited oscillations in power systems experiencing SSR have been analyzed in [26, 27]. Perturbation methods, e.g., multiscale method, have been used for conducting local nonlinear analysis in these studies. The models used in these studies are based on highly simplified second-order classical model of power systems.

As is known, SSR defines a condition where one or more mechanical shaft and/or electrical modes of a series compensated power system becomes unstable with changing series compensation level of the system. If our investigation is confined to a single unstable system mode, the condition coincides with the most important condition for the occurrence of Hopf bifurcations [28, 29, 30]. When Hopf bifurcation occurs, the system may experience limited oscillations which may be analyzed by applying the appropriate bifurcation theory. This may result in more accurate explanation of the SSR dynamic phenomenon.

In this chapter, an analysis of Hopf bifurcations [28] for a SMIB power system experiencing SSR is presented. The system models the BOARDMAN plant with respect

to the rest of the NWAPS, representing the system by a 15th-order set of differential equations. A Hopf bifurcation in the system at a series compensation level of 61.85% is predicted, along with the stable bifurcated periodic orbits. The stability of the bifurcated periodic orbits in the Hopf bifurcation is also analyzed by a numerical method, the essence of which is solving a two-point boundary value problem. Compared with the analytical bifurcation analysis method of applying the Hopf bifurcation theorem, the numerical method is easier to implement, and can yield more information about the periodic orbits in the Hopf bifurcation. In particular, it can predict a series compensation level, greater than, but local to, the bifurcation value, at which the bifurcated periodic orbits change from stable to unstable.

The Hopf bifurcation approach [28, 29, 30] followed in this thesis is often referred to as a "time-domain approach", since the analysis is entirely based on the differential equations [56]. In contrast to this, another Hopf bifurcation approach is based on harmonic balancing methods and is similar to the generalized Nyquist stability analysis[45, 56]. This latter approach is often referred to as a "frequency-domain approach" [56], and is most attractive for analyzing feedback systems. Though it is possible to obtain a required feedback representation for the set of differential equations considered in this study, tremendous effort would be needed to accomplish the task. Thus, the time-domain approach is followed in this study, which seems to be more suitable for the problem considered.

3.2 Introduction of Terms, Definitions and Theorem

In this section, several terms, definitions, and a theorem are introduced, which are important for the study presented in this chapter.

3.2.1 Stability of Nonlinear Autonomous Systems

Since the study presented in this chapter addresses nonlinear SSR dynamical problems in a power system, it is important to introduce the concept of stability. The stability of a nonlinear dynamical system is often addressed in two sense, i.e., Liapunov stability (or, equilibrium stability), and orbital stability of the system. Both concepts are involved in Hopf bifurcations, and the latter is especially relevant. Consider the following nonlinear system

$$d\mathbf{x} / dt = \mathbf{f}(\mathbf{x}) \quad \mathbf{x} \in \mathbf{R}^n \tag{3.1}$$

The Liapunov stability and the orbital stability of the system are defined in the following [44].

Definition 3.1 Let ϕ_t denote the flow of the differential equation (3.1) defined for all $t \in R$. An equilibrium point $\mathbf{x}_0$ of (3.1) is *stable* if for all $\varepsilon > 0$ there exists a $\delta > 0$ such that for all $\mathbf{x} \in N_\delta(\mathbf{x}_0)$ (a δ neighborhood of $\mathbf{x}_0$) and $t \geq 0$ there is

$$\phi_t(\mathbf{x}) \in N_\varepsilon(\mathbf{x}_0) .$$

The equilibrium point $\mathbf{x}_0$ is *unstable* if it is not stable. And $\mathbf{x}_0$ is asymptotically stable if there exists a $\delta > 0$ such that for all $\mathbf{x} \in N_\delta(\mathbf{x}_0)$ there is

$$\lim_{t\to\infty} \phi_t(\mathbf{x}) = \mathbf{x}_0 .$$

It is an immediate consequence of the definition that if an equilibrium point $\mathbf{x}_0$ of (3.1) is asymptotically stable then $\mathbf{x}_0$ is stable.

Definition 3.2 A *cycle or periodic orbit* of (3.1) is any closed solution curve of (3.1) which is not an equilibrium point of (3.1). A periodic orbit Γ is called stable if for each $\varepsilon > 0$ there is a neighborhood U of Γ such that for all $\mathbf{x} \in U$, $d(\phi(t,\mathbf{x}), \Gamma) < \varepsilon$. A periodic orbit Γ is called *unstable* if it is not stable; and Γ is called *asymptotically stable* if for all points $\mathbf{x}$ in some neighborhood U of Γ

$$\lim_{t\to\infty} d(\phi(t, \mathbf{x}), \Gamma) = 0$$

where $d(\phi(t, \mathbf{x}), \Gamma)$ is defined as

$$d(\phi(t, \mathbf{x}), \Gamma) = \inf_{\mathbf{a} \in \phi(t,\mathbf{x}),\, \mathbf{b} \in \Gamma} |\mathbf{a} - \mathbf{b}| .$$

3.2.2 Center manifold Theorem [29]

The center manifold theorem, as introduced in the following [29], is used in the Hopf bifurcation theorem [28] to reduce the vector field of a high dimensional system to two dimensions.

Theorem 3.1 (Center Manifold Theorem) Let $\mathbf{f}$ be a C^r vector field on $\mathbf{R}^n$ vanishing at the origin ($\mathbf{f}(\mathbf{0}) = \mathbf{0}$) and let $A = D\mathbf{f}(\mathbf{0})$. Divide the spectrum of A into three parts, σ^s, σ^c, σ^u with

$$\text{Re}\,\lambda \begin{cases} < 0 \text{ if } \lambda \in \sigma^s \\ = 0 \text{ if } \lambda \in \sigma^c \\ > 0 \text{ if } \lambda \in \sigma^u . \end{cases}$$

Let the (generalized) eigenspaces of σ^s, σ^c, and σ^u be E^s, E^c, and E^u, respectively. Then there exist C^r stable and unstable invariant manifolds W^s and W^u tangent to E^s, and E^u at $\mathbf{0}$ and a C^{r-1} center manifold W^c tangent to E^c at $\mathbf{0}$. The manifolds W^s, W^u, and W^c are all invariant for the flow of $\mathbf{f}$. The stable and unstable manifolds are unique, but W^c need not be.

Consider a system with empty unstable manifold, it is shown [29, 51] that the local stability at the origin of the system is determined by the local stability of its center manifold.

3.2.3 The Poincare Map [44]

The Poincare map is a basic tool for studying the stability of periodic orbits. The idea of the Poincare map is introduced in the following [44].

If Γ is a periodic orbit of the system

$$dx / dt = \mathbf{f}(\mathbf{x}) \quad \mathbf{x} \in \mathbf{R}^n, \mathbf{f} \in C^1(E) \tag{3.2}$$

where E is an open subset of $\mathbf{R}^n$ and contains Γ, through the point $\mathbf{x}_0$, as shown in Fig 3.1, and Σ is a hyperplane perpendicular to Γ at $\mathbf{x}_0$, then for any point $\mathbf{x} \in \Sigma$ sufficiently near $\mathbf{x}_0$, the solution of (3.2) through $\mathbf{x}$ at t=0, $\phi_t(\mathbf{x})$, will cross Σ again at a point $\mathbf{P}(\mathbf{x})$ near $\mathbf{x}_0$. The mapping $\mathbf{x} \rightarrow \mathbf{P}(\mathbf{x})$ is called the *Poincare map*, or first return map. The theorem and its proof on the existence of the Poincare map $\mathbf{P}(\mathbf{x})$ and its first derivative $D\mathbf{P}(\mathbf{x})$ can be found in [44]. The Poincare map $\mathbf{P}(\mathbf{x})$ is an (n-1) dimensional map, and $D\mathbf{P}(\mathbf{x}_0)$ at a point $\mathbf{x}_0 \in \Gamma$ is an (n-1) x (n-1) matrix.

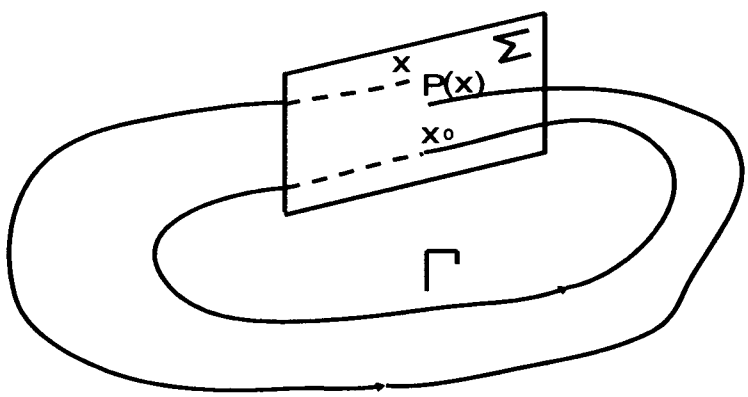

Fig.3.1 The Poincare map

The stability of the periodic orbit Γ is completely described by its Poincare map $\mathbf{P}(\mathbf{x})$, where $\mathbf{x}$ is near an $\mathbf{x}_0 \in \Gamma$. If $\mathbf{P}(\mathbf{x})$ takes $\mathbf{x}$ closer to $\mathbf{x}_0$, the periodic orbit is attracting, otherwise, it is repelling.

For a planar system, if the origin is translated to a point $\mathbf{x}_0 \in \Gamma \cap \Sigma$, the normal line Σ will be a line through the origin, as shown in Fig 3.2. The *displacement function*

associated with the poincare map for the periodic orbit Γ of the planar system is defined as [44]

$$d(s) = P(s) - s.$$

Then

$$d'(s) = P'(s) - 1.$$

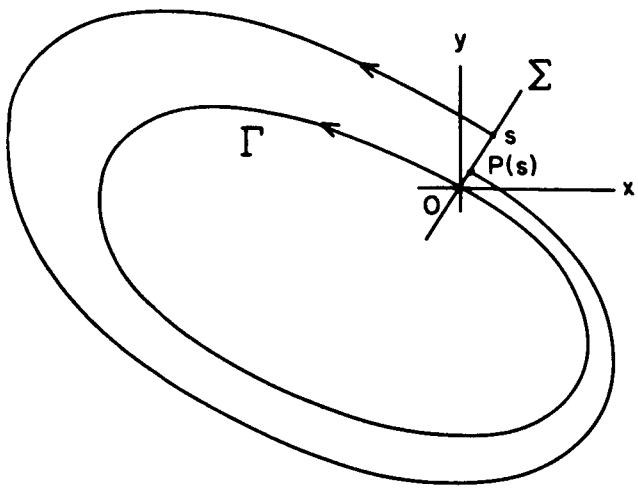

Fig.3.2 The Poincare map for a planar system

It is shown that the stability of the periodic orbit Γ of the planar system is determined by the Poincare map (respectively, the displacement function) according to [44]

if $P'(0) > 1$ (respectively, $d'(0) > 0$), Γ is unstable;

if $P'(0) < 1$ (respectively $d'(0) < 0$), Γ is stable.

3.2.4 Local Bifurcations

Hopf bifurcation approach belongs to *local bifurcation analysis* the idea of which is introduced in the following.

As are many physical problems, power systems are generally modelled by sets of differential equations which involve high nonlinearity and depend on certain parameters, such as line reactance, resistance, mechanical damping, etc.. As the parameters are varied, qualitative changes may occur in the system dynamic behavior. For example, the stability of an equilibrium of a power system model can change from locally asymptotically stable to unstable at certain values of system parameters. These changes are called *bifurcations* and the parameter values at which the changes occur are called *bifurcation values* [29]. Particularly, consider bifurcations of isolated equilibria of a system. The analysis of such bifurcations considers the local behavior around an individual degenerating equilibrium or periodic orbit of the system, and the parameter values in a neighborhood of the bifurcation values. Thus, the analysis is referred to as *local bifurcation analysis* [29].

Now, consider the following system

$$d\mathbf{x} / dt = \mathbf{f}_{\mu}(\mathbf{x}); \quad \mathbf{x} \in \mathbf{R}^n, \mu \in \mathbf{R}^k \tag{3.3}$$

where $\mathbf{f}$ is a C^k (i.e., the k-th derivative of $\mathbf{f}$ is continuous) ($k \geq 1$) function and depends on the k-dimensional parameter μ, and suppose that (3.3) has an equilibrium $(\mathbf{x}_0, \mu_0)$.

If the equilibrium is hyperbolic (i.e., none of the eigenvalues of $D\mathbf{f}(\mathbf{x}_0, \mu_0)$ lie on the imaginary axis, where D represents the partial derivative with respect to $\mathbf{x}$), it can be seen that the local stability of $(\mathbf{x}_0, \mu_0)$ of (3.3) is determined by the linearized system of (3.3), i.e., by the eigenvalues of $D\mathbf{f}(\mathbf{x}_0, \mu_0)$. Since $D\mathbf{f}(\mathbf{x}_0, \mu_0)$ is invertible, by the implicit function theorem, there thus exists a unique C^k function $\mathbf{x}(\mu)$, such that

$$\mathbf{f}(\mathbf{x}(\mu), \mu) = 0$$

for μ sufficiently close to μ_0, with

$$\mathbf{x}(\mu_0) = \mathbf{x}_0 .$$

Now, by the continuity of the eigenvalues with respect to parameters, for μ sufficiently close to μ_0,

$$D_{\mathbf{x}}\mathbf{f}(\mathbf{x}, \mu)$$

has no eigenvalues on the imaginary axis [51]. Therefore, for μ sufficiently close to μ_0, the hyperbolic fixed point $(\mathbf{x}_0, \mu_0)$ of (3.3) persists and its stability type remains unchanged [51]. Thus, for hyperbolic equilibria of (3.3), there are no local bifurcations [29].

Bifurcations in (3.3) may occur when the equilibrium $(\mathbf{x}_0, \mu_0)$ is non-hyperbolic (i.e. $D\mathbf{f}(\mathbf{x}_0, \mu_0)$ has eigenvalues on the imaginary axis). In such cases, when μ changes through μ_0 locally, various nonlinear dynamics may occur, e.g., periodic, quasiperiodic, and chaotic behavior.

Now, consider a simple class of bifurcations by assuming $\mu \in R^1$ in (3.3). The simplest bifurcations in the system (3.3) with k = 1 occur when the linearized system of (3.3) with k = 1 has a simple zero eigenvalue or a unique pair of pure imaginary eigenvalues. Particularly, the latter is of interest, which addresses *Hopf bifurcations.*

3.3 Review of the Hopf Bifurcation Theorem [28, 29, 44]

Consider the nonlinear system

$$d\mathbf{x} / dt = \mathbf{f}_\mu(\mathbf{x}) \quad \mathbf{x} \in \mathbf{R}^n, \mu \in R \tag{3.4}$$

where the vector field $\mathbf{f}_\mu(\mathbf{x})$ depends on a parameter μ.

Assume that

(1) $\mathbf{f}_\mu(\mathbf{x}) \in C^{k+1}(\mathbf{E})$, where $\mathbf{E}$ is an open subset of $\mathbf{R}^n$, and $k \geq 4$,

(2) $\mathbf{f}_\mu(\mathbf{0}) = \mathbf{0}$ for all μ,

(3) $\mathbf{Df}_{\mu}(\mathbf{0})$ ($\mathbf{Df}_{\mu}(\mathbf{x})$ represents the partial derivative of **f** with respect to **x**) has a distinct pair of complex eigenvalues $\lambda(\mu)$ and $\lambda^*(\mu)$. For some $\mu < \mu_0$, $\mathrm{Re}(\lambda(\mu_0)) < 0$; at $\mu = \mu_0$, $\mathrm{Re}(\lambda(\mu_0)) = 0$, and $d\,(\mathrm{Re}(\lambda(\mu_0))) / d\mu > 0$; for some $\mu > \mu_0$, $\mathrm{Re}(\lambda(\mu_0)) > 0$. The other eigenvalues of $\mathbf{Df}_{\mu}(\mathbf{0})$ remain in the left half plane bounded away from the imaginary axis for both $\mu < \mu_0$ and $\mu \geq \mu_0$ with μ local to μ_0.

Under these circumstances, bifurcations to periodic orbits occur for $\mu \in (\mu_0-\delta, \mu_0+\delta)$ for some $\delta \geq 0$. As investigated next, if $d'''(0) \neq 0$, the periodic orbits are unique local to the origin. Also, if the coefficient $d'''(0)$ is negative, the periodic orbits occur for $\mu > \mu_0$ and are attracting. If $d'''(0) > 0$, the orbits occur for $\mu < \mu_0$, and are repelling. The periods of the orbits are close to $2\pi/|\lambda(\mu_0)|$, and the radius of the orbits increases with increasing $|\mu - \mu_0|$. μ_0 is called a bifurcation value.

Computation of d'''(0)

d(.) is the displacement function associated with the Poincare map for the orbit of the origin on a second-order center manifold of (3.4) [28]. The center manifold determines the local stability of the origin of (3.4) for some μ local to the bifurcation value μ_0, and is tangent at the origin to the subspace spanned by the eigenvectors of the complex pair [28]. The coefficient $d'''(0)$ is the third derivative of d(.) with respect to its argument evaluated at the origin, which can be completely determined by the vector field of (3.4) and the associated derivatives up to third-order, evaluated at the origin of (3.4) [28]. The formulae for calculating the coefficient $d'''(0)$ is shown in the following [28].

Assume coordinates, such that $\mathbf{f}_{\mu 0} = [f^1_{\mu 0}, f^2_{\mu 0}, (\mathbf{f}^3_{\mu 0})^T]^T$,

where

$$\mathbf{Df}_{\mu 0}(\mathbf{0}) = \begin{bmatrix} 0 & |\lambda(\mu_0)| & 0 \\ -|\lambda(\mu_0)| & 0 & 0 \\ 0 & 0 & \mathbf{Df}^3_{\mu 0}(\mathbf{0}) \end{bmatrix},$$

and define $\mathbf{x} = [x_1, x_2, \mathbf{X}_3^T]^T$, where $\mathbf{X}_3 = [x_3, ..., x_n]^T$.

$$
\begin{aligned}
d'''(0) = \; & 3\pi/(4|\lambda(\mu_0)|) \, [\, \partial^3 g^1{}_{\mu 0}(\mathbf{0}) / \partial x_1^3 + \partial^3 g^1{}_{\mu 0}(\mathbf{0}) / \partial x_1 \partial x_2^2 \\
& + \partial^3 g^2{}_{\mu 0}(\mathbf{0}) / \partial x_1^2 \partial x_2 + \partial^3 g^2{}_{\mu 0}(\mathbf{0}) / \partial x_2^3 \,] \\
& + 3\pi/(4|\lambda(\mu_0)|^2) \, [\, - (\partial^2 f^1{}_{\mu 0}(\mathbf{0}) / \partial x_1^2)(\partial^2 f^1{}_{\mu 0}(\mathbf{0}) / \partial x_1 \partial x_2) \\
& + (\partial^2 f^2{}_{\mu 0}(\mathbf{0}) / \partial x_2^2)(\partial^2 f^2{}_{\mu 0}(\mathbf{0}) / \partial x_1 \partial x_2) \\
& + (\partial^2 f^2{}_{\mu 0}(\mathbf{0}) / \partial x_1^2)(\partial^2 f^2{}_{\mu 0}(\mathbf{0}) / \partial x_1 \partial x_2) \\
& - (\partial^2 f^1{}_{\mu 0}(\mathbf{0}) / \partial x_2^2)(\partial^2 f^1{}_{\mu 0}(\mathbf{0}) / \partial x_1 \partial x_2) \\
& + (\partial^2 f^1{}_{\mu 0}(\mathbf{0}) / \partial x_1^2)(\partial^2 f^2{}_{\mu 0}(\mathbf{0}) / \partial x_1^2) \\
& - (\partial^2 f^1{}_{\mu 0}(\mathbf{0}) / \partial x_2^2)(\partial^2 f^2{}_{\mu 0}(\mathbf{0}) / \partial x_2^2) \,] \qquad (3.5)
\end{aligned}
$$

where

$$
\begin{aligned}
d_\iota d_k d_j \, g^i{}_{\mu 0}(\mathbf{0}) = \; & d_\iota d_k d_j f^i{}_{\mu 0}(\mathbf{0}) + d_3 d_j f^i{}_{\mu 0}(\mathbf{0}) \circ d_\iota d_k \mathbf{h}(\mathbf{0}) \\
& + d_3 d_k f^i{}_{\mu 0}(\mathbf{0}) \circ d_\iota d_j \mathbf{h}(\mathbf{0}) \\
& + d_3 d_\iota f^i{}_{\mu 0}(\mathbf{0}) \circ d_k d_j \mathbf{h}(\mathbf{0}) \qquad (3.6)
\end{aligned}
$$

for i, j, k, ι = 1, 2, in which d_m, m being integer, represents the operator of partial derivative with respect to x_m, with x_m being a scalar or a vector. "$\circ$" represents the operator of inner product, and

$$
\begin{bmatrix} d_1 d_1 \mathbf{h}(\mathbf{0}) \\ d_1 d_2 \mathbf{h}(\mathbf{0}) \\ d_2 d_2 \mathbf{h}(\mathbf{0}) \end{bmatrix} =
$$

$$
\Delta^{-1} \begin{bmatrix} 2|\lambda(\mu_0)|^2 \mathbf{I}_d + (d_3 \mathbf{f}^3{}_{\mu 0}(\mathbf{0}))^2 & -2|\lambda(\mu_0)| \, d_3 \mathbf{f}^3{}_{\mu 0}(\mathbf{0}) & 2|\lambda(\mu_0)|^2 \mathbf{I}_d \\ |\lambda(\mu_0)| \, d_3 \mathbf{f}^3{}_{\mu 0}(\mathbf{0}) & (d_3 \mathbf{f}^3{}_{\mu 0}(\mathbf{0}))^2 & 2|\lambda(\mu_0)| \, d_3 \mathbf{f}^3{}_{\mu 0}(\mathbf{0}) \\ 2|\lambda(\mu_0)|^2 \mathbf{I}_d & - |\lambda(\mu_0)| \, d_3 \mathbf{f}^3{}_{\mu 0}(\mathbf{0}) & 2|\lambda(\mu_0)|^2 \mathbf{I}_d + (d_3 \mathbf{f}^3{}_{\mu 0}(\mathbf{0}))^2 \end{bmatrix} \begin{bmatrix} -d_1 d_1 \mathbf{f}^3{}_{\mu 0}(\mathbf{0}) \\ -d_1 d_2 \mathbf{f}^3{}_{\mu 0}(\mathbf{0}) \\ -d_2 d_2 \mathbf{f}^3{}_{\mu 0}(\mathbf{0}) \end{bmatrix} \qquad (3.7)
$$

where

$$
\Delta = [d_3 \mathbf{f}^3{}_{\mu 0}(\mathbf{0})] \, [(d_3 \mathbf{f}^3{}_{\mu 0}(\mathbf{0}))^2 + 4|\lambda(\mu_0)|^2 \mathbf{I}_d \,] \qquad (3.8)
$$

and $\mathbf{I}_d$ is an identity matrix with the same dimension as $d_3 \mathbf{f}^3{}_{\mu 0}(\mathbf{x})$.

3.4 Power System Model and Verification of Hopf Bifurcation Conditions

The configuration of the SMIB power system used in this study is shown in Fig 3.3. Model and parameters are chosen to represent the characteristics of the *BOARDMAN* generator with respect to the rest of the North-Western American Power System(NWAPS) [43], assuming heavy generator loading. The model is represented by a 15th-order set of differential equations (3.9). The electrical sub-system is represented by a 5th-order set of differential equations, where the dynamics of the Automatic Voltage Regulator (AVR) and the damper windings are neglected. The mechanical sub-system is represented by a 10th-order set of differential equations, where the dynamics of the turbine-governor are neglected. The vector field of (3.9) depends on a parameter μ, i.e., the series compensation level of the system.

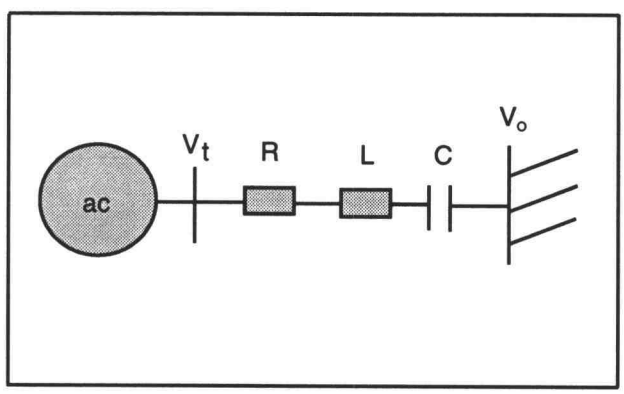

Fig.3.3 SMIB power system with series capacitor compensation

$$
\left\{
\begin{aligned}
& -(x_d + x_t)\, di_d/dt + xad\, di_f/dt = \omega_b [(r_a+r)\, i_d - x_t\, i_q - \omega\, x_q\, i_q + e_{cd} + v_o \sin\delta\,] \\
& -x_{ad}\, di_d/dt + x_f\, di_f/dt = \omega_b [r_f\, E_{fd} / x_{ad} - r_f\, i_f\,] \\
& -(x_q + x_t)\, di_q/dt = \omega_b [x_t\, i_d + (r_a+r)\, i_q + \omega\, x_d\, i_d - \omega\, x_{ad}\, i_f + e_{cq} + v_o \cos\delta\,] \\
& de_{cd}/dt = \omega_b [\mu\, x_t\, i_d + e_{cq}\,] \\
& de_{cq}/dt = \omega_b [\mu\, x_t\, i_q - e_{cd}\,] \\
& d\omega_1/dt = 1/M_1 [-D_1\, \omega_1 - K_{12}\, \theta_1 + K_{12}\, \theta_2] \\
& d\theta_1/dt = \omega_b\, \omega_1 \\
& d\omega_2/dt = 1/M_2 [-D_2\, \omega_2 + K_{12}\, \theta_1 - (K_{12} + K_{23})\, \theta_2 + K_{23}\, \theta_3] \\
& d\theta_2/dt = \omega_b\, \omega_2 \\
& d\omega_3/dt = 1/M_3 [-D_3\, \omega_3 + K_{23}\, \theta_2 - (K_{23} + K_{34})\, \theta_3 + K_{34}\, \delta] \\
& d\theta_3/dt = \omega_b\, \omega_3 \\
& d\omega/dt = 1/M_4 [-T_e + T_m - D_4\, \omega + K_{34}\, \theta_3 - (K_{34} + K_{45})\, \delta + K_{45}\, \theta_5] \\
& d\delta/dt = \omega_b\, \omega \\
& d\omega_5/dt = 1/M_5 [-D_5\, \omega_5 + K_{45}\, \delta - K_{45}\, \theta_5] \\
& d\theta_5/dt = \omega_b\, \omega_5
\end{aligned}
\right. \qquad (3.9)
$$

where $T_e = (x_q - x_d)\, i_d\, i_q + x_{ad}\, i_f\, i_q$, and T_m is constant.

Parameters of the system are as follows:

Parameters in p.u. for the synchronous generator and the line:

$x_{ad} = 1.66$, $x_d = 1.79$,

$x_q = 1.71$, $x_f = 1.70$,

$r_f = 0.01$, $r_a = 0.015$,

$x_l = 0.30$, $r = 0.0165$

The equilibrium operation condition (in p.u.) in this study:

$P_e = 0.876$, $Q_e = -0.115$, $v_t = 1.09$, $v_o = 1.0$

The mechanical damping, inertia and stiffness constants in p.u.:

$D_{m1} = 0.518 \quad M_1 = 0.6695$

$D_{m2} = 0.224 \quad M_2 = 1.4612 \quad K_{12} = 33.07$

$D_{m3} = 0.224 \quad M_3 = 1.6307 \quad K_{23} = 28.59$

$D_{m4} = 0.000 \quad M_4 = 1.5228 \quad K_{34} = 44.68$

$D_{m5} = 0.145 \quad M_5 = 0.0903 \quad K_{45} = 21.98$

Subscripts 1, 2, 3, 4 and 5 indicates HP(high-pressure turbine), IP (medium-pressure turbine), LP(low-pressure turbine), GEN(generator) and EX(exciter), respectively.

In addition to a 2.2 Hz local *swing mode*, the BOARDMAN generator has the following 4 shaft modes:

mode 1: 12.5 Hz, *mode 2*: 25.0 Hz,

mode 3: 29.0 Hz, *mode 4*: 50.0 Hz

Since the vector field of (3.9) is highly smooth within a certain region around the equilibrium representing steady-state operation of the system, (3.9) can be represented by its Taylor expansion around the equilibrium, which can be denoted as:

$$d\mathbf{z} / dt = \mathbf{p}_\mu(\mathbf{z}), \quad \mathbf{z} \in \mathbf{R}^{15}, \mu \in R \tag{3.10}$$

Note that μ appears in the linear coefficients of the state variables i_d and i_q in (3.9). Thus, by taking the Taylor expansion, the equilibrium is transferred to the origin for all μ. That is,

$$\mathbf{p}_\mu(\mathbf{0}) = \mathbf{0}, \quad \text{for any given } \mu \in R.$$

It is shown that the vector field of (3.10) satisfies the assumption (2) in the Hopf-Bifurcation Theorem. Also, because of the assumed smoothness of the vector field of

(3.9) (as well as its Taylor expansion), within a certain region around the origin, the vector field of (3.10) satisfies the assumption (1) in the Hopf bifurcation theorem.

So far, it has been verified that (3.10) satisfies conditions (1) and (2) in the Hopf bifurcation theorem for the occurrence of Hopf bifurcations. From the theorem, it can also be seen that the third condition is determined entirely by the linearized system of (3.10). Specifically, the conditions state that the linearized system has all eigenvalues with negative real parts for μ less than a particular value μ_0, and when μ increases through μ_0, there is a unique complex pair of eigenvalues passing through the imaginary axis with a non-zero speed, while the rest of the eigenvalues remain in the left half of the complex plane.

As mentioned before, in power systems with series capacitor compensation, SSR defines a condition where with changing series compensation level, one or more mechanical and/or electrical modes become unstable. In this study, the analysis is restricted to those cases where only one of the system modes becomes unstable. It can be seen that the physical features of this class of SSR problems fit the condition (3) in the Hopf bifurcation theorem naturally, if it is assumed that the complex pair passes the imaginary axis with a non-zero speed (This is usually satisfied and can be approximately verified by examining the plot of μ versus the real part of the complex pair [30] for each studied case, which will be demonstrated in an example in section 3.6).

3.5 Algorithms for the Computation of d'''(0)

In the previous section, it is demonstrated that at certain series compensation levels, the SMIB power system, modelled by (3.9), or equivalently by (3.10), satisfies the conditions for the occurrence of Hopf bifurcations. When a Hopf bifurcation occurs, the

system may undergo sustained oscillations. Consequently, it is necessary to determine how a bifurcation occurs at a bifurcation value, and the stability of bifurcated periodic orbits. These can be resolved by computing d'''(0) for the SMIB power system using the formulae given in the Hopf bifurcation theorem, which is a more difficult task than verifying the satisfaction of the Hopf bifurcation conditions in the system.

In this section, the development of a set of algorithms for computing the coefficient d'''(0) for (3.10) by applying (3.5) - (3.8) in the Hopf bifurcation theorem is presented. The developed algorithms can be implemented conveniently using software packages, such as MATLAB.

First, it is necessary to transform (3.10) into a form for which (3.5) - (3.8) can be applied.

Since the Hopf-Bifurcation Theorem indicates that the Hopf bifurcation analysis for (3.10) will not be influenced by higher than third-order terms (in case $d'''(0) \neq 0$) in its vector field [29], those terms may be truncated for this study. Denoting the equilibrium values of (3.9) by suffix "e", equation (3.11) (shown in the next page) is obtained which is the Taylor expansion of (3.9) including terms up to third order.

Equation (3.11) can be denoted as in the following:

$$\mathbf{dy} / dt = \mathbf{b}_{\mu}(\mathbf{y}) \quad \mathbf{y} \in \mathbf{R}^n, \mu \in R \tag{3.12}$$

where n = 15,

$\mathbf{y} = [i_d, i_f, i_q, e_{cd}, e_{cq}, \omega_1, \theta_1, \omega_2, \theta_2, \omega_3, \theta_3, \omega, \delta, \omega_5, \theta_5]^T$,

and $\mathbf{b}_{\mu}(\mathbf{y})$ depends on the series compensation level, or, μ, of the SMIB power system.

$$
\begin{cases}
di_d/dt &= \omega_b/Q_1\,[(r_a+r)\,x_f\,i_d + r_f\,x_{ad}\,i_f - (x_t+x_q)\,x_f\,i_q + x_f\,e_{cd} \\
&\quad - x_q\,x_f\,i_{qe}\,\omega + x_f\,v_o\cos\delta_e\,\delta] \\
&\quad + w_b/Q_1\,[\,-x_q\,x_f\,i_q\,\omega + x_f\,v_o\,(-1/2\sin\delta_e\,\delta^2 - 1/6\cos\delta_e\,\delta^3)\,] \\
di_f/dt &= \omega_b/Q_1\,[(r_a+r)x_{ad}\,i_d + r_f(x_d + x_t)\,i_f - (x_t+x_q)x_{ad}\,i_q \\
&\quad + x_{ad}\,e_{cd} - x_q\,x_{ad}\,i_{qe}\,\omega + x_{ad}\,v_o\cos\delta_e\,\delta] \\
&\quad + w_b/Q_1\,[\,-x_q\,x_{ad}\,i_q\,\omega + x_{ad}\,v_o\,(-1/2\sin\delta_e\,\delta^2 - 1/6\cos\delta_e\,\delta^3)\,] \\
di_q/dt &= \omega_b/Q_2\,[(x_t+x_d)\,i_d - x_{ad}\,i_f + (r_a+r)\,i_q + e_{cq} \\
&\quad + (x_d i_{de} - x_{ad} i_{fe})\,\omega - v_o\sin\delta_e\,\delta] \\
&\quad + \omega_b/Q_2\,[x_d\,i_d\,\omega - x_{ad}\,i_f\,\omega + v_o\,(-1/2\cos\delta_e\,\delta^2 + 1/6\sin\delta_e\,\delta^3)] \\
de_{cd}/dt &= \omega_b\,[\,\mu\,x_t\,i_d + e_{cq}\,] \\
de_{cq}/dt &= \omega_b\,[\,\mu\,x_t\,i_q - e_{cd}\,] \\
d\omega_1/dt &= 1/M_1\,[-D_1\,\omega_1 - K_{12}\,\theta_1 + K_{12}\,\theta_2] \\
d\theta_1/dt &= \omega_b\,\omega_1 \\
d\omega_2/dt &= 1/M_2\,[-D_2\,\omega_2 + K_{12}\,\theta_1 - (K_{12} + K_{23})\,\theta_2 + K_{23}\,\theta_3] \\
d\theta_2/dt &= \omega_b\,\omega_2 \\
d\omega_3/dt &= 1/M_3\,[-D_3\,\omega_3 + K_{23}\,\theta_2 - (K_{23} + K_{34})\,\theta_3 + K_{34}\,\delta] \\
d\theta_3/dt &= \omega_b\,\omega_3 \\
d\omega/dt &= 1/M_4\,[(x_d - x_q)\,i_{qe}\,i_d - x_{ad}\,i_{qe}\,i_f + (x_d - x_q)\,i_{de}\,i_q \\
&\quad - x_{ad}\,i_{fe}\,i_q - D_4\,\omega + K_{34}\,\theta_3 - (K_{34} + K_{45})\,\delta + K_{45}\,\theta_5] \\
&\quad + 1/M_4\,[(x_d - x_q)\,i_d\,i_q - x_{ad}\,i_f\,i_q] \\
d\delta/dt &= \omega_b\,\omega \\
d\omega_5/dt &= 1/M_5\,[-D_5\,\omega_5 + K_{45}\,\delta - K_{45}\,\theta_5] \\
d\theta_5/dt &= \omega_b\,\omega_5
\end{cases}
\tag{3.11}
$$

where $Q_1 = x_{ad}^2 - x_f\,(x_d + x_t)$, $Q_2 = -\,(x_q + x_t)$, and $\mu = x_c / x_t$.

Now, transform the nonlinear system (3.12) into a form in which the vector field has its linear portion in real Jordan canonical form. Subsequently, Eqns (3.5) - (3.8) can be applied directly.

Note that the vector field of (3.12) is expressed explicitly in the form:

$$\mathbf{b}_\mu(\mathbf{y}) = \mathbf{A}_\mu\, \mathbf{y} + \mathbf{b}^n{}_\mu(\mathbf{y})$$

where $\mathbf{A}_\mu\, \mathbf{y}$ is the linear portion of the vector field, and $\mathbf{b}^n{}_\mu(\mathbf{y})$ is the nonlinear portion, and $\mathbf{y} \in R^n$, $\mathbf{b}_\mu(\mathbf{y}) \in R^n$, $\mathbf{b}^n{}_\mu(\mathbf{y}) \in R^n$, $\mathbf{A}_\mu$ is an n x n matrix, and n=15. Thus, the linearized system of (3.12) is

$$\mathbf{du} / dt = \mathbf{A}_\mu\, \mathbf{u} \tag{3.13}$$

Assuming a Hopf bifurcation occurs at $\mu = \mu_0$, and assigning $\mu = \mu_0$ in (3.12), change the coordinates of (3.12) according to the following

$$\mathbf{x} = \mathbf{P}^{-1}\, \mathbf{y}$$

where $\mathbf{P}$ is composed of the real and imaginary parts of the eigenvectors of $\mathbf{A}_{\mu 0}$. Thus,

$$\mathbf{dx} / dt = \mathbf{L}_{\mu 0}\, \mathbf{x} + \mathbf{Q}\, \mathbf{b}^n{}_{\mu 0}(\mathbf{Px}) \tag{3.14}$$

where $\mathbf{Q} = \mathbf{P}^{-1}$, $\mathbf{L}_{\mu 0} = \mathbf{Q}\, \mathbf{A}_{\mu 0}\, \mathbf{P}$. $\mathbf{P}$ and $\mathbf{Q}$ are chosen, such that $\mathbf{L}_{\mu 0}$ is in the real Jordan canonical form:

$$\mathbf{L}_{\mu 0} = \begin{bmatrix} 0 & -\lambda(\mu_0) & 0 \\ \lambda(\mu_0) & 0 & 0 \\ 0 & 0 & \mathbf{L}^3{}_{\mu 0} \end{bmatrix},$$

in which $\mathbf{L}^3{}_{\mu 0}$ is in real Jordan canonical form, resulting from the linear transformation.

Assuming $\mathbf{z}_{\mu 0}\ (\mathbf{x}) = \mathbf{Q}\ \mathbf{b}^n{}_{\mu 0}(\mathbf{Px})$, $p_{ij}(1 \le i \le 15,\ 1 \le j \le 15)$ are entries of $\mathbf{P}$, and $q_{ij}(1 \le i \le 15,\ 1 \le j \le 15)$ are entries of $\mathbf{Q}$, it can be obtained

$$\mathbf{z}_{\mu 0}(\mathbf{x}) = [z^1{}_{\mu 0}(\mathbf{x}), \ldots, z^i{}_{\mu 0}(\mathbf{x}), \ldots, z^{15}{}_{\mu 0}(\mathbf{x})]^T,$$

in which

$$z^i_{\mu 0}(\mathbf{x}) = \alpha(i)\,(\Sigma_{j=1,15}\, p_{1,j}\, x_j)\,(\Sigma_{k=1,15}\, p_{3,k}\, x_k)$$
$$+ \beta(i)\,(\Sigma_{j=1,15}\, p_{2,j}\, x_j)\,(\Sigma_{k=1,15}\, p_{3,k}\, x_k)$$
$$+ \gamma(i)\,(\Sigma_{j=1,15}\, p_{2,j}\, x_j)\,(\Sigma_{k=1,15}\, p_{12,k}\, x_k)$$
$$+ \rho(i)\,(\Sigma_{j=1,15}\, p_{3,j}\, x_j)\,(\Sigma_{k=1,15}\, p_{12,k}\, x_k)$$
$$+ \eta(i)\,(\Sigma_{j=1,15}\, p_{1,j}\, x_j)\,(\Sigma_{k=1,15}\, p_{12,k}\, x_k)$$
$$+ \upsilon(i)\,(\Sigma_{j=1,15}\, p_{13,j}\, x_j)\,(\Sigma_{k=1,15}\, p_{13,k}\, x_k)$$
$$+ \xi(i)\,(\Sigma_{j=1,15}\, p_{13,j}\, x_j)(\Sigma_{k=1,15}\, p_{13,k}\, x_k)(\Sigma_{t=1,15}\, p_{13,t}\, x_t),$$

where

$$\alpha(i) = -\, q_{i,12}/M_4\,(x_q - x_d)$$

$$\beta(i) = -\, q_{i,12}/M_4\, x_{ad}$$

$$\gamma(i) = -\, q_{i,3}\, \omega_b/Q_2\, x_{ad}$$

$$\rho(i) = -\, q_{i,1}\, \omega_b/Q_1\, x_f\, x_q - q_{i,2}\, \omega_b/Q_1\, x_{ad}\, x_q$$

$$\eta(i) = q_{i,3}\, \omega_b/Q_2\, x_d$$

$$\upsilon(i) = -\, 1/2\, q_{i,1}\, \omega_b/Q_1\, x_f\, v_o \sin\delta_e - 1/2\, q_{i,2}\, \omega_b/Q_1\, x_{ad}\, v_o \sin\delta_e$$
$$- 1/2\, q_{i,3}\, \omega_b/Q_2\, v_o \cos\delta_e$$

$$\xi(i) = -\, 1/6\, q_{i,1}\, \omega_b/Q_1\, x_f\, v_o \cos\delta_e - 1/6\, q_{i,2}\, \omega_b/Q_1\, x_{ad}\, v_o \cos\delta_e$$
$$+ 1/6\, q_{i,3}\, \omega_b/Q_2\, v_o \sin\delta_e\,.$$

Defining

(1) $\mathbf{x} = [\, x_1, x_2, \mathbf{X}_3^T\,]^T$, in which $\mathbf{X}_3 = [x_3, \ldots, x_{15}]^T$,

(2) $\mathbf{r}_{\mu 0}(\mathbf{x}) = [r^1_{\mu 0}(\mathbf{x}), r^2_{\mu 0}(\mathbf{x}), (\mathbf{r}^3_{\mu 0}(\mathbf{x}))^T]^T$, in which

$r^1_{\mu 0}(\mathbf{x}) = z^1_{\mu 0}(\mathbf{x})$

$r^2_{\mu 0}(\mathbf{x}) = z^2_{\mu 0}(\mathbf{x})$

$\mathbf{r}^3_{\mu 0}(\mathbf{x}) = [\, z^3_{\mu 0}(\mathbf{x}), \ldots, z^{15}_{\mu 0}(\mathbf{x})]^T$, and

(3) $$\begin{bmatrix} f^1_{\mu 0}(\mathbf{x}) \\ f^2_{\mu 0}(\mathbf{x}) \end{bmatrix} = \begin{bmatrix} 0 & -\lambda(\mu_0) \\ \lambda(\mu_0) & 0 \end{bmatrix} \begin{bmatrix} x_1 \\ x_2 \end{bmatrix} + \begin{bmatrix} r^1_{\mu 0}(\mathbf{x}) \\ r^2_{\mu 0}(\mathbf{x}) \end{bmatrix},$$

and $\mathbf{f}^3_{\mu 0}(\mathbf{x}) = \mathbf{L}^3_{\mu 0}\, \mathbf{X}_3 + \mathbf{r}^3_{\mu 0}(\mathbf{x})$,

it is seen that

$$\mathbf{dx} / dt = \mathbf{f}_{\mu 0}(\mathbf{x}) \tag{3.15}$$

in which $\mathbf{x} = [\, x_1, x_2, \mathbf{X}_3^T \,]^T$,

and $\mathbf{f}_{\mu 0}(\mathbf{x}) = [f^1{}_{\mu 0}(\mathbf{x}), f^2{}_{\mu 0}(\mathbf{x}), (\mathbf{f}^3{}_{\mu 0}(\mathbf{x}))^T]^T$.

Based on (3.15), the algorithms for the computation of the coefficient d'''(0) can be derived by applying (3.5) - (3.8). The results are summarized in Appendix B.

3.6 A Hopf Bifurcation in the SMIB Power System

An example of Hopf bifurcations in the SMIB power system with series capacitor compensation modelled by (3.9) is presented in this section. Both an analytical prediction of stable periodic orbits, as well as nonlinear simulation results will be shown.

3.6.1 Analytical Prediction of a Hopf Bifurcation

It was observed from the eigenvalue analysis based on the linearized system (3.13) that a pair of complex eigenvalues corresponding to the generator shaft mode 3 of around 29 Hz (or, 180.4 rad/sec) changes from stable to unstable when the series compensation level increases through 61.85% of line reactance. The remaining eigenvalues remain in the left half plane. Figure 3.4 shows how the complex pair crosses the imaginary axis with a non-zero speed while increasing the series compensation level through 61.85%. Table 3.1 shows the eigenvalues of the system with $\mu = 0.6185$. It is shown that the complex pair corresponding to shaft mode 3 has zero real part.

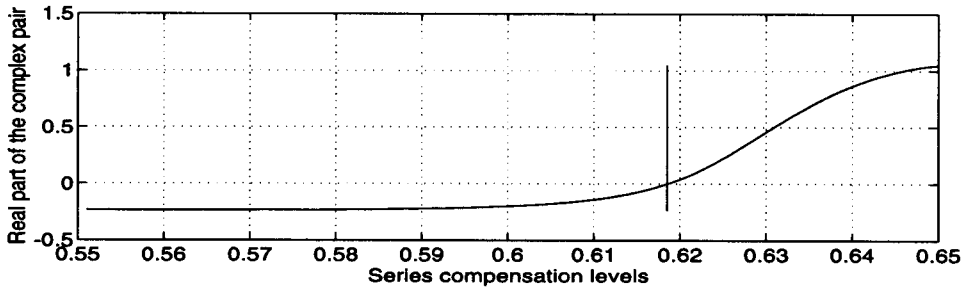

Fig.3.4 Real part of the complex pair changing from negative to positive around series compensation level of 61.85%
* vertical line indicating the series compensation level of 61.85%

Table 3.1 Eigenvalues of the SMIB power system with series compensation level of 61.85%

1.0e+02 *
-0.0963 ± j 5.6444 -0.0049 ± j 1.5404
-0.0073 ± j 3.1307 -0.0314 ± j 1.8390
-0.0611 ± j 0.1260 0.0000 ± j 1.8039
-0.0060 ± j 0.8106 -0.0239

Based on the discussions presented in the previous sections, it can be seen that a Hopf bifurcation occurs at a series compensation level of 61.85%, and $\mu_0 = 61.85\%$ is a bifurcation value. To investigate how the bifurcation occurs and the stability of the bifurcated periodic orbits, the coefficient d'''(0) is computed. Using the algorithms developed and summarized in Appendix B, the coefficient follows from

$$d'''(0) = 3\pi/(4\,|\lambda(\mu_0)|)\,(-0.39) + 3\pi/(4\,|\lambda(\mu_0|^2)\,(-0.071)$$

where $\lambda(\mu_0) = 180.39$.

Since $d'''(0) < 0$, a Hopf bifurcation occurs for $\mu > \mu_0$. The bifurcated periodic orbits are stable.

3.6.2 Simulation Cases at Several Series Compensation Levels

Case I series compensation level of 61.5%

Table 3.2 shows the eigenvalues when $\mu = 0.615$, which is less than $\mu_0 = 0.6185$. It is shown that all the eigenvalues of the system have negative real parts. Figure 3.5 shows

the simulation result based on the linearized model (3.13), which matches the eigenvalue analysis. Figure 3.6 shows the simulation result based on the nonlinear model (3.9). It is shown that the system is stable and there is no periodic orbit at the compensation level.

Table 3.2 Eigenvalues of the SMIB power system with series compensation level of 61.5%

1.0e+02 *

-0.0962 ± j 5.6391	-0.0048 ± j 1.5402
-0.0073 ± j 3.1307	-0.0311 ± j 1.8458
-0.0609 ± j 0.1259	-0.0007 ± j 1.8031
-0.0059 ± j 0.8105	-0.0239

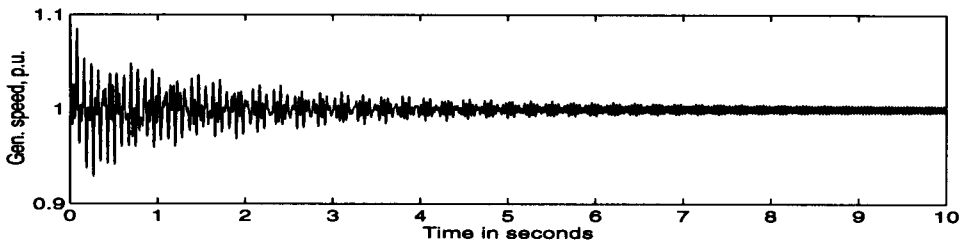

Fig.3.5 System response after a 10% initial disturbance in generator rotor speed, 61.5% series compensation, linear model

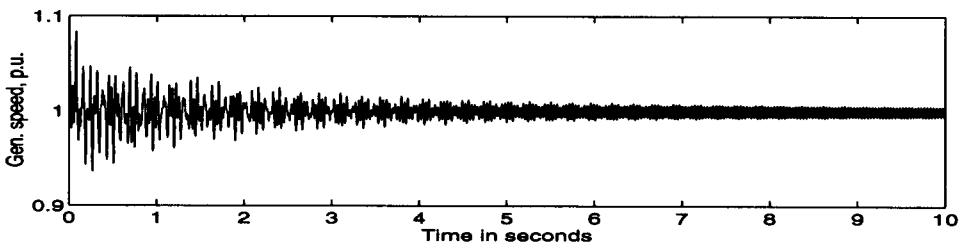

Fig.3.6 System response after a 10% initial disturbance in generator rotor speed, 61.5% series compensation, nonlinear model

Case II series compensation level of 62.5%

Table 3.3 shows eigenvalues of the system when $\mu = 0.625$, which is greater than $\mu_0 = 0.6185$. It can be seen that the pair of eigenvalues corresponding to shaft mode 3 is

Table 3.3 Eigenvalues at a series compensation level of 62.5%

1.0e+02 *

-0.0963 ± j 5.6544	-0.0050 ± j 1.5409
-0.0073 ± j 3.1307	-0.0330 ± j 1.8266
-0.0615 ± j 0.1262	0.0022 ± j 1.8050
-0.0060 ± j 0.8107	-0.0240

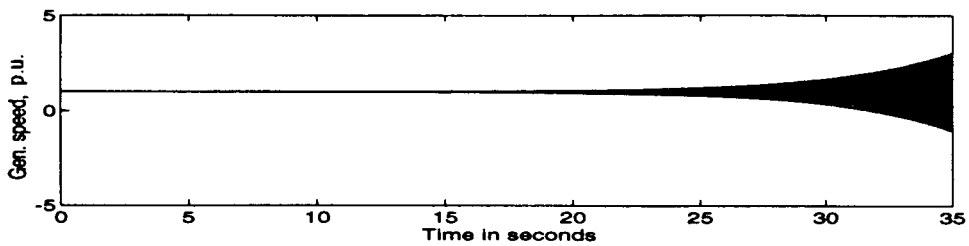

Fig.3.7 System response after a 1% initial disturbance in generator rotor speed, 62.5% series compensation, linear model

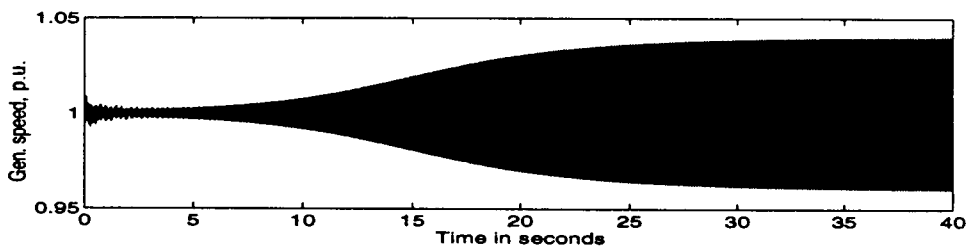

(a)

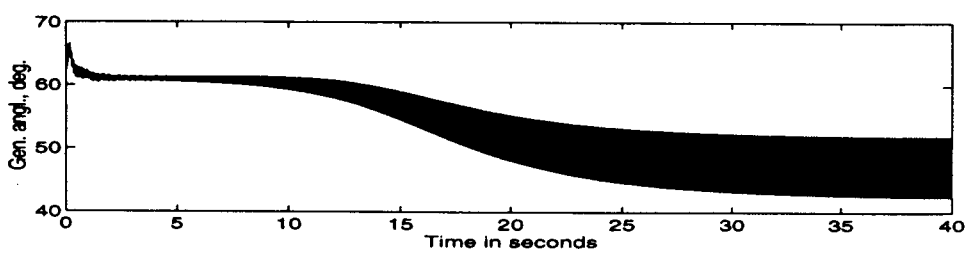

(b)

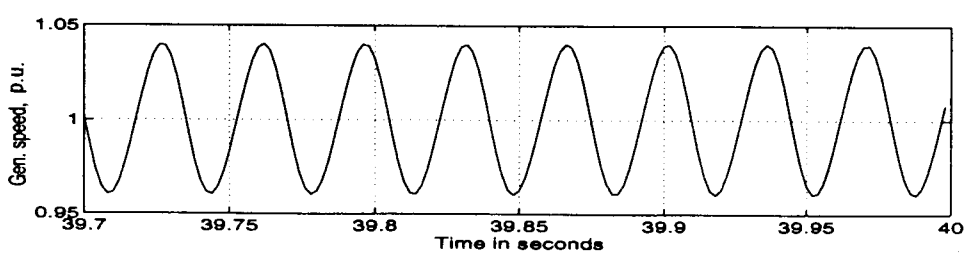

(c)

Fig.3.8 System response after a 1% initial disturbance in generator rotor speed, 62.5% series compensation, nonlinear model

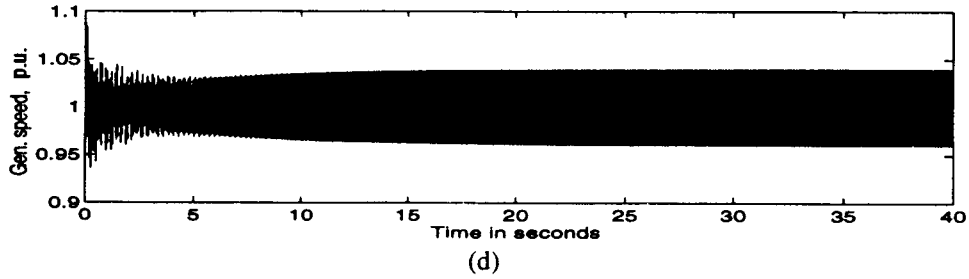

(d)

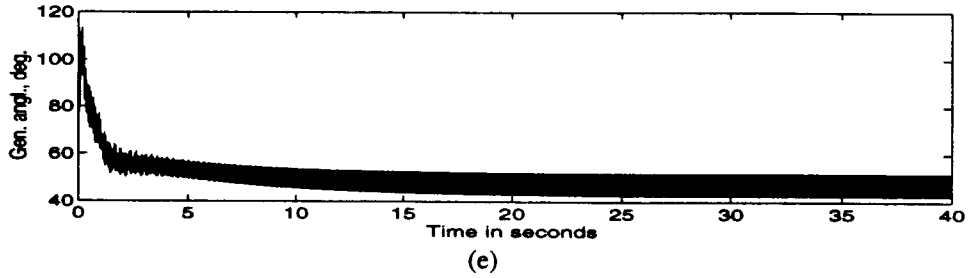

(e)

Fig.3.8, Continued. System response after a 10% initial disturbance in generator rotor speed, 62.5% series compensation, nonlinear model

unstable at the compensation level. Figure 3.7 shows the simulation result based on the linearized model (3.13), which indicates an exponentially increasing oscillation at shaft mode 3. Figure 3.8 shows the simulation results based on the nonlinear model (3.9), which indicate limited oscillations at frequencies close to shaft mode 3, instead of exponentially increasing oscillations. Figure 3.8(a), (b) and (c) show the system response after a relatively small disturbance, and Fig 3.8(d) and (e) show the system response after a larger disturbance. Figure 3.8 (c) shows a section of Fig 3.8(a), which indicates that the frequency of the periodic orbit is close to shaft mode 3 of 29.0 Hz. The nonlinear simulations show a stable periodic orbit at the compensation level.

Case III series compensation level of 63%

Table 3.4 shows eigenvalues of the system when $\mu = 0.63$, which is greater than μ_0=0.6185. It can be seen that the pair of eigenvalues corresponding to shaft mode 3 is unstable at the compensation level. Figure 3.9 shows the simulation results based on the

nonlinear model (3.9), which indicate stable limited oscillations at frequencies close to shaft mode 3 at the compensation level.

It is shown that the analytical prediction of the bifurcation of stable periodic orbits at series compensation level of 61.85% is supported by the nonlinear simulations for the cases studied.

Table 3.4 Eigenvalues of the SMIB power system with series compensation level of 63.0%

1.0e+02 *
-0.0964 ± j 5.6621 -0.0051 ± j 1.5413
-0.0073 ± j 3.1307 -0.0348 ± j 1.8179
-0.0617 ± j 0.1263 0.0046 ± j 1.8050
-0.0061 ± j 0.8109 -0.0241

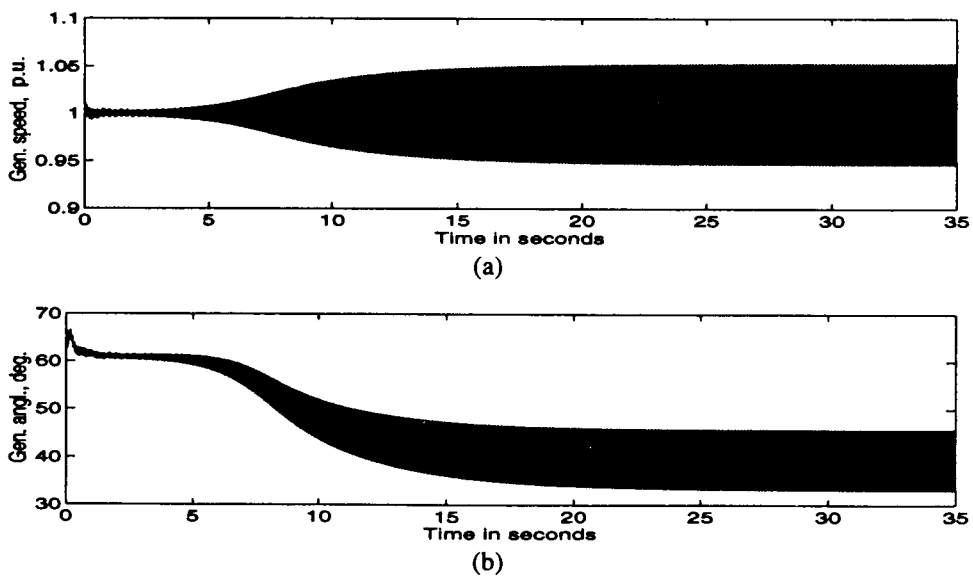

Fig.3.9 System response after a 1% initial disturbance in generator rotor speed, 63% series compensation, nonlinear model

3.7 Numerical Analysis of the Stability of Periodic Orbits in the Hopf Bifurcation

In the previous sections, bifurcation behavior in a SMIB power system with series capacitor compensation is analyzed, by applying the Hopf bifurcation theorem. It has been shown that the system satisfies the Hopf bifurcation conditions when it is vulnerable to SSR at a particular mode of the system. A Hopf bifurcation at a series compensation level of 61.85%, and stable periodic orbits at series compensation levels greater than, but local to, the bifurcation value (i.e., $\mu_0 = 0.6185$) are predicted and verified via nonlinear simulations. The stability of the bifurcated periodic orbits was determined by computing the coefficient d'''(0) for the studied case following a set of algorithms developed for the SMIB power system.

Since the analysis follows the Hopf bifurcation theorem, the prediction of how the bifurcation occurs and the stability of bifurcated periodic orbits is quite accurate. However, since the model considered is high dimensional, the algorithm derivation is extremely complicated. Further, as mentioned before, Hopf bifurcation analysis is of local nature. The limited oscillation behavior in the Hopf bifurcation is local to the bifurcation value of the parameter the system depends on, i.e., the series compensation level in this study. Analytical studies applying the Hopf bifurcation theorem can not determine the parameter range, for which the stable property of the periodic orbits is sustained. That is, it can not determine a particular value $\mu = \mu_p$, which is greater than, but local to, μ_0, at which the bifurcated periodic orbits change from stable to unstable.

An alternative for analyzing the stability of the bifurcated periodic orbits is via a numerical method, the essence of which is solving a two-point boundary value problem [30]. The numerical method is easier to implement than the analytical method for high dimensional systems. In addition, the numerical analysis, as will be presented in the

following sections, can yield the value of μ_p, at which the periodic orbits in the Hopf bifurcation change from stable to unstable.

First, some theorems on the stability analysis of periodic orbits are reviewed.

3.7.1 The Poincare Map and the Monodromy Matrix

In section 3.2, the concept of the Poincare map for a periodic orbit is introduced. Also, it is shown that for a planar system, $DP(\mathbf{x}_0)$ determines the stability of a periodic orbit Γ of the system, with $\mathbf{x}_0 \in \Gamma$. It can be shown that similar results hold for higher dimensional systems [44]:

$$d\mathbf{x} / dt = \mathbf{f}(\mathbf{x}) \quad \mathbf{x} \in \mathbf{R}^n, \mathbf{f} \in C^1(E) \tag{3.16}$$

where E is an open subset of $\mathbf{R}^n$.

Assume Γ is a periodic orbit of the system (3.16), it is shown [44] that the stability of the periodic orbit Γ is determined by the first derivative of the Poincare map, $\mathbf{DP}(\mathbf{x}_0)$ (an (n-1) x (n-1) matrix), at an $\mathbf{x}_0 \in \Gamma$, as summarized in the following theorem [30]:

Theorem 3.2

(a) If the moduli of all eigenvalues of $\mathbf{DP}(\mathbf{x}_0)$ are smaller that 1, then Γ is attracting.

(b) If the modulus of at least one eigenvalue of $\mathbf{DP}(\mathbf{x}_0)$ is larger than 1, then Γ is repelling.

The (n-1) x (n-1) matrix $\mathbf{DP}(\mathbf{x}_0)$ is determined by a fundamental matrix for the linearized system of (3.16) about the periodic orbit Γ [44], which will be shown in the following.

Assuming T is the period of Γ, and

$$\Gamma: \mathbf{x} = \gamma(t), 0 \le t \le T$$

the linearization of (3.16) about Γ is defined as the following linear time-varying system [44, 45]:

$$d\mathbf{x} / dt = A(t)\,\mathbf{x} \tag{3.17}$$

with $A(t) = Df(\gamma(t))$.

The n x n matrix A(t) is a T-periodic function of t. A fundamental matrix for (3.17) is a nonsingular n x n matrix $\Phi(t)$ which satisfies

$$d\,\Phi(t) / dt = A(t)\,\Phi(t) \tag{3.18}$$

A solution of (3.17) satisfying the initial condition $\mathbf{x}(0) = \mathbf{x}_0$ is thus given by [44, 45]

$$\mathbf{x}(t) = \Phi(t)\,\Phi^{-1}(0)\,\mathbf{x}_0$$

The monodromy matrix, which plays an important role in determining stabilities of periodic orbits, is closely related to the fundamental matrix $\Phi(t)$, as shown in the following definition [30].

Definition 3.3 The n x n monodromy matrix M of the periodic solution $\gamma(t)$ of (3.16) with period T is defined by

$$M = \Phi(T)$$

where $\Phi(t)$ is a fundamental matrix for the linearized system (3.17), which satisfies (3.18) with initial condition $\Phi(0) = I$.

Following the Floquet theorem [44, 45, 46], it can be found that a fundamental matrix $\Phi(t)$ for (3.17) satisfies

$$\Phi(t) = Q(t)\,e^{Bt}$$

where Q(t) is a nonsingular, differentiable, T-periodic matrix, and B is a constant matrix. Further, if $\Phi(0) = I$, then $Q(0) = I$.

Consequently, it is easy to see that the monodromy matrix satisfies [44]

$$M = e^{BT}$$

The eigenvalues of B are called *characteristic exponents*, and the eigenvalues of e^{BT}, or M, are called *characteristic multipliers* [44].

It can be shown [44] that the n x n monodromy matrix M for the periodic orbit Γ of (3.16) has unity as an eigenvalue. Also, it is proved [44] that the other n-1 eigenvalues of M are those of $DP(\mathbf{x}_0)$, where $\mathbf{x}_0 \in \Gamma$. Following theorem 3.2, it is clear that the characteristic multipliers of M are critical for determining the stability of the periodic orbit Γ. There can thus be following summary [30]:

Summary 3.1: Let $\gamma(t)$ be a periodic solution of (3.16) with period T. The monodromy matrix M is defined by $M = \Phi(T)$, where $\Phi(t)$ solves the matrix initial value problem

$$d\,\Phi(t) / dt = Df(\gamma(t))\,\Phi(t),\ \Phi(0) = I\,.$$

The matrix M has n eigenvalues $\mu_1, \ldots \mu_n$. One of them is equal to unity, say μ_n. The other n-1 eigenvalues determine (local) orbital stability by the following rule:

$\gamma(t)$ is orbitally asymptotically stable if $|\mu_j| < 1$ for j=1, ... n-1;

$\gamma(t)$ is unstable if $|\mu_j| > 1$ for some j.

3.7.2 Statement of a Two-Point Boundary Value Problem

It has been shown that the monodromy matrix M plays an important role in determining the stability of a periodic orbit of a nonlinear system. Though it is generally difficult to obtain an analytical solution of the monodromy matrix M, a numerical solution of the matrix can be achieved.

If the periodic solution of (3.16) would be known apriori (which is normally not the case), M can be obtained by integrating the initial value problem (3.18), with an initial condition $\Phi(0) = I$.

An alternative is to solve for the periodic solution and its monodromy matrix M simultaneously via solving a two-point boundary value problem [30, 47, 48].

Of interest is the following nonlinear system:

$$d\mathbf{x}(\tau) / d\tau = \mathbf{f}(\mathbf{x}(\tau), \mu) \quad \mathbf{x} \in \mathbf{R}^n, \mu, \tau \in R, \tau \geq 0 \tag{3.19}$$

which has a periodic solution with period T. The vector field of (3.19) depends on a parameter μ. Note that for a periodic solution of the system, there is

$$\mathbf{x}(0) = \mathbf{x}(T) \tag{3.20}$$

Since T is not known apriori, it is desirable that T not appear in the boundary conditions. This can be achieved by linearly mapping the time interval [0 T] to [0 1]. Following the mapping [30], (3.19) and (3.20) are transformed into follows:

$$d\mathbf{x}(t) / dt = T\,\mathbf{f}(\mathbf{x}(t), \mu) = \mathbf{g}(\mathbf{x}(t), T, \mu) \tag{3.21}$$

$$\mathbf{x}(0) = \mathbf{x}(1) \tag{3.22}$$

where $t = \tau/T$.

The system (3.21) can be augmented to include T as an unknown constant by including the following equation:

$$dT / dt = 0 \tag{3.23}$$

An additional boundary condition is needed for fixing the phase condition, so that a unique periodic solution can be obtained. Following phase condition can be posed [30]:

$$x_k(0) = c, \text{ for any } 1 \leq k \leq n \tag{3.24}$$

where c should be a value between the minimum and maximum of the periodic oscillation $x_k(t)$, for $0 \leq t \leq T$.

In summary, the two-point boundary-value problem (3.21)-(3.24) is obtained, which can be restated as in the following:

$$d\mathbf{x}(t) / dt = \mathbf{g}(\mathbf{x}(t), T, \mu) \tag{3.25}$$

$$dT / dt = 0 \tag{3.26}$$

$$E\,\mathbf{x}(0) + F\,\mathbf{x}(1) = \upsilon \tag{3.27}$$

in which $\mathbf{g}(\mathbf{x}(t), T, \mu) = T\,\mathbf{f}(\mathbf{x}(t), \mu)$, and $\mathbf{f}$ is defined in (3.19). E and F are $(n + 1) \times n$ matrices, and $\upsilon \in R^{n+1}$, as shown in the following:

$$E = \begin{bmatrix} & & & & & \\ & & I_n & & & \\ & & & & & \\ 0 & .. & 1 & 0 & .. & 0 \end{bmatrix}$$

↓
kth-column

$$F = \begin{bmatrix} & & & & \\ & & -I_n & & \\ & & & & \\ 0 & & .... & 0 & 0 \end{bmatrix}$$

and
$\upsilon = [0\ 0\ ...\ 0\ c]^T$

in which I_n denotes an identity matrix of dimension n, and c is a real constant, as defined in (3.24).

The problem can be solved by following the Newton-Fox method [48, 49], by which the periodic solution and its monodromy matrix M can be obtained simultaneously.

3.7.3 Newton-Fox Procedure [48, 49]

Consider the initial value problem for (3.25)-(3.27) in the following:

$$dy / dt = \mathbf{g}(\mathbf{y}(t), T, \mu) \tag{3.28}$$

$$dT / dt = 0 \tag{3.29}$$

$$\mathbf{y}(0) = \mathbf{s} \tag{3.30}$$

where $\mathbf{y}, \mathbf{s}, \mathbf{g} \in \mathbf{R}^n$.

Denoting $\phi(\mathbf{s}, T, \mu) = E\,\mathbf{y}(\mathbf{s}, T, \mu, 0) + F\,\mathbf{y}(\mathbf{s}, T, \mu, 1) - \upsilon$, it is desirable that $\mathbf{s}$ and T satisfy

$$\phi(\mathbf{s}, T, \mu) = 0 \tag{3.31}$$

Eqn (3.31) can be solved iteratively by the basic Newton-Raphson scheme as following:

Given $\mathbf{s}_0$, T_0

$$\mathbf{s}_{k+1} = \mathbf{s}_k + \Delta\mathbf{s}_k$$

$$T_{k+1} = T_k + \Delta T_k$$

in which

$$Q(\mathbf{s}_k, T_k, \mu) \begin{bmatrix} \Delta\mathbf{s}_k \\ \Delta T_k \end{bmatrix} = -\phi(\mathbf{s}_k, T_k, \mu)$$

and $Q(\mathbf{s}, T, \mu)$ is defined as:

$$Q(\mathbf{s}, T, \mu) = [d\phi / d\mathbf{s}, d\phi / dT]$$

$$= [E + F\,W(\mathbf{s}, T, \mu, 1), F\,V(\mathbf{s}, T, \mu, 1)]$$

W (an n x n matrix, n=15) and V ($\in \mathbf{R}^n$, n=15) solve the following initial value problems:

$$dW / dt = A(t, \mathbf{s}, T, \mu)\,W \tag{3.32}$$

$$W(\mathbf{s}, T, \mu, 0) = \mathbf{I}_n, \text{ with } \mathbf{I}_n \text{ an identity matrix of dimension 15} \tag{3.33}$$

$$dV / dt = A(t, \mathbf{s}, T, \mu)\,V + G(t, \mathbf{s}, T, \mu) \tag{3.34}$$

$$V(\mathbf{s}, T, \mu, 0) = \mathbf{0} \tag{3.35}$$

and

$$A(t, \mathbf{s}, T, \mu) = d\mathbf{g}(\mathbf{y}(\mathbf{s}, T, \mu, t), T, \mu) / d\mathbf{y}$$
$$= T\, J(\mathbf{y}(\mathbf{s}, T, \mu, t), \mu)$$
$$G(t, \mathbf{s}, T, \mu) = d\mathbf{g}(t, \mathbf{y}(\mathbf{s}, T, \mu, t), T, \mu) / dT$$
$$= \mathbf{f}(\mathbf{y}(\mathbf{s}, T, \mu, t), \mu)$$

where

$J = d\mathbf{f}(\mathbf{y}(\mathbf{s}, T, \mu, t), \mu) / d\mathbf{y}$.

For each iteration of $\mathbf{s}_k$, T_k, the initial value problems (3.28)-(3.30) and (3.32)-(3.35) are integrated simultaneously. The iteration terminates either after a user-defined maximum iteration number, or when $\Delta\mathbf{s}$ and ΔT are small in some norm sense, e.g. $\max(|\Delta s_j|, j=1,...n, |\Delta T|)$ is less than a small pre-defined real number.

Following the iterative Newton-Fox procedure, which can be recognized as a shooting procedure [50], desirable initial conditions $\mathbf{s}^*$ and T^* for integrating the initial value problem (3.28)-(3.30) may be obtained, through which the periodic solution (either stable or unstable) of (3.19) can be obtained.

Also, notice that A (respectively J) is actually the Jacobian matrix of $\mathbf{g}$ (respectively $\mathbf{f}$) along a solution path. Thus, provided that the iteration process converges (the periodic solution is achieved), $W(\mathbf{s}, T, \mu, 1)$ is the monodromy matrix M [30, 48], whose eigenvalues decide the stability of the periodic solution.

In summary, following the Newton-Fox method, a periodic solution of (3.18), and its monodromy matrix M can be obtained simultaneously.

3.7.4 Stability of the Periodic Orbits in the SMIB Power System

In section 3.6, a Hopf bifurcation in the SMIB power system at series compensation level μ_0 = 61.85% of line reactance is presented. Stable periodic orbits bifurcated in the Hopf bifurcation were predicted for some μ greater than, but local to, μ_0 by the analytical method and verified using nonlinear simulations. Following the Hopf bifurcation theorem, the periods of the bifurcated periodic orbits are predicted to be close to shaft mode 3 in the eigenvalue analysis at μ_0.

In this section, the numerical method presented is applied to the stability analysis of the bifurcated periodic orbits in the SMIB power system modelled by (3.9).

Following the eigenvalue analysis, as discussed in section 3.6, it is assumed that the periodic orbits occur for $\mu>\mu_0$ (if one can not succeed in obtaining a single periodic solution at this side of μ_0, the other side can be tried). Consider a series of μ (which are greater than, but local to, μ_0), and solve for a corresponding series of periodic solutions of (3.9) and their monodromy matrices using the numerical method presented. In each case, μ is a fixed parameter.

For applying the numerical procedure, following information is needed:

(1) the vector field **f**;

(2) the Jacobian matrix J of **f**;

(3) the initial guess of $\mathbf{s}_0$ and T_0,

(4) a phase condition by following (3.24)

For the SMIB power system, **f** is given by (3.9), and the Jacobian of **f** is presented in Appendix C. The initial guess of **s** as shown in the following was found to be able to lead to good convergence:

$$s_0 = x_e + \varepsilon x_e$$

where the subscript "e" indicates the equilibrium of the system, and ε is a small real number.

The initial guess T_0 is taken to be the period corresponding to the shaft mode 3 in the eigenvalue analysis at $\mu = \mu_0$.

For fixing a phase condition by (3.24), select an initial value of the generator speed to be 1.01 p.u. for the studied cases, which was observed to be appropriate.

The results of the numerical solutions can be presented by a bifurcation diagram [29, 30], which contains a plot of μ versus a scalar measure [**x**] of the periodic oscillations of (3.9). For a periodic oscillation **x**(t) with period T, a scalar measure of **x**(t) can be defined as [30]:

$$[\mathbf{x}] = \text{maximum and minimum values of } x_k(t)$$

for $0 \le t \le T$, and any k, such that $1 \le k \le n$.

In this study, k is selected such that x_k is the state variable representing the generator rotor angle, or speed.

It was observed that the modulus of a pair of complex characteristic multipliers of the monodromy matrix M crosses the unit circle at a series compensation level μ_p between 63.8% and 64%. The rest of the multipliers of M were observed to remain in the unit circle for series compensation levels between 61.85% and 64.50%. Table 3.5 shows the modulus of the complex pair and the unit multiplier of M at several series compensation levels. The result indicates that at the series compensation level $\mu = \mu_p$, the bifurcated periodic orbits in the Hopf bifurcation changes from stable to unstable.

Table 3.5 Multipliers of the monodromy matrix M

μ	A	B
0.620	1.0000	0.8161
0.630	1.0000	0.9225
0.635	1.0000	0.9751
0.638	1.0000	0.9969
0.640	1.0000	1.0094
0.645	1.0000	1.0378

μ - series compensation level;
A - unit multiplier of M; B - modulus of the complex pair

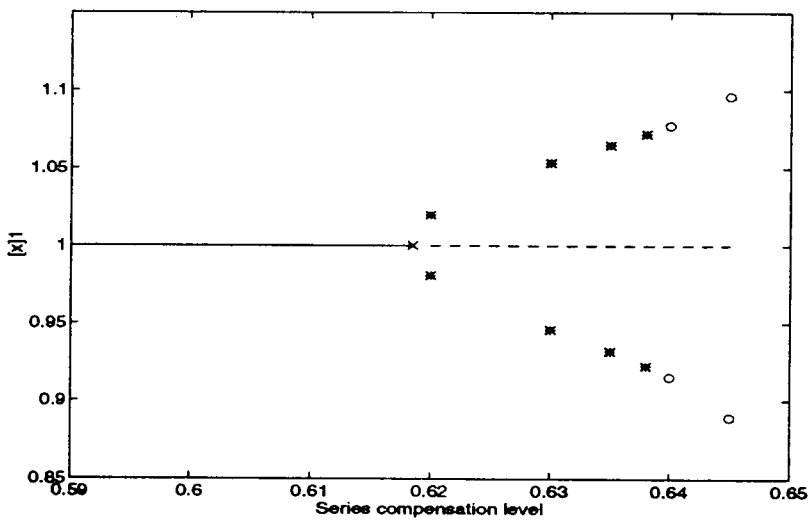

(a)

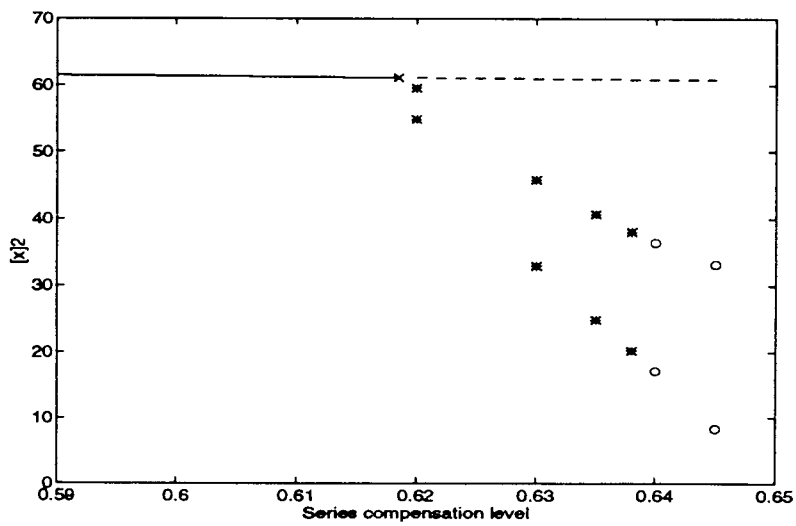

(b)

Fig.3.10 The bifurcation diagrams
[x]1 = maximum and minimum of the generator rotor speed within a period; [x]2 = maximum and minimum of the generator rotor angle within a period
"*" indicates stable periodic orbits; "o" indicates unstable periodic orbits;
"___" indicates stable equilibria; "---" indicates unstable equilibria; "x" indicates bifurcation point

Figures 3.10(a) and (b) show the resulting bifurcation diagrams at the compensation levels. Figure 3.10(a) shows the diagram in which the generator rotor speed is used for measuring the periodic oscillations; Figure 3.10(b) uses generator rotor angle. It can be observed that with increasing μ (locally to μ_0), the stable periodic oscillations become larger. And at a particular value of $\mu = \mu_p$ between 63.8% and 64.0%, the periodic oscillations become unstable. The region of the series compensation levels within which the periodic orbits are stable, and beyond which they are unstable in the Hopf bifurcation is shown clearly in the bifurcation diagrams.

It also can be observed, from Fig 3.10(b), that the center of the periodic orbits of the generator rotor angle deviates from its equilibrium values obviously, which matches the nonlinear simulation results shown in section 3.6 (see Figs 3.8 and 3.9).

Table 3.6 Periods of the periodic orbits in the Hopf bifurcation

μ	T (seconds)
0.620	0.03484
0.630	0.03490
0.635	0.03492
0.638	0.03493
0.640	0.03494
0.645	0.03496

μ - series compensation level; T - period

Table 3.6 shows the orbit periods at the series compensation levels considered. It is seen that the periods are close to that of shaft mode 3 in the eigenvalue analysis at $\mu = \mu_0$, i.e., 0.0348 second (= 2π / 180.39 rad/sec).

The numerical analysis predicts stable periodic orbits for the series compensation level μ greater than, but local to, μ_0. The results match those presented in section 3.6 for the analytical method. As illustrated, the analysis technique can yield the particular value

μ_p of series compensation level, at which the periodic orbits in the Hopf bifurcation change from stable to unstable. It also results in numerical solutions of periodic orbits.

Depending on how the characteristic multiplier(s) of the monodromy matrix for a periodic orbit crosses the unit circle, there are different kinds of unstable behavior. In particular, when [28, 29, 30, 51] (1) a multiplier crosses the unit circle along the positive real axis, then two periodic orbits may bifurcate from the unstable periodic orbit; (2) a multiplier crosses the unit circle along the negative real axis, then a period doubling may bifurcate from the unstable periodic orbit; (3) a pair of complex multipliers crosses the unit circle with the imaginary part of the multipliers different from zero, then a torus may bifurcate from the unstable periodic orbit. And it is known that all three routes may lead to chaotic behavior in the system [28, 29, 30, 51].

For the Hopf bifurcation in the SMIB power system, it was observed that a pair of complex multipliers crosses the unit circle at μ_p. This indicates that tori will bifurcate from the unstable periodic orbits when the series compensation level increases through μ_p.

More detailed studies on the bifurcations from the non-hyperbolic periodic orbits and chaotic behaviors in the system are out of scope of this thesis, since there does not seem to be rather complete theory for analyzing strange attractors (observable chaotic behavior) for a general high dimensional nonlinear system. In the following, a simulation result at a series compensation level of 64.0% (greater than μ_p) is shown in Fig 3.11. It is shown that the stable periodic oscillations no longer exist at the compensation level, and the system response demonstrates 2-torus [51] behavior . It is also shown that the system response is unstable, which indicates that the bifurcated torus is unstable at the given compensation level.

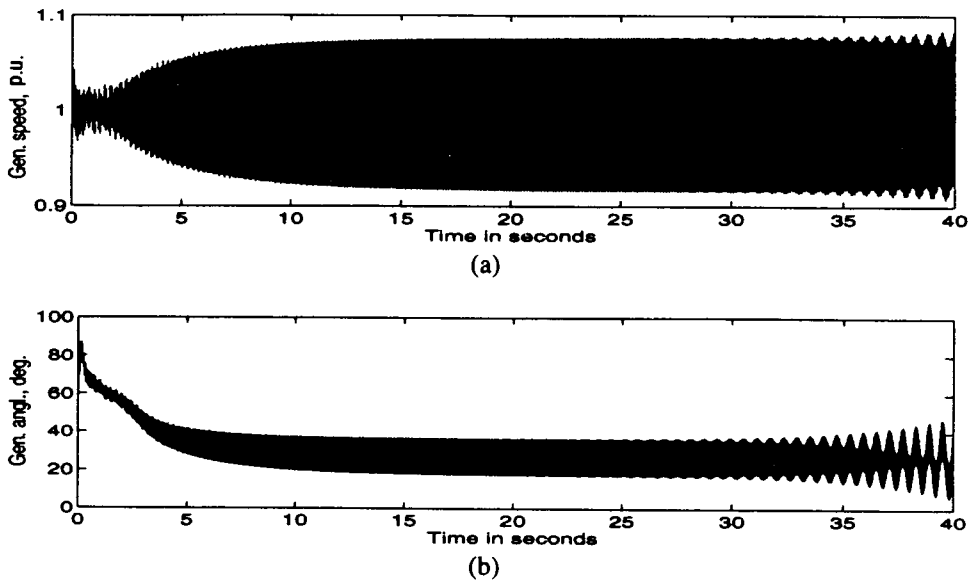

Fig.3.11 System response after a 1% initial disturbance in generator rotor speed at series compensation level of 64.0%

3.8 Conclusion

In this chapter, it has been shown that the limited oscillation behavior in a certain class of SSR problems (i.e., only one of the system modes becomes unstable while varying the series compensation level) can be explained by Hopf bifurcations. This has been analyzed for a SMIB power system with series capacitor compensation, which models the BOARDMAN generator with respect to the rest of the NWAPS. The model used for the analysis is represented by a 15th-order set of differential equations. A Hopf bifurcation at a series compensation level of 61.85% is predicted by applying the Hopf bifurcation theorem, and the stability of the bifurcated periodic orbits is analyzed by applying the same theory. The stability of the bifurcated periodic orbits has also been analyzed by a numerical method, the essence of which is solving a two-point boundary value problem. Stable periodic orbits in the Hopf bifurcation at series compensation levels greater than, but local to, the bifurcation value $\mu_0 = 61.85\%$ are predicted by both the analytical and the numerical study. Both results match those of the detailed nonlinear

simulations. Compared with the analytical method, the numerical method is less complicated to implement. In addition, it can result in more information about the bifurcated periodic orbits, e.g., a particular series compensation level value μ_p, at which the bifurcated periodic orbits change from stable to unstable, and numerical solutions of the periodic orbits.

Chapter IV
An EMTP Study of SSR Mitigation Effects Provided by the Thyristor Controlled Series Capacitor Operated in Vernier Mode

4.1 Introduction

The Thyristor Controlled Series Capacitor (TCSC) is one of the FACTS (flexible AC Transmission Systems) devices, which has received a lot of interest. It is known that series capacitor compensation benefits power systems in more than one way, such as enhancing transient stability limits, increasing power transfer capability, etc.[1]. It is also known that fixed series capacitor compensation may cause Subsynchronous Resonance (SSR) in steam-turbine power systems, which can lead to severe problems, such as damage to the machine shaft[1]. However, it has been noted that the newly developed Thyristor Controlled Series Compensation (TCSC) operated in vernier mode benefits the mitigation of SSR[40,41]. This is among several TCSC benefits which include higher transient stability limits compared to fixed series compensation, flexible load flow control, and control of loop flows[40, 41]. A detailed simulation study of the SSR mitigation effect of TCSC vernier operation, compared with fixed series compensation case is necessary for each application. Also, it is desirable to base the simulation on realistic power system models and to use standard power system simulation programs, such as EMTP. Moreover, analytic techniques to integrate and explain the underlying characteristics are needed. Assuming slow dynamics of SSR, one approximate method of analyzing the mitigation effect is to view the TCSC as an electrical element in the power system and study the frequency domain characteristics of the equivalent TCSC impedance for a typical level of excitation. In this chapter, the studies as mentioned are presented. The studies focus on the SSR mitigation effect of TCSC vernier operation compared with fixed series compensation. This phenomenon has been observed repeatedly in our simulation studies, and is supported by previous studies[40]. A field test

of the TCSC device installed[41] is currently being planned by the Bonneville Power Administration (BPA) with a view to assessing TCSC performance of SSR mitigation.

The analysis of SSR mitigation effects provided by the TCSC presented in this chapter is based on EMTP simulation studies. It is expected that satisfactory theoretical explanations of the beneficial effect follow the exploratory studies presented in this chapter, as well as in previous documents [40, 42].

4.2 Model Considerations

The simulation studies discussed are based on a model representing the 500kV-level network of the North-Western American Power System (NWAPS) and use the standard EMTP.

A diagram of the power system model used is shown in Fig 4.1. The TCSC is installed between SLATT and BUCKLEY. It has been noted that when the generator at BOARDMAN, shown in Fig 4.1, is radialized to BUCKLEY and beyond, the generator is most vulnerable to the excitation of SSR at one or more of its shaft modes through the effect of the SLATT series compensation and the fixed series compensation beyond GRIZZLY in the NWAPS. Thus, in the model used, the BOARDMAN generator is modelled in detail by a system of differential equations while the remaining 21 generators are modelled by voltage sources. The BOARDMAN generator is radialized to BUCKLEY and beyond by operating the breakers at SLATT and GRIZZLY. Both transient and subtransient electrical sub-system dynamics of the BOARDMAN generator are represented. Five masses, namely, mass #1 through mass #5, are mounted on the shaft of the generator. Masses #1 through #5 represents high-pressure turbine, low-pressure-1

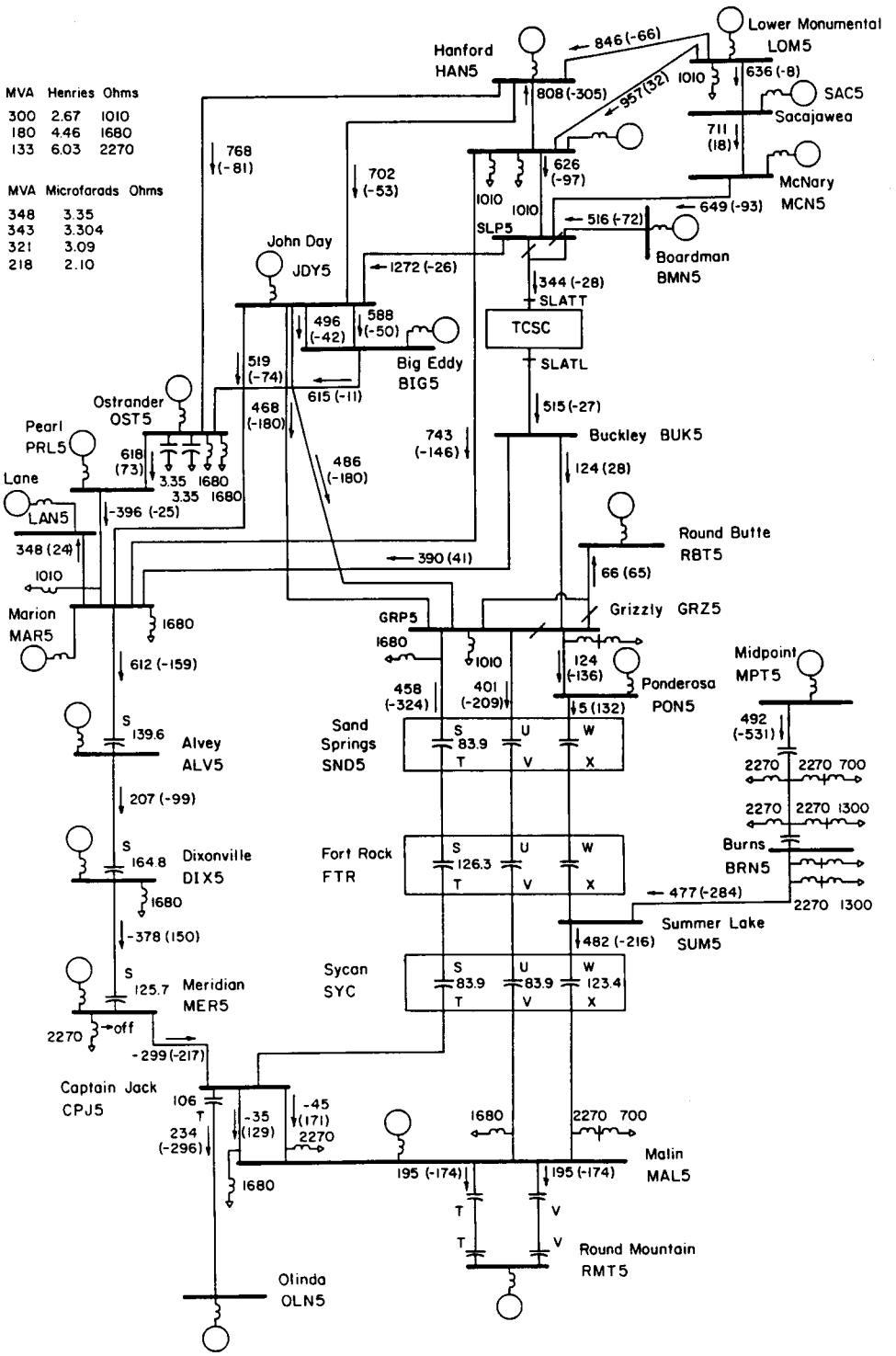

Fig.4.1 NWAPS model used in the SSR simulation study

turbine, lower-pressure-2 turbine, generator, and exciter, respectively. The mechanical damping values used represent nominal values. The BOARDMAN generator field tests are needed to establish actual damping constants. In addition to a 2.2 Hz local *swing mode*, the BOARDMAN generator has the following 4 shaft modes:

mode 1 - 12.5 Hz; *mode 2* - 25.0 Hz;
mode 3 - 29.0 Hz; *mode 4* - 50.0 Hz

The transmission lines are described by distributed parameters, while the fixed series compensation installations in the system are modelled accordingly. The load flow of the system is regulated such that it represents the heavy load condition of the NWAPS. The real and imaginary power output of the BOARDMAN generator is 540MW and - 62MVar, respectively.

The simplified TCSC model used in this study is simulated using the "MODELS" feature of EMTP, which is loosely patterned after the TCSC model developed at Clarkson University under EPRI sponsorship. An earlier version of the model was used in [52, 53]. Details regarding the EMTP implementation of the TCSC are shown in Appendix D. As shown in Fig 4.2, the TCSC model used in this study is represented by an 8 ohm equivalent internal capacitor, in parallel with antiparallel thyristor switches and commutation inductance. The actual SLATT TCSC consists of six segments of 1.33 ohms each. Also provided is a bypass breaker, as shown in Fig 4.2. The TCSC can be operated in three basic modes. In the bypassed mode, the thyristor path is conducting continuously, short circuiting the capacitor. In the blocked mode, the thyristor path is blocked continuously, which is equivalent to fixed series compensation at the capacitor reactance, i.e., 8 ohms in this study. Finally, in the vernier mode, the thyristor path is partially conducting to achieve a specified ohms order. In the vernier mode, partial

thyristor firing results in a loop current flowing through the inductor in the opposite direction of the internal capacitor current[54, 55], as shown in Fig 4.2. This loop current results in an increase of the equivalent TCSC impedance over the internal capacitor reactance with respect to synchronous frequency. The term "ohms order", or "Xorder" is used to describe the series compensation capability of the TCSC [54, 42]. In this study it is defined as the ratio of the 60 Hz equivalent TCSC impedance to the internal capacitor reactance, i.e., 8 ohms in this study, under steady-state operating conditions. The larger the Xorder, the higher the series compensation level with respect to synchronous frequency in the steady state. Achievable Xorder values are limited by a number of practical considerations [54], mainly thyristor current rating considerations. This study considers Xorder values between 1.0 p.u. and 3.0 p.u., with a base value equal to the internal capacitor reactance, i.e., 8 ohms.

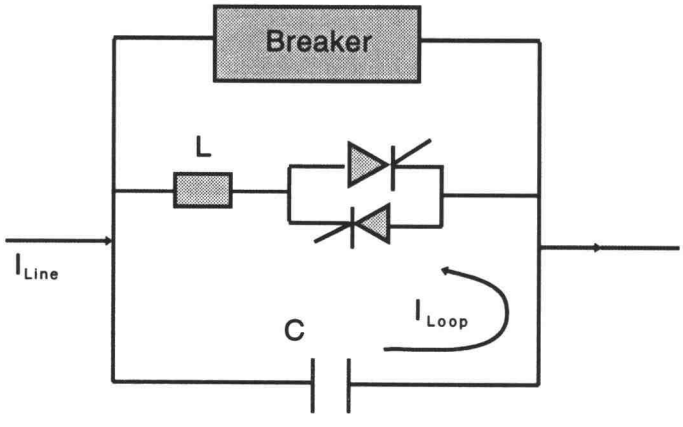

Fig.4.2 The TCSC model

4.3 Simulation Results

In this section, simulation results for three different cases are presented along with the effect of TCSC Xorder control. Post-disturbance system responses with the TCSC in vernier mode are compared with system performances using fixed series compensation.

Case I

A disturbance is applied by switching in the series compensation initially. The operational scenario is as follows:

In the case of the TCSC,

At t = 0-, TCSC is bypassed;

At t = 0+, TCSC is switched into vernier mode,

and in the case of the fixed series compensation,

At t = 0-, TCSC is bypassed;

At t = 0+, TCSC is blocked.

Figures 4.3 through 4.6 show the speed responses of the BOARDMAN generator shaft elements after the disturbance. Figure 4.3 shows the post-disturbance system response with 8 ohms fixed compensation. It can be seen that SSR at shaft mode 4 (50.0 Hz) is dominantly excited after the disturbance, as shown in the mass #4 and #5 speed responses. Also, oscillation at shaft mode 1 (12.5 Hz) can be observed in the mass #1 and mass #2 speed responses, and oscillation at shaft mode 2 (25.0 Hz) can be observed in the mass #3 speed response. Figures 4.4 through 4.6 show the post-disturbance speed responses with the TCSC at Xorder values of 1.5, 2.0, and 3.0 p.u., respectively. It is shown that with TCSC vernier operation at the studied Xorder values, the amplitude of

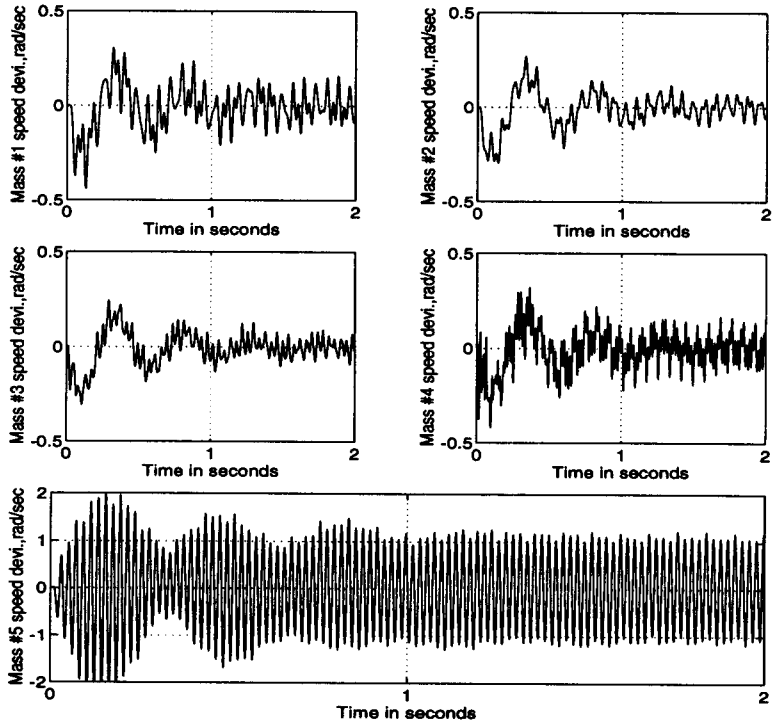

Fig.4.3 Post-disturbance system response, 8 ohms fixed compensation

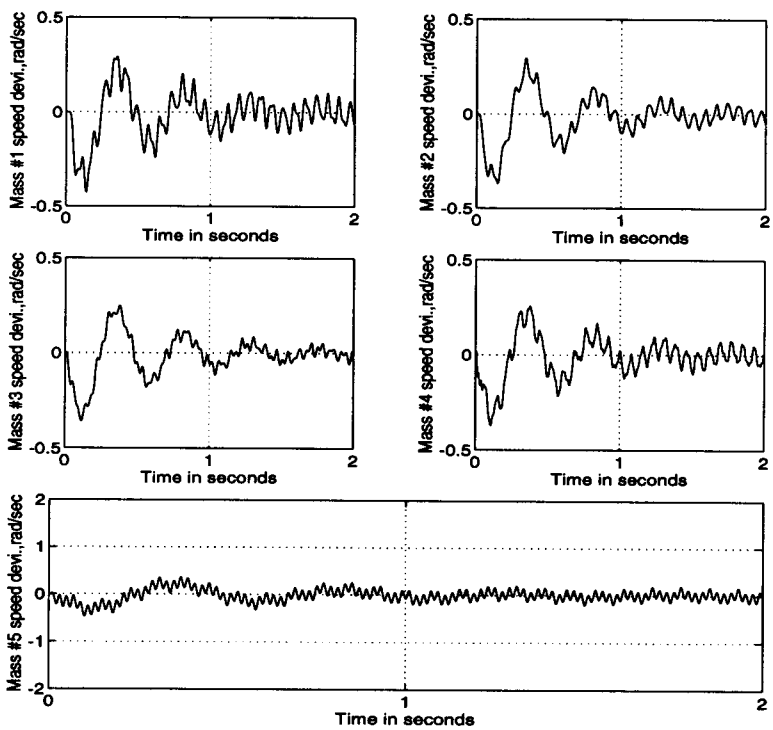

Fig.4.4 Post-disturbance system response, Xorder = 1.5 p.u.

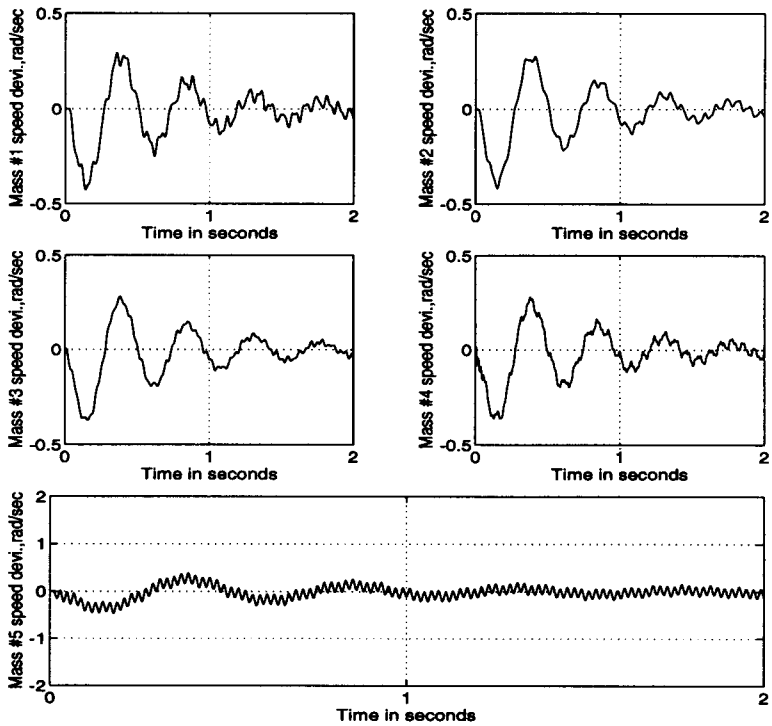

Fig.4.5 Post-disturbance system response, Xorder = 2.0 p.u.

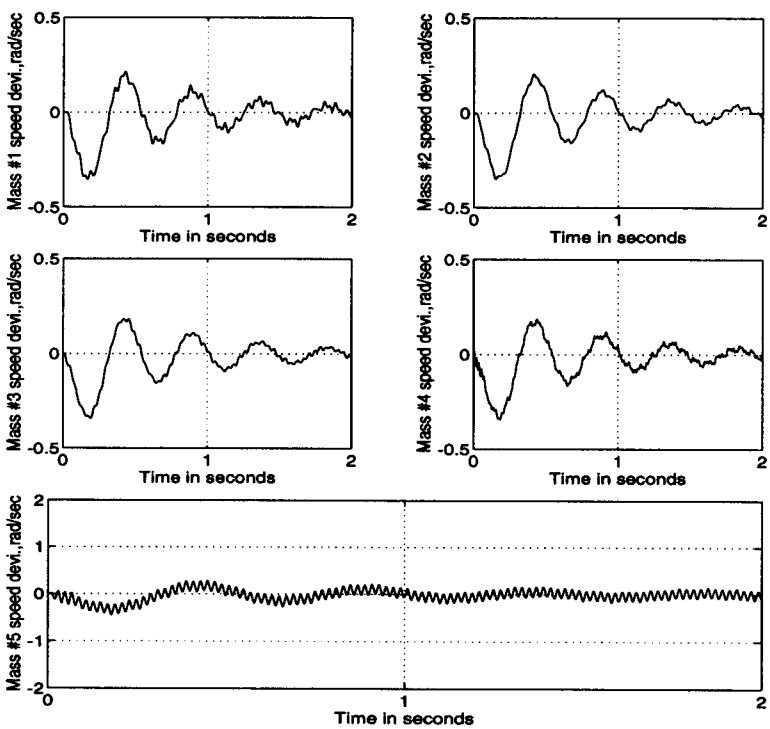

Fig.4.6 Post-disturbance system response, Xorder = 3.0 p.u.

the dominant shaft mode 4 oscillation is reduced significantly compared with the fixed compensation. This can be explained by the changes in network characteristics due to TCSC vernier control, which affect system SSR modes. Figures 4.4 through 4.6 also show that shaft mode 1 and 2 oscillations are better mitigated with increasing Xorder, as seen by comparing the mass #1 through mass #4 speed responses in the figures.

Figures 4.7 through 4.9 show the electrical responses of the system after the disturbance. Figure 4.7 shows the blocked TCSC (which is equivalent to 8 ohms fixed compensation) voltage of the system, after the disturbance. The electrical oscillation due to the interaction between the electrical and mechanical subsystems after the disturbance can be seen clearly from the response during the first 0.5 second simulation time. Figures 4.8(a), (b), and (c) show the TCSC voltage of the system with the Xorder of 1.5, 2.0, and 3.0 p.u., respectively. The increase of the TCSC voltage reflects the increase of Xorder. It is shown that the electrical oscillation is well mitigated in the cases of the TCSC vernier operation, in contrast to the case of the fixed series compensation. Figure 4.9 shows the thyristor currents when TCSC is in vernier mode at the studied Xorder values.

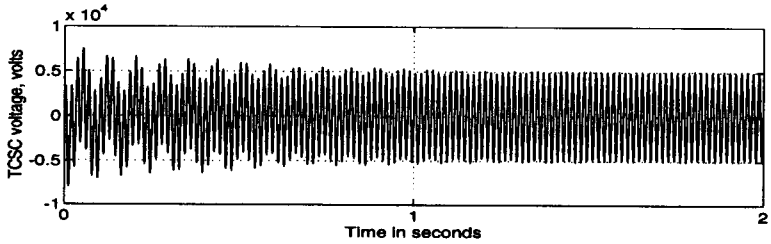

Fig.4.7 Post-disturbance system response, 8 ohms fixed compensation

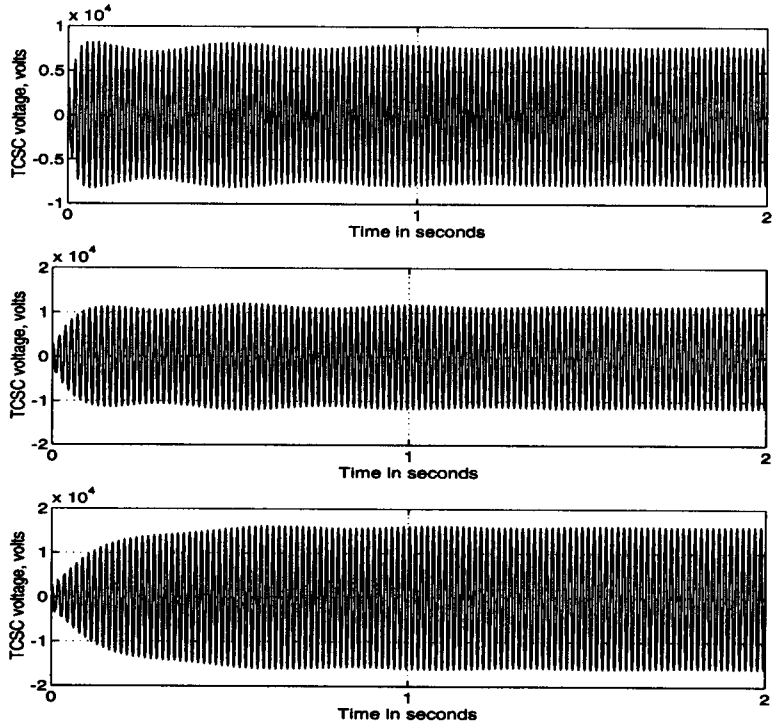

Fig.4.8 Post-disturbance system responses
(a) Xorder = 1.5 (upper plot), (b) Xorder = 2.0 p.u. (middle plot)
(c) Xorder = 3.0 p.u. (lower plot)

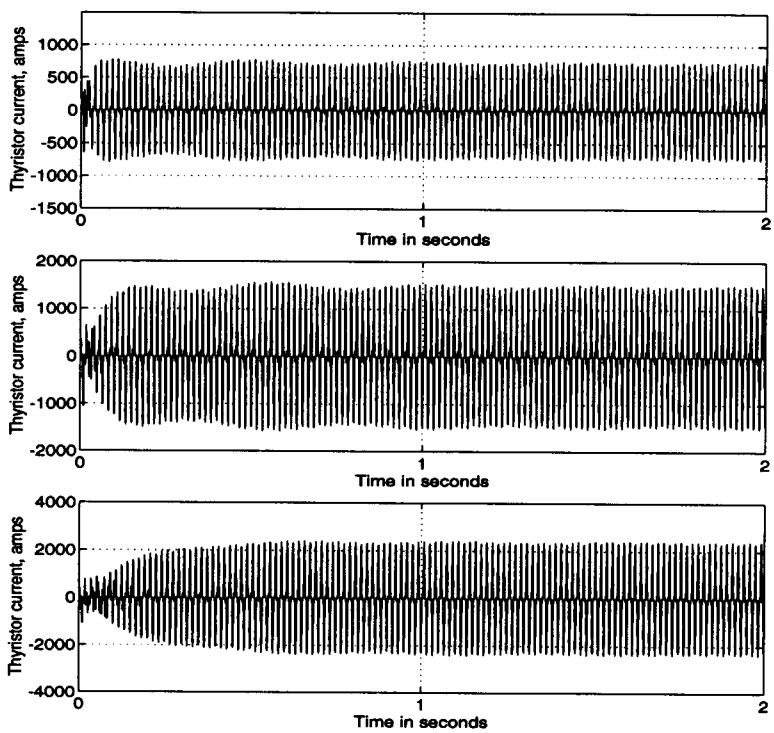

Fig.4.9 Post-disturbance system responses
(a) Xorder = 1.5 p.u. (upper plot), (b) Xorder = 2.0 p.u. (middle plot)
(c) Xorder = 3.0 p.u. (lower plot)

Case II

In this simulation, the *Case I* disturbance is enlarged by switching out a small shunt impedance branch at SLATT initially. The operation scenario is as follows:

At t = 0-, TCSC is bypassed and the shunt branch at SLATT is in the system;

At t = 0+, TCSC is either blocked (in the case of fixed compensation), or switched into vernier mode; and the shunt branch is switched out of the system.

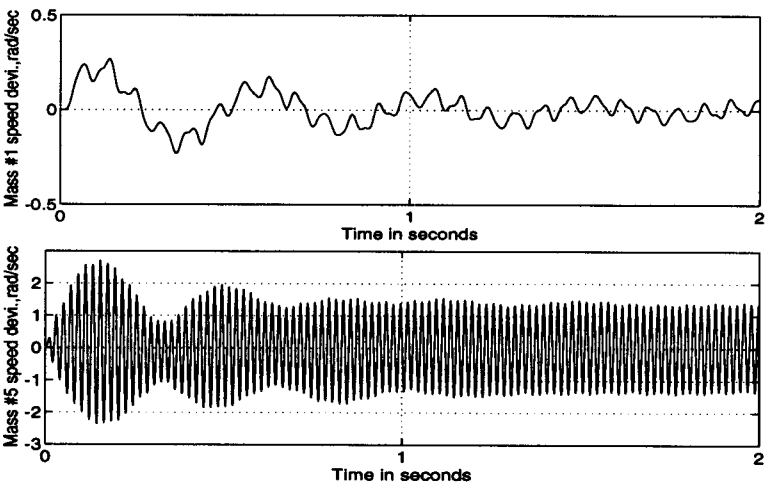

Fig.4.10 Post-disturbance system response, 8 ohms fixed compensation

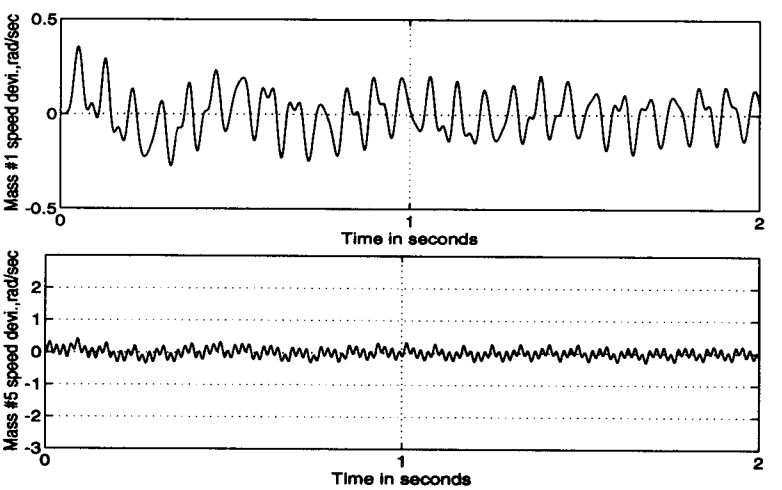

Fig.4.11 Post-disturbance system response, Xorder = 1.5 p.u.

As in *Case I*, shaft mode 4 is dominantly excited, which can be seen from the mass #5 speed response in Fig 4.10. Oscillation at shaft mode 1 can also be observed, as shown in the mass #1 speed response in Fig 4.10. Figure 4.11 shows the system response with a TCSC Xorder value of 1.5 p.u.. It can be seen that compared with fixed series compensation, TCSC vernier control provides significant mitigation of the shaft mode 4 oscillations. However, although the magnitudes of shaft mode 1 oscillations for both fixed compensation and TCSC vernier operation, the oscillation is notably more active in the latter case, as seen by comparing the mass #1 speed responses shown in Figs 4.10 and 4.11. Further investigation of the cause of this phenomenon is needed.

Case III

In this simulation, a 4 ohm internal capacitor reactance and an Xorder value of 2.0 p.u. are considered. Thus, there is an 8 ohm TCSC effective reactance. The fault scenario is as follows:

At t = 0-, TCSC is bypassed;

At t = 0+, TCSC (with an Xorder value of 2.0 p.u.) is switched into vernier mode

In this case, the shaft mode 4 oscillation is dominantly excited with 4 ohms fixed compensation, as shown in mass #3, #4 and #5 speed responses in Fig 4.12. Comparing Fig 4.12 with Fig 4.3 (in *case I*), it can be observed that the shaft mode 4 is excited much more severely in the case of 4 ohms fixed compensation than 8 ohms fixed compensation. Fig 4.13 shows the system response with a TCSC Xorder value of 2.0 p.u.. It is shown that using the TCSC vernier control, oscillations at the dominant shaft mode 4 is well mitigated compared with 4 ohms fixed compensation. Also, comparing Fig 4.13 with Fig 4.3 (in *case I*), it is shown that the dominant shaft mode 4 oscillation is significantly reduced in this case of TCSC vernier operation, compared with the case of 8

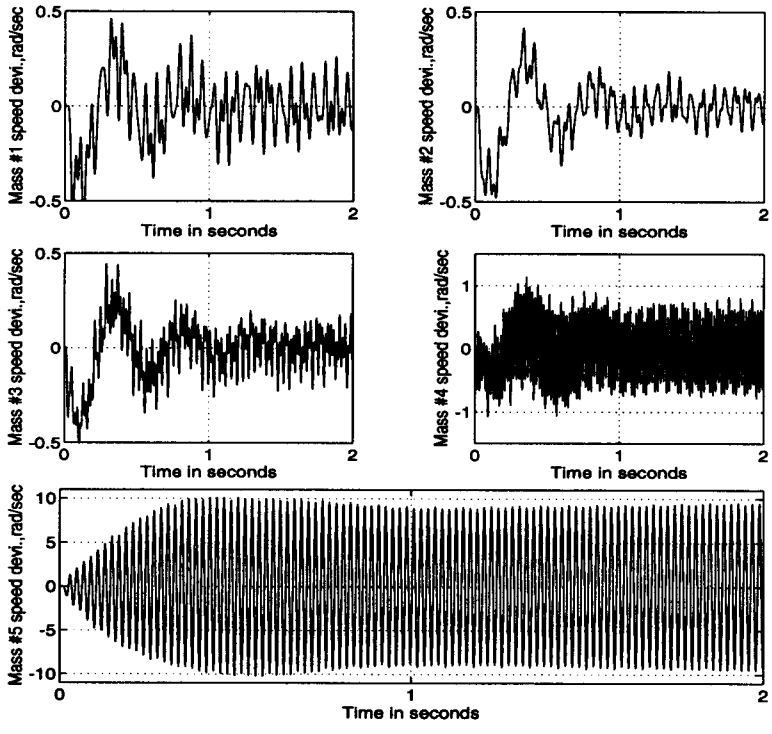

Fig.4.12 Post-disturbance system response, 4 ohms fixed compensation

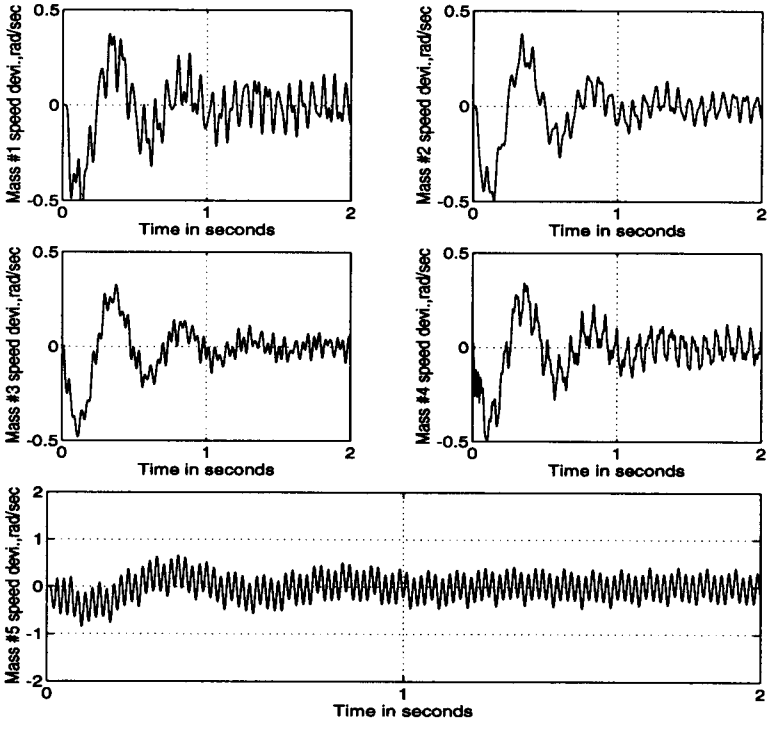

Fig.4.13 Post-disturbance system response, Xorder = 2.0 p.u., 4 ohms base

ohms fixed compensation. It is also shown that oscillations at shaft mode 1 and 2 remain small in this case of TCSC vernier operation, as in the case of 8 ohms fixed compensation. It can be seen that using TCSC vernier control, an effective 8 ohms series compensation can be achieved while significantly reducing the shaft mode 4 oscillations which is dominantly excited in the case of 8 ohms fixed compensation, without worsening small oscillations at other shaft modes.

4.4 Frequency Domain Study of the Equivalent Impedance of TCSC

An analysis of the equivalent TCSC impedance can offer an explanation for the effectiveness of the TCSC at different oscillation frequencies. In the following, the frequency domain characteristics of the equivalent TCSC impedance using a 1.33 ohm internal capacitive reactance (one segment at SLATT) is presented.

A network including the TCSC in series with the network impedance and voltage sources at both synchronous and subsynchronous frequency is simulated in EMTP. The relationship between the voltage across the TCSC and the current through the TCSC at synchronous frequency and at different subsynchronous frequencies can be studied to determine the equivalent frequency-dependent TCSC impedance. The network for the simulation is shown in Fig 4.14, where the magnitudes of the subsynchronous voltage sources are chosen to be much smaller than the magnitude of the synchronous voltage source.

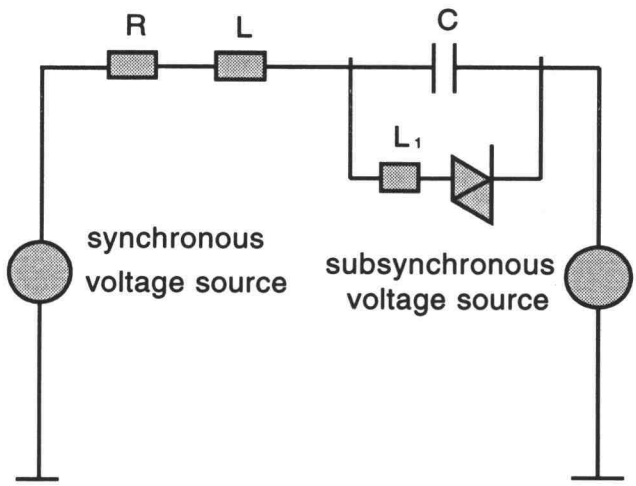

Fig.4.14 Network for the simulation study of the TCSC equivalent impedance

As an example, voltage sources at frequencies of 60 Hz and 10 Hz are considered with a thyristor conduction time of 70 electrical degrees per half cycle. The simulated TCSC voltage is shown in Fig 4.15, with the corresponding square root of the Power Density Spectrum (PDS) characteristic illustrated in Fig 4.16. It can be seen that the two main frequency components of the response are at 60 Hz and 10 Hz. Similarly, the TCSC current, which is equal to the line current, has the two main frequency components at 60 Hz and 10 Hz. The filtered 60 Hz and 10 Hz components are shown in Fig 4.17, where a Chebychev second-order filter was used. This analysis can be done conveniently using design packages, such as MATLAB. From the magnitude and phase angle relationship between voltage and current at a given frequency, the equivalent TCSC impedance at these frequencies for the excitation level used can be obtained. In this case, the equivalent TCSC impedances at 60 Hz and 10 Hz are $1.65\angle -90.0°$ ohms and $3.40\angle -8.5°$ ohms, respectively. The Xorder is 1.2 (=1.65/1.33) p.u., with a base value equal to the internal capacitor reactance, i.e., 1.33 ohms in this case.

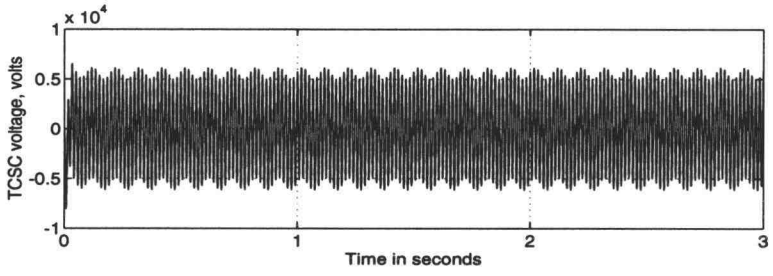

Fig.4.15 The simulated TCSC voltage

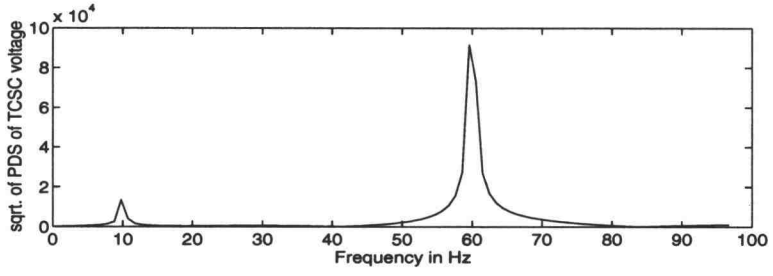

Fig.4.16 The square root(sqrt.) of the Power Density Spectrum (PDS) of the simulated TCSC voltage

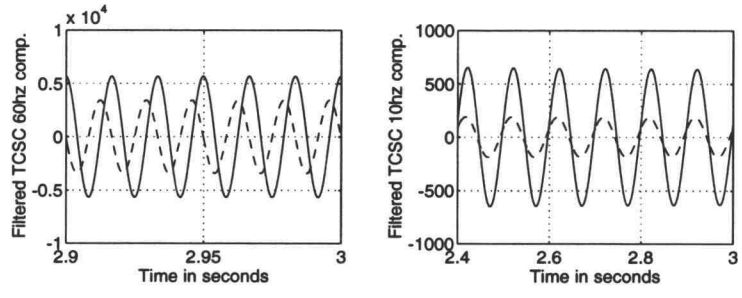

Fig.4.17 Filtered frequency components of the system responses
__ voltage in volts, --- current in amps

Based on the simulation studies and the analysis procedure illustrated, values of the equivalent TCSC impedance for different frequencies and Xorder values are obtained. Fig 4.18 shows the resulting real and imaginary parts of the equivalent TCSC impedance. It can be seen that for the studied values of Xorder, the equivalent TCSC impedance has negative(capacitive) imaginary parts and positive (resistive) real parts, with respect to subsynchronous and synchronous frequencies. Thus, if the TCSC is viewed as an electrical element, it can be represented as a resistor in series with a capacitor as follows:

$$Z_e(\omega) = R_e(\omega) + jX_e(\omega),$$

where the subscript "e" stands for "equivalent", and $R_e \geq 0$, $X_e < 0$.

Figure 4.18(a) shows that $R_e(\omega)$ tends towards zero at synchronous frequency for any studied Xorder. Figure 4.18(b) shows that the equivalent TCSC reactance at synchronous frequency is enlarged over the internal capacitor reactance, which reflects the increased series compensation capability. Thus, it can be reasoned that with respect to synchronous frequency, the TCSC in vernier mode behaves as a lossy capacitor in an average sense.

Figure 4.18(a) shows that $R_e(\omega)$ is nonzero and positive with respect to subsynchronous frequencies for any studied Xorder. Consequently, the TCSC provides resistive damping to SSR. Fig 4.18(b) shows that for any studied Xorder, the frequency domain characteristic of $X_e(\omega)$ deviates from that of the TCSC internal capacitor reactance with respect to subsynchronous frequencies, as well as with respect to synchronous frequency. Thus, the TCSC operated in vernier mode avoids a resonant condition by changing the capacitive reactance at SSR frequencies and by introducing equivalent resistive damping.

Figure 4.18 shows that for a given Xorder value, the value of $R_e(\omega)$ is somewhat larger and the deviation of $X_e(\omega)$ from the internal capacitor reactance is somewhat more significant at lower network frequencies. Since the electrical frequencies of SSR are the complementary frequencies of the shaft modes[1, 2], it can be reasoned that the SSR mitigation effect of TCSC vernier operation may be more significant with respect to higher frequency shaft modes, e.g., shaft mode 4 of 50.0 Hz in the studied system. Note further that for network frequencies between 28 and 60 Hz, the value of $R_e(\omega)$ increases as Xorder is increased, as shown in Fig 4.18(a). This may indicate that higher Xorder

introduces a larger effective resistance at relatively low shaft mode frequencies (high network frequencies), e.g., at shaft mode 1 of 12.5 Hz.

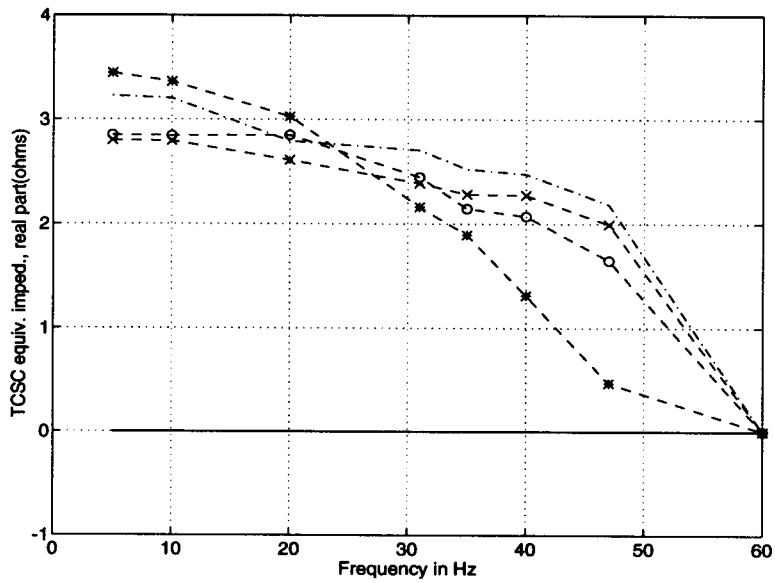

(a)

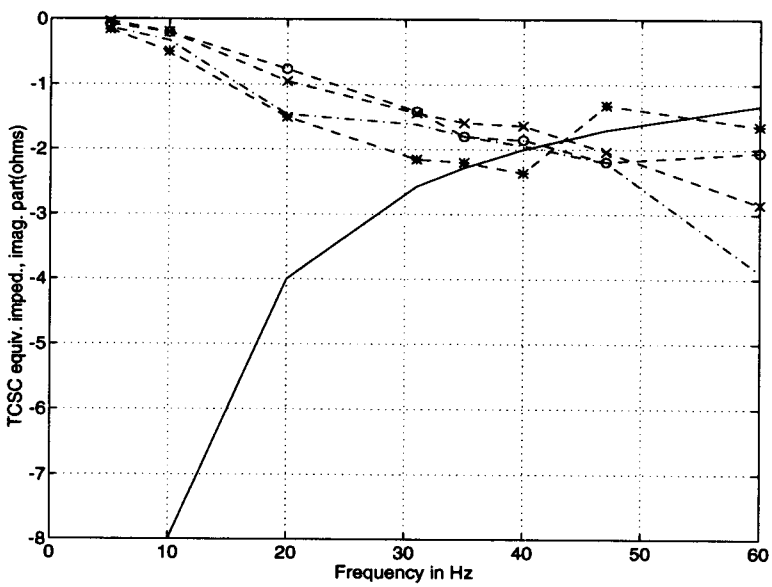

(b)

Fig.4.18 Frequency domain characteristics of the real part & imaginary part of the TCSC equivalent impedance

———	TCSC internal capacitor
--*--	Xorder = 1.2
--o--	Xorder = 1.5
--x--	Xorder = 2.1
-.-.-.-.	Xorder = 2.9

4.5 Conclusion

An exploratory simulation study of SSR mitigation effects due to TCSC vernier operation has been performed using a model of the NWAPS and the standard EMTP simulation program. The frequency domain characteristics of the equivalent TCSC impedance obtained based on EMTP simulations has been used to give an explanation of the issues involved. It is shown that TCSC vernier operation provides significant mitigation of the 50 Hz shaft mode which is dominantly excited with fixed series compensation.

The equivalent TCSC impedance study shows that the TCSC in vernier mode no longer behaves as a pure capacitor in an average sense with respect to subsynchronous frequencies for the studied values of Xorders. TCSC vernier operation may benefit SSR mitigation in two aspects. One is that vernier control provides equivalent resistive damping to subsynchronous oscillations, and the other is that the equivalent TCSC reactance in vernier mode deviates from the internal capacitor reactance with respect to subsynchronous frequencies, as well as at synchronous frequency. These effects lead to a change of the system characteristics and suppression of SSR.

The frequency domain analysis also shows that the SSR mitigation effects due to TCSC vernier operation may change with the dominant SSR frequencies. Both the simulation study (*Case I*) and the equivalent TCSC impedance consideration suggest that with respect to SSR at shaft modes of relatively low frequencies (e.g., shaft mode 1 of 12.5 Hz in the studied system), the TCSC SSR mitigation effect increases with increasing Xorder. Small values of Xorders can provide good mitigation of SSR at shaft modes of relatively high frequencies, e.g., shaft mode 4 of 50.0 Hz in the studied system.

As in any dynamic system studies, the results of the simulation studies presented can be influenced by a number of factors, such as system configuration, system parameters, TCSC operating conditions, etc. Thus, the conclusions presented are related to the specified problems studied and should not be taken out of context. Additional investigations are needed to account for the larger mode 1 amplitude with TCSC control (Fig 4.11). Moreover, the analysis of TCSC SSR mitigation effects, as presented in this chapter, is based on EMTP simulations. Further theoretical analysis is needed to verify the relationships suggested.

Chapter V
Conclusions

Subsynchronous Resonance (SSR) problems in series compensated power systems co-exist with the beneficial effects provided by series capacitors. Since early 1930s, numerous researchers have addressed issues relating to these problems.

Linear analysis of SSR has provided a fundamental understanding of the phenomenon, along with system parameters and operation conditions which are critical to excitation of SSR. Eigen-based methods and frequency domain techniques are two main linear methods of SSR analysis. Among the frequency domain techniques, there are two main categories. The techniques in the first category derive equivalent circuits for evaluating induction generator effects, and strictly follow the principles of analyzing electrical damping torque coefficient as related to torsional interactions. Extensive work on developing these techniques started in 1970s; and the investigations seem to have been concluded in 1982 [4]. The second frequency domain technique was proposed by Canay in 1982 [20, 21]. It only addresses analysis of torsional interactions, and does not strictly follow the principles of analyzing electrical damping torque coefficients. While the technique has some advantages (e.g., yielding analysis over a range of frequencies including vicinities of shaft modes, which enables a closer study of the danger of torsional interactions) over those in the first category, problems are apparent as pointed out in chapter 2 of this thesis. Maturity in the field of linear SSR analysis is evident in the literature in 1982 [4, 20, 21]. Since then, publications on the subject are scarce. Problems relating to the second frequency domain technique seem to have been neglected by researchers previous of this dissertation.

In chapter II, these problems are pointed out and analyzed in detail. The development of a generalized frequency scan method is presented, which overcomes the

shortcomings of the original technique, while maintaining its unique advantages. The new method is developed for a SMIB power system. Future work is needed to extend the results to multimachine power systems, which will significantly enhance the usefulness of the proposed technique.

Nonlinear analysis of SSR has been reported since the late 1980s. Perturbation methods have been used as a main tool for analyzing several dynamic phenomena in power systems with SSR. Among the nonlinear dynamic phenomena analyzed is Hopf bifurcation. Since perturbation methods for high dimensional systems are either extremely complicated, or even impossible, published results have been restricted mostly to second-order power system models.

It is noted that since the theory of Hopf bifurcation analysis in high dimensional systems is available, its application may result in more accurate analysis of the phenomenon than possible previously. In chapter III, the Hopf bifurcation phenomenon in a SMIB power system (modelled by a 15th-order set of differential equations) is analyzed by applying a Hopf bifurcation theorem. The stability of the bifurcated periodic orbits in the system is analyzed both analytically, and by a numerical method, the essence of which is solving a two-point boundary value problem. Compared with the analytical approach, the numerical study has several advantages. For example, it can result in a series compensation value (which can not be obtained by the analytical study) greater than, but local to, the bifurcation value, at which the bifurcated periodic orbits in the Hopf bifurcation change from stable to unstable. It can also result in numerical solutions of the periodic orbits, which can not be obtained by the analytical study. Hopf bifurcation analysis is not new in many research fields, as such chemistry, biology, and even the voltage stability problems in power systems. The unique contribution of the study as presented in chapter III of this thesis is the application of these methods to explaining the

Hopf bifurcation phenomenon in a high dimensional SMIB power system with SSR. As presented, the work successfully handles situations of high complexity. It is hoped that the study leads to a more clear and better understanding of the SSR dynamic phenomenon in power systems.

Compared with fixed series capacitors in power systems, Thyristor Controlled Series Compensation (TCSC) has several advantages, such as increasing the dynamic and transient stability limits to higher levels, controlling load flows more flexibly and controlling loop flows. It has been noticed that vernier mode operation of TCSC contributes to the mitigation of SSR, as demonstrated in [40-43], and in chapter IV of this thesis. The encouraging results have aroused a lot of interest in the power industry, since capacitor based SSR mitigation schemes are generally favored over the generator based methods.

On the other hand, switching operation of TCSC adds nonlinearity and complexity to the power system analysis of SSR and associated problems and mitigation strategies of TCSC vernier control. In chapter IV, the beneficial effect of TCSC vernier control is demonstrated by EMTP simulation studies, and verified via an equivalent impedance method. It is intended that satisfactory theoretical studies of the effect follow the exploring studies as presented in [40-43] and in chapter IV of this dissertation. An EMTP model of the TCSC used is given in appendix D. It is intended to be useful to other interested researchers.

The thesis addresses both linear and nonlinear perspectives of SSR analysis in SMIB power systems equipped with fixed series compensation, and analyzed the phenomenon of SSR mitigation provided by the Thyristor Controlled Series Compensation (TCSC). The EMTP studies presented are based on realistic

representation, such as the North-Western American Power System (NWAPS). The thesis aims at contributing to a better understanding of SSR related problems in power systems.

References

[1] IEEE Committee Report,"Reader's Guide to SSR," *IEEE Transactions on Power Systems*, vol.7, No.2, pp.150-157, February 1992

[2] IEEE Power System Engineering Committee Report, "Terms, Definitions & Symbols for Subsynchronous Oscillations," *IEEE Transactions on PAS*, vol.PAS-104, No.6, pp.1326-1334, June 1985

[3] L.A.Kilgore, D.G.Ramey, M.C.Hall,"Simplified Transmission & Generation System Analysis Procedures for SSR Problems," *IEEE Transactions on PAS*, vol.PAS-96, No.6, pp.1840-1846, Nov./Dec. 1977

[4] T.H.Putnam, D.G.Ramey,"Theory of The Modulated Reactance Solution For SSR," *IEEE Transactions on PAS*, vol.PAS-101. No.6, pp.1527-1535, June 1982

[5] Erwin Kreyszig, "Advanced Engineering Mathematics,", fifth edition, pp.110-111, *Wiley Eastern Limited*, 1985

[6] J.W.Butler, C.Concordia,"Analysis of Series Capacitor Application Problems," *AIEE Transactions*, vol.56, pp.975-988, August 1937

[7] C.Concordia & G.K.Carter,"Negative Damping of Electrical Machinery", *AIEE Transactions*, Vol.60, pp.116-118, March 1941

[8] J. W. Ballance & S. Goldberg, "Subsynchronous Resonance in Series Compensated Transmission Lines," *IEEE Transactions on PAS*, Vol.PAS-92, pp.1649-1658, September/October 1973

[9] IEEE Committee Report,"A Bibliography for the Study of SSR between Rotating Machines & Power Systems," *IEEE Transactions on PAS*, vol. PAS-95, No.1, pp.216-218, January/February 1976

[10] IEEE Committee Report,"First Supplement to a Bibliography for the Study of SSR between Rotating Machines & Power Systems," *IEEE Transactions on PAS*, vol. PAS-98, No.6, pp.1872-1875, Nov./Dec. 1979

[11] IEEE Committee Report,"Second Supplement to a Bibliography for the Study of SSR between Rotating Machines & Power Systems," *IEEE Transactions on PAS*, vol. PAS-104, No.2, pp.321-327, February 1985

[12] IEEE Committee Report,"Third Supplement to a Bibliography for the Study of SSR Between Rotating Machines & Power Systems," *IEEE Transactions on Power Systems*, vol.6, No.2, pp.830-834, May 1991

[13] Homer, M. Rustebakke, Charles Concordia, "Self-Excited Oscillations in a Transmission System Using Series Capacitors," *IEEE Transactions on PAS*, vol. PAS-89, No.7, pp.1504-1512, September/October 1970

[14] L.A. Kilgore, L.C. Elliot, E.R. Taylor, Jr., "The prediction and Control of Self-Excited Oscillations due to Series Capacitors in Power Systems," *IEEE Transactions on PAS*, Vol. PAS-90, No.3, pp.1305-1311, May/June 1971

[15] J.M. Undrill, T.E. Kostyniak, "Subsynchronous Oscillations, Part 1 - Comprehensive System Stability Analysis," *IEEE Transactions on PAS*, Vol. PAS-95, No.4, pp.1446-1455, July/August 1976

[16] J.M. Undrill, T.E. Kostyniak, "Subsynchronous Oscillations, Paer 2 - Shaft System Dynamic Interactions," *IEEE Transactions on PAS*, Vol. PAS-95, No.4, pp.1456-1464, July/August 1976

[17] M.C. Hall, R.L. Daniels, D.G. Ramey, "A New Technique for Subsynchronous Resonance Analysis and an Application to the Kaiparowits System," *IEEE Transactions on PAS*, Vol. PAS-96, No.4, pp.1251-1255, July/August 1977

[18] B.L.Agrawal, R.G.Farmer,"Use of Frequency Scanning Techniques for SSR Analysis", *IEEE Transactions on PAS*, Vol.PAS-98, pp.341-349, March/April 1979

[19] I.M. Canay, "A Novel Approach to the Torsional Interaction and Electrical Damping of the Synchronous Machine, Part I: Theory, *IEEE Transactions on PAS*, Vol.PAS-101, No.10, pp.3630-3638, October 1982

[20] I.M. Canay, "A Novel Approach to the Torsional Interaction and Electrical Damping of the Synchronous Machine, Part II: Application to an Arbitary Network, *IEEE Transactions on PAS*, Vol.PAS-101, No.10, pp.3639-3647, October, 1982

[21] Colin E.J. Bowler, Donald N. Ewart, "Self-Excited Torsional Frequency Oscillations with Series Capacitors," *IEEE Transactions on PAS*, Vol.PAS-92, pp.1688-1695, 1973

[22] Yao-Nan-Yu,"*Electric Power System Dynamics*", Academic Press, New York, 1983

[23] P.M. Anderson, B.L. Agrawal, J.E. Van Ness, "Subsynchronous Resonance in Power Systems," *IEEE Press*, 1990

[24] W. Zhu, V. Rajkumar, R. Spee, R.R. Mohler, "On the Analysis of Subsynchronous Resonance in Power Systems," accepted for publication, *American Power Conference, Chicago,* April 1994

[25] N.Yorino, Y.Tamura, R.Yokoyama,"A Generalized Analysis Method of Auto-Parametric Resonances in Power Systems", *IEEE Transactions on Power Systems*, vol.4, No.3, pp.1057-1064, August 1989

[26] A.M.A.Hamdan, A.H.Nayfeh,"The Effect of Nonlinearities on the Response of a Single-Machine-Quasi-Infinite-Busbar System", *IEEE Transactions on Power Systems*, vol.4, No.3, pp.843-849, August 1989

[27] M.R.Iravani, A.Semlyen,"Hopf Bifurcations in Torsional Dynamics", *IEEE Transactions on Power Systems*, vol.7, No.1, pp.28-36, February 1992.

[28] J.E. Marsden, M. McCracken, "The Hopf Bifurcation and Its Applications," *Springer-Verlag*, New York, 1976

[29] John Gukenheimer, Philip Holmes, "Nonlinear Oscillations, Dynamical Systems, and Bifurcation Fields," *Springer-Verlag*, New York, 1983

[30] R. Seydel, "From Equilibrium to Chaos, Practical Bifurcation and Stability Analysis," *Elsevier Science Publishing Co.*, New York, 1988

[31] W. Zhu, R.R. Mohler, R. Spee, "Hopf Bifurcation Analysis for an Electrical Power System Experiencing Subsynchronous Resonance," submitted to *the IEEE Conference on Decision and Control*, 1994

[32] IEEE SSR Working Group,"Countermeasures to SSR Problems", *IEEE Transactions on PAS*, vol.PAS-99, No.5, pp.1810-1818, Sept./Oct. 1980

[33] Q.H.Li, D.Z.Zhao, Y.N.Yu,"A New Pole-Placement Method for Excitation Control Design to Damp SSR of a Nonidentical Two-Machine System", *IEEE Transactions on Power Systems*, vol.4, No.3, pp.1176-1181, August 1989

[34] R.A.Achilles, S.A.Hidronor, A.R.Ramirez,"An In-depth Analysis of Critical Parameters Affecting Leading SSR Countermeasures", *IEEE Transactions on PAS*, vol.PAS-104,No.2, pp.357-365, February 1985

[35] M.R.Iravani, R.M.Mathur,"Damping Subsynchronous Oscillations in Power Systems Using a Static Phase-Shifter", *IEEE Transactions on Power Systems*, vol.PWRS-1, No.2, pp.76-83, May 1986

[36] IEEE SSR Working Group,"Series Capacitor Controls And Settings As Countermeasures To SSR", *IEEE Transactions on PAS*, vol.PAS-101, No.6, pp.1281-1287, June 1982

[37] R.A.Hedin, K.B.Stump, N.G.Hingorani,"A New Scheme For SSR Dampng of Torsional Oscillations and Transient Torque - Part II, Performance", *IEEE Transactions on PAS*, vol.PAS-100, No.4, pp.1856-1863, April 1981

[38] N.G.Hingorani, B.Bhargava, G.F.Garrigue, G.D.Rodriguez,"Prototype NGH SSR Damping Scheme. Part I - Field Installation & Operating Experience", *IEEE Transactions on Power Systems*, vol.2, pp.1034-1039, Nov.1987

[39] N.G.Hingorani, B.Bhargava, G.F.Garrigue, G.D.Rodriguez,"Prototype NGH SSR Damping Scheme. Part II - Switching and Short Circuit Tests," *IEEE Transactions on Power Systems*, vol.2, pp.1040-1049, Nov.1987

[40] E.V. Larsen, C.E.J. Bowler, B.L. Damsky, S.L. Nilsson, "Benefits of Thyristor -Controlled Series Compensation," CIGRE Paper 14/37/38-04, Paris, 1992

[41] J. Urbanek, R.J. Piwko, E.V. Larsen, B.L. Damsky, B.C. Furumasu, W.A. Mittelstadt, J.D. Eden, "Thyristor Controlled Series Compensation Prototype Installation at the Slatt 500 kV Substation," *IEEE PES Paper 92-SM-467-1PWRD*, Seattle, July 1992

[42] S. Nyati C.A. Wegner, R.W. Delmerico, R.J. Piwko, D.H. Baker, A. Edris, "Effectiveness of Thyristor Controlled Series Capacitor in Enhancing Power System Dynamics: an Analog Simulator Study," *IEEE PES Paper 93-SM-432-5PWRD*, Vancouver, B.C., Canada, July, 1993

[43] W. Zhu, R. Spee, R.R. Mohler, G.C. Alexander, W.A. Mittelstadt, D. Maratukulam, "An EMTP Study of SSR Mitigation Using the Thyristor Controlled Series Capacitor," accepted for publication, IEEE PES Summer Meeting, San Francisco, 1994, to appear in *IEEE Transactions on Power Delivery*

[44] Lawrence Perko, "Differential Equations and Dynamical Systems", Springer -Verlag, New York, 1991

[45] R. Mohler, "Nonlinear Systems", Prentice Hall, Englewood Cliffs, New Jersey, 1991

[46] J. A. Richards, "Analysis of Periodically Time-Varying Systems", Springer-Verlag, Berlin, Heidelberg, 1983

[47] R. Seydel, "Numerical Computation of Periodic Orbits That Bifurcate from Stationary Solutions of Ordinary Differential Equations", *Appl. Math. Comput.*, 9: 257-271, 1981

[48] Mobolaji Aluko, Hsueh-Chia Chang, "PEFLOQ: An Algorithm for the Bifurcational Analysis of Periodic Solutions of Autonomous Systems", *Computers & Chemical Engineering*, Vol.8, No. 6, pp.355-365, 1984

[49] M. Kubicek, Hlavecek, "Numerical Solution of Nonlinear Boundary Value Problems with Applications", Prentice Hall, Englewood Cliffs, New Jersey, 1983

[50] Sanford M. Roberts, Jerome S. Shipman, "Two-Point Boundary Value Problems: Shooting Methods", American Elsevier Publishing Company, Inc., New York, 1972

[51] S. Wiggins, "Introduction to Applied Nonlinear Dynamical Systems and Chaos", Springer-Verlag, New York, 1990

[52] R. Spee, W.Zhu, "Flexible AC Transmission Systems - Simulation and Control", Proc. Africon, Swaziland, 1992

[53] Advanced Concepts Studies Related to FACTS: Operation and Nonlinear Control - Phase II, OSU ECE Technical Report FACTS 9201, February, 1992, EPRI Contract No. RP 4000-06, BPA Contract No. DE B179-90BP08423

[54] E.V. Larsen, K. Clark, S.A. Miske, Jr., J.Urbanek, "Characteristics and Rating Considerations of Thyristor Controlled Series Compensation," IEEE PES Paper 93-SM-433-3PWRD, Vancouver, B.C., Canada, July, 1993

[55] Scott G. Helbing, G.G. Karady, "Investigation of an Advanced Form of Series Compensation," IEEE PES Paper 93-SM-431-7PWRD, Vancouver, B.C., Canada, July, 1993

[56] Alistair I. Mees, Leon O. Chua, "The Hopf Bifurcation Theorem and Its Applications to Nonlinear Oscillations in Circuits and Systems," IEEE Transactions on Circuits and Systems, Vol. CAS-26, No.4, April, 1979

Appendices

Appendix A Derivation of T_{ec} and T_{sc}

1. Derivation of T_{sc}

We solve for T_{sc} from the mechanical sub-system described by(2.10), (2.11) and (2.12), with $\delta = F_\delta e^{\sigma t} e^{j\Omega t} + cc_1$ and its derivatives $d\delta/dt$ and $d\delta^2/dt^2$ acting as forcing functions on the sub-system.

First, we solve for the particular solution of (2.10) under the forcing function δ of the time function(2.8). We assume that

$$\theta' = \mathbf{S} F_\delta e^{\sigma t} e^{j\Omega t} + cc_5, \qquad \text{(A–1)}$$

where $\mathbf{S} = [s_1\ s_2\ s_3\ s_4]^T$, with "T" indicating vector transpose, and cc_5 indicates the complex conjugate of the first term in (A-1). From (A-1), we can obtain

$$d\theta'/dt = \mathbf{S} F_\delta (\sigma+j\Omega) e^{\sigma t} e^{j\Omega t} + cc_6 , \qquad \text{(A–2)}$$

where cc_6 indicates the complex conjugate of the first term in (A-2), and

$$d\theta'^2/dt^2 = \mathbf{S} F_\delta (\sigma+j\Omega)^2 e^{\sigma t} e^{j\Omega t} + cc_7 , \qquad \text{(A–3)}$$

where cc_7 indicates the complex conjugate of the first term in (A-3).

Substituting (A-1), (A-2) and (A-3) into (2.10), we obtain

$$\mathbf{S} = [\mathbf{M}'(\sigma+j\Omega)^2 + \mathbf{D}'(\sigma+j\Omega) + \mathbf{K}']^{-1} \begin{bmatrix} 0 \\ 0 \\ 0 \\ K_{45} \end{bmatrix}.$$

Now, solving for the particular solution of the differential equation(2.11), under the forcing function δ of the time function(2.8), we obtain

$$\theta_6 = s_6 F_\delta e^{\sigma t} e^{j\Omega t} + cc_8 \qquad \text{(A-4)}$$

where

$$s_6 = K_{56} / [M_6(\sigma+j\Omega)^2 + D_{m6}(\sigma+j\Omega) + K_{56}],$$

and cc_8 indicates the complex conjugate of the first term in eqn(A-4).

Substituting (A-1), (A-4), δ and its derivatives $d\delta/dt$ and $d\delta^2/dt^2$ into (2.12), we obtain

$$T_s = T_{sc} F_\delta e^{\sigma t} e^{j\Omega t} + cc_4 \qquad \text{(A-5)}$$

where cc_4 indicates the complex conjugate of the first term in (A-5), and

$$T_{sc} = -M_5 (\sigma+j\Omega)^2 - D_{m5} (\sigma+j\Omega) + K_{45} s_4 - (K_{45}+K_{56}) + K_{56} s_6 \qquad \text{(A-6)}$$

2. Derivation of T_{ec}

The electrical sub-system (2.2) under the forcing functions δ and ω of the time function(2.8), can be expressed as following:

$$\mathbf{H}\, d\mathbf{x}/dt = \mathbf{G}\,\mathbf{x} + \mathbf{B}\,\mathbf{u}, \qquad \text{(A-7)}$$

where

$\mathbf{x} = [i_d\ i_f\ i_q\ i_Q\ e_{cd}\ e_{cq}]^T$, and "T" indicates vector transpose,

$$\mathbf{H} = \begin{bmatrix} -x_l-x_d & x_{ad} & & & & \\ -x_{ad} & x_f & & & & \\ & & -x_l-x_q & x_{aq} & & \\ & & -x_{aq} & x_Q & & \\ & & & & 1 & \\ & & & & & 1 \end{bmatrix},$$

$$\mathbf{G} = \omega_b \begin{bmatrix} r_a+r & 0 & -(x_l+x_q) & x_{aq} & 1 & 0 \\ 0 & -r_f & 0 & 0 & 0 & 0 \\ x_l+x_d & -x_{ad} & r_a+r & 0 & 0 & 1 \\ 0 & 0 & 0 & -r_Q & 0 & 0 \\ x_c & 0 & 0 & 0 & 0 & 1 \\ 0 & 0 & x_c & 0 & -1 & 0 \end{bmatrix},$$

$$\mathbf{B} = \omega_b \begin{bmatrix} (-x_q i_{qe})\rho+v_o\cos(\delta_e) & (-x_q i_{qe})\rho+v_o\cos(\delta_e) \\ 0 & 0 \\ (x_d i_{de}-x_{ad} i_{fe})\rho-v_o\sin(\delta_e) & (x_d i_{de}-x_{ad} i_{fe})\rho-v_o\sin(\delta_e) \\ 0 & 0 \\ 0 & 0 \\ 0 & 0 \end{bmatrix},$$

$\omega_b = 377$(rad/sec), which is synchronous speed, and

$$\mathbf{u} = \begin{bmatrix} F_\delta\, e^{\sigma t} e^{j\Omega t} \\ F_\delta^*\, e^{\sigma t} e^{-j\Omega t} \end{bmatrix},$$

where F_δ^* indicates the complex conjugate of F_δ.

Subscript "e" indicates the equilibrium operation condition.

In general, **H** has full rank. Thus, from (A-7), we obtain

$$d\mathbf{x}/dt = \mathbf{H}^{-1}\,\mathbf{G}\,\mathbf{x} + \mathbf{H}^{-1}\,\mathbf{B}\,\mathbf{u}$$

or,

$$d\mathbf{x}/dt = \mathbf{A}\,\mathbf{x} + \mathbf{H}^{-1}\,\mathbf{B}\,\mathbf{u}, \text{ where } \mathbf{A} = \mathbf{H}^{-1}\mathbf{G}\,.$$

Supposing $\mathbf{A} = \mathbf{P}\Lambda\mathbf{P}^{-1}$, where

$$\Lambda = \begin{bmatrix} \lambda_1 & & & & & \\ & \lambda_2 & & & & \\ & & \lambda_3 & & & \\ & & & \lambda_4 & & \\ & & & & \lambda_5 & \\ & & & & & \lambda_6 \end{bmatrix},$$

we have

$$\mathbf{P}^{-1}\, d\mathbf{x}/dt = \Lambda\,\mathbf{P}^{-1}\,\mathbf{x} + \mathbf{P}^{-1}\,\mathbf{H}^{-1}\,\mathbf{B}\,\mathbf{u}$$

or

$$d\mathbf{z}/dt = \Lambda\,\mathbf{z} + \mathbf{B}_1\,\mathbf{u}\,, \tag{A-8}$$

where $\mathbf{z} = \mathbf{P}^{-1}\mathbf{x}$, and $\mathbf{B}_1 = \mathbf{P}^{-1}\mathbf{H}^{-1}\mathbf{B}$.

Suppose that the particular solution of (A-8) under the forcing function u is:

$$\mathbf{z} = \mathbf{C}\,F_\delta\, e^{\sigma t} e^{j\Omega t} + cc_9 \tag{A-9}$$

where

$\mathbf{C} = [c_1\ c_2\ c_3\ c_4\ c_5\ c_6]^T$, and "T" indicates vector transpose.

From (A-9), we can obtain

$$d\mathbf{z}/dt = \mathbf{C}\,(\sigma + j\Omega)\,F_\delta\, e^{\sigma t} e^{j\Omega t} + cc_{10} \tag{A-10}$$

Substituting (A-9) and (A-10) into (A-8), we can obtain

$$\mathbf{C} = \begin{bmatrix} b_1 / (\sigma + j\Omega - \lambda_1) \\ b_2 / (\sigma + j\Omega - \lambda_2) \\ b_3 / (\sigma + j\Omega - \lambda_3) \\ b_4 / (\sigma + j\Omega - \lambda_4) \\ b_5 / (\sigma + j\Omega - \lambda_5) \\ b_6 / (\sigma + j\Omega - \lambda_6) \end{bmatrix}.$$

Since $\mathbf{x} = \mathbf{Pz}$, we have the particular solution $\mathbf{x}$ of (A-7) under the forcing function $\mathbf{u}$ as following:

$$\mathbf{x} = \mathbf{P}\,\mathbf{C}\,F_\delta\, e^{\sigma t}\, e^{j\Omega t} + cc_{11} \tag{A-11}$$

where cc_{11} indicates the complex conjugate of the first term in (A-11), or

$$\mathbf{x} = \mathbf{L}\,F_\delta\, e^{\sigma t}\, e^{j\Omega t} + cc_{11} \tag{A-12}$$

where

$\mathbf{L} = \mathbf{PC} = [l_1\ l_2\ l_3\ l_4\ l_5\ l_6]^T$, while "T" indicates vector transpose.

Substitute (A-12) into (2.3), we have

$$T_e = T_{ec}\,F_\delta\, e^{\sigma t}\, e^{j\Omega t} + cc_3 \tag{A-13}$$

where cc_3 indicates the complex conjugate of the first term in (A-13), and

$$T_{ec} = (x_q - x_d)\, i_{qe}\, l_1 + [(x_q - x_d)\, i_{de} + x_{ad}\, i_{fe}]\, l_3 + x_{ad}\, i_{qe}\, l_2 - x_{aq}\, i_{de}\, l_4 \tag{A-14}$$

Appendix B
Algorithms for Computing d'''(0) for the SMIB Power System Model (3.10)

(1): Algorithm for implementing (3.8)

$$\Delta = \mathbf{L}^3_{\mu 0} [\, \mathbf{L}^3_{\mu 0} \mathbf{L}^3_{\mu 0} + 4\, |\lambda(\mu_0)|^2\, \mathbf{I}_d \,]$$

where $\mathbf{I}_d$ represents the identity matrix with same dimension as $\mathbf{L}^3_{\mu 0}$.

(2): Algorithms for implementing (3.7)

$$\begin{aligned} d_1 d_1 \mathbf{h}(\mathbf{0}) = \; & \Delta^{-1} [\, -(2\,|\lambda(\mu_0)|^2\, \mathbf{I}_d + \mathbf{L}^3_{\mu 0} \mathbf{L}^3_{\mu 0})\, (d_1 d_1 \mathbf{f}^3_{\mu 0}(\mathbf{0})) \\ & + (2\,|\lambda(\mu_0)|\, \mathbf{L}^3_{\mu 0})\, (d_1 d_2 \mathbf{f}^3_{\mu 0}(\mathbf{0})) - 2\,|\lambda(\mu_0)|^2\, (d_2 d_2 \mathbf{f}^3_{\mu 0}(\mathbf{0}))\,] \end{aligned}$$

$$\begin{aligned} d_1 d_2 \mathbf{h}(\mathbf{0}) = \; & \Delta^{-1} [\, -(|\lambda(\mu_0)|\, \mathbf{L}^3_{\mu 0})\, (d_1 d_1 \mathbf{f}^3_{\mu 0}(\mathbf{0})) \\ & - (\mathbf{L}^3_{\mu 0} \mathbf{L}^3_{\mu 0})\, (d_1 d_2 \mathbf{f}^3_{\mu 0}(\mathbf{0})) + (|\lambda(\mu_0)|\, \mathbf{L}^3_{\mu 0})\, (d_2 d_2 \mathbf{f}^3_{\mu 0}(\mathbf{0}))\,] \end{aligned}$$

$$\begin{aligned} d_2 d_2 \mathbf{h}(\mathbf{0}) = \; & \Delta^{-1} [\, -2\,|\lambda(\mu_0)|^2\, (d_1 d_1 \mathbf{f}^3_{\mu 0}(\mathbf{0})) \\ & - (2\,|\lambda(\mu_0)|\, \mathbf{L}^3_{\mu 0})\, (d_1 d_2 \mathbf{f}^3_{\mu 0}(\mathbf{0})) - 2\,|\lambda(\mu_0)|^2\, (d_2 d_2 \mathbf{f}^3_{\mu 0}(\mathbf{0})) \\ & - (\mathbf{L}^3_{\mu 0} \mathbf{L}^3_{\mu 0})\, (d_2 d_2 \mathbf{f}^3_{\mu 0}(\mathbf{0}))\,], \end{aligned}$$

where

$$d_1 d_1 \mathbf{f}^3_{\mu 0}(\mathbf{0}) = [\partial^2 z^3_{\mu 0}(\mathbf{0}) / \partial x_1^2, \ldots, \partial^2 z^i_{\mu 0}(\mathbf{0}) / \partial x_1^2, \ldots, \partial^2 z^{15}_{\mu 0}(\mathbf{0}) / \partial x_1^2]^T,$$

$$d_1 d_2 \mathbf{f}^3_{\mu 0}(\mathbf{0}) = [\partial^2 z^3_{\mu 0}(\mathbf{0}) / \partial x_1 \partial x_2, \ldots, \partial^2 z^i_{\mu 0}(\mathbf{0}) / \partial x_1 \partial x_2, \ldots, \partial^2 z^{15}_{\mu 0}(\mathbf{0}) / \partial x_1 x_2]^T,$$

$$d_2 d_2 \mathbf{f}^3_{\mu 0}(\mathbf{0}) = [\partial^2 z^3_{\mu 0}(\mathbf{0}) / \partial x_2^2, \ldots, \partial^2 z^i_{\mu 0}(\mathbf{0}) / \partial x_2^2, \ldots, \partial^2 z^{15}_{\mu 0}(\mathbf{0}) / \partial x_2^2]^T,$$

in which

$$\begin{aligned} \partial^2 z^i_{\mu 0}(\mathbf{0}) / \partial x_1^2 = \; & \alpha(i)\, p_{1,1}\, p_{3,1} + \beta(i)\, p_{2,1}\, p_{3,1} + \gamma(i)\, p_{2,1}\, p_{12,1} \\ & + \rho(i)\, p_{3,1}\, p_{12,1} + \eta(i)\, p_{1,1}\, p_{12,1} + \upsilon(i)\, p_{13,1}\, p_{13,1}\,, \\ \partial^2 z^i_{\mu 0}(\mathbf{0}) / \partial x_1 \partial x_2 = \; & \alpha(i)\, (p_{1,1}\, p_{3,2} + p_{1,2}\, p_{3,1}) + \beta(i)\, (p_{2,1}\, p_{3,2} + p_{2,2}\, p_{3,1}) \\ & + \gamma(i)\, (p_{2,1}\, p_{12,2} + p_{2,2}\, p_{12,1}) + \rho(i)\, (p_{3,1}\, p_{12,2} + p_{3,2}\, p_{12,1}) \\ & + \eta(i)\, (p_{1,1}\, p_{12,2} + p_{1,2}\, p_{12,1}) + \upsilon(i)\, (p_{13,1}\, p_{13,2} + p_{13,2}\, p_{13,1}) \end{aligned}$$

$$\partial^2 z^i{}_{\mu 0}(\mathbf{0}) / \partial x_2{}^2 = \alpha(i)\, p_{1,2}\, p_{3,2} + \beta(i)\, p_{2,2}\, p_{3,2} + \gamma(i)\, p_{2,2}\, p_{12,2} + \rho(i)\, p_{3,2}\, p_{12,2} + \eta(i)\, p_{1,2}\, p_{12,2} + \upsilon(i)\, p_{13,2}\, p_{13,2}\,.$$

(3): Algorithms for implementing (3.6)

$$\partial^3 g^1{}_{\mu 0}(\mathbf{0}) / \partial x_1{}^3 = \partial^3 f^1{}_{\mu 0}(\mathbf{0}) / \partial x_1{}^3 + 3\, \partial^2 f^1{}_{\mu 0}(\mathbf{0}) / \partial \mathbf{X}_3 \partial x_1 \circ d_1 d_1 \mathbf{h}(\mathbf{0}),$$

$$\partial^3 g^1{}_{\mu 0}(\mathbf{0}) / \partial x_1 \partial x_2{}^2 = \partial^3 f^1{}_{\mu 0}(\mathbf{0}) / \partial x_1 \partial x_2{}^2 + 2\partial^2 f^1{}_{\mu 0}(\mathbf{0}) / \partial \mathbf{X}_3 \partial x_2 \circ d_1 d_2 \mathbf{h}(\mathbf{0}) + \partial^2 f^1{}_{\mu 0}(\mathbf{0}) / \partial \mathbf{X}_3 \partial x_1 \circ d_2 d_2 \mathbf{h}(\mathbf{0})$$

$$\partial^3 g^2{}_{\mu 0}(\mathbf{0}) / \partial x_1{}^2 \partial x_2 = \partial^3 f^2{}_{\mu 0}(\mathbf{0}) / \partial x_1{}^2 \partial x_2 + \partial^2 f^2{}_{\mu 0}(\mathbf{0}) / \partial \mathbf{X}_3 \partial x_2 \circ d_1 d_1 \mathbf{h}(\mathbf{0}) + 2\partial^2 f^2{}_{\mu 0}(\mathbf{0}) / \partial \mathbf{X}_3 \partial x_1 \circ d_1 d_2 \mathbf{h}(\mathbf{0})$$

$$\partial^3 g^2{}_{\mu 0}(\mathbf{0}) / \partial x_2{}^3 = \partial^3 f^2{}_{\mu 0}(\mathbf{0}) / \partial x_2{}^3 + 3\, \partial^2 f^2{}_{\mu 0}(\mathbf{0}) / \partial \mathbf{X}_3 \partial x_2 \circ d_2 d_2 \mathbf{h}(\mathbf{0}),$$

where

$$\partial^3 f^1{}_{\mu 0}(\mathbf{0}) / \partial x_1{}^3 = \xi(1)\, p_{13,1}\, p_{13,1}\, p_{13,1}$$

$$\partial^3 f^1{}_{\mu 0}(\mathbf{0}) / \partial x_1 \partial x_2{}^2 = 3\, \xi(1)\, p_{13,1}\, p_{13,2}\, p_{13,2}$$

$$\partial^3 f^2{}_{\mu 0}(\mathbf{0}) / \partial x_1{}^2 \partial x_2 = 3\, \xi(2)\, p_{13,1}\, p_{13,1}\, p_{13,2}$$

$$\partial^3 f^2{}_{\mu 0}(\mathbf{0}) / \partial x_2{}^3 = \xi(2)\, p_{13,2}\, p_{13,2}\, p_{13,2},$$

and

$$\partial^2 f^1{}_{\mu 0}(\mathbf{0}) / \partial \mathbf{X}_3 \partial x_1 = [\partial^2 f^1{}_{\mu 0}(\mathbf{0}) / \partial x_3 \partial x_1, \ldots, \partial^2 f^1{}_{\mu 0}(\mathbf{0}) / \partial x_i \partial x_1, \ldots, \partial^2 f^1{}_{\mu 0}(\mathbf{0}) / \partial x_{15} \partial x_1]^T,$$

in which

$$\partial^2 f^1{}_{\mu 0}(\mathbf{0}) / \partial x_i \partial x_1 = \alpha(1)\,(p_{1,i}\, p_{3,1} + p_{1,1}\, p_{3,i}) + \beta(1)\,(p_{2,i}\, p_{3,1} + p_{2,1}\, p_{3,i}) + \gamma(1)\,(p_{2,i}\, p_{12,1} + p_{2,1}\, p_{12,i}) + \rho(1)\,(p_{3,i}\, p_{12,1} + p_{3,1}\, p_{12,i}) + \eta(1)\,(p_{1,i}\, p_{12,1} + p_{1,1}\, p_{12,i}) + \upsilon(1)\,(p_{13,i}\, p_{13,1} + p_{13,1}\, p_{13,i}),$$

$$\partial^2 f^1{}_{\mu 0}(\mathbf{0}) / \partial \mathbf{X}_3 \partial x_2 = [\partial^2 f^1{}_{\mu 0}(\mathbf{0}) / \partial x_3 \partial x_2, \ldots, \partial^2 f^1{}_{\mu 0}(\mathbf{0}) / \partial x_i \partial x_2, \ldots, \partial^2 f^1{}_{\mu 0}(\mathbf{0}) / \partial x_{15} \partial x_2]^T,$$

in which

$$\partial^2 f^1{}_{\mu 0}(\mathbf{0}) / \partial x_i \partial x_2 = \alpha(1)\,(p_{1,i}\, p_{3,2} + p_{1,2}\, p_{3,i}) + \beta(1)\,(p_{2,i}\, p_{3,2} + p_{2,2}\, p_{3,i}) + \gamma(1)\,(p_{2,i}\, p_{12,2} + p_{2,2}\, p_{12,i}) + \rho(1)\,(p_{3,i}\, p_{12,2} + p_{3,2}\, p_{12,i}) + \eta(1)\,(p_{1,i}\, p_{12,2} + p_{1,2}\, p_{12,i}) + \upsilon(1)\,(p_{13,i}\, p_{13,2} + p_{13,2}\, p_{13,i}),$$

$\partial^2 f^2_{\mu 0}(\mathbf{0}) / \partial \mathbf{X}_3 \partial x_2 = [\partial^2 f^2_{\mu 0}(\mathbf{0}) / \partial x_3 \partial x_2, \ldots, \partial^2 f^2_{\mu 0}(\mathbf{0}) / \partial x_i \partial x_2, \ldots, \partial^2 f^2_{\mu 0}(\mathbf{0}) / \partial x_{15} \partial x_2]^T$,
in which

$$\begin{aligned}\partial^2 f^2_{\mu 0}(\mathbf{0}) / \partial x_i \partial x_2 = {} & \alpha(2)\,(p_{1,i}\,p_{3,2} + p_{1,2}\,p_{3,i}) + \beta(2)\,(p_{2,i}\,p_{3,2} + p_{2,2}\,p_{3,i}) \\ & + \gamma(2)\,(p_{2,i}\,p_{12,2} + p_{2,2}\,p_{12,i}) + \rho(2)\,(p_{3,i}\,p_{12,2} + p_{3,2}\,p_{12,i}) \\ & + \eta(2)\,(p_{1,i}\,p_{12,2} + p_{1,2}\,p_{12,i}) + \upsilon(2)\,(p_{13,i}\,p_{13,2} + p_{13,2}\,p_{13,i})\,,\end{aligned}$$

$\partial^2 f^2_{\mu 0}(\mathbf{0}) / \partial \mathbf{X}_3 \partial x_1 = [\partial^2 f^2_{\mu 0}(\mathbf{0})/\partial x_3 \partial x_1, \ldots, \partial^2 f^2_{\mu 0}(\mathbf{0})/\partial x_i \partial x_1, \ldots, \partial^2 f^2_{\mu 0}(\mathbf{0})/\partial x_{15} \partial x_1]^T$,
in which

$$\begin{aligned}\partial^2 f^2_{\mu 0}(\mathbf{0}) / \partial x_i x_1 = {} & \alpha(2)\,(p_{1,i}\,p_{3,1} + p_{1,1}\,p_{3,i}) + \beta(2)\,(p_{2,i}\,p_{3,1} + p_{2,1}\,p_{3,i}) \\ & + \gamma(2)\,(p_{2,i}\,p_{12,1} + p_{2,1}\,p_{12,i}) + \rho(2)\,(p_{3,i}\,p_{12,1} + p_{3,1}\,p_{12,i}) \\ & + \eta(2)\,(p_{1,i}\,p_{12,1} + p_{1,1}\,p_{12,i}) + \upsilon(2)\,(p_{13,i}\,p_{13,1} + p_{13,1}\,p_{13,i})\,.\end{aligned}$$

To this point, the algorithms have been presented for implementing the computations of the first 4 terms in (3.5). The algorithms for computation of the last 6 terms in (3.5) are more straight-forward, and are presented in the following.

(4): Algorithms for the last 6 terms in (3.5)

$$\begin{aligned}\partial^2 f^1_{\mu 0}(\mathbf{0}) / \partial x_1^2 = {} & \alpha(1)\,p_{1,1}\,p_{3,1} + \beta(1)\,p_{2,1}\,p_{3,1} + \gamma(1)\,p_{2,1}\,p_{12,1} \\ & + \rho(1)\,p_{3,1}\,p_{12,1} + \eta(1)p_{1,1}\,p_{12,1} + \upsilon(1)\,p_{13,1}\,p_{13,1}\end{aligned}$$

$$\begin{aligned}\partial^2 f^1_{\mu 0}(\mathbf{0}) / \partial x_1 \partial x_2 = {} & \alpha(1)\,(p_{1,1}\,p_{3,2} + p_{1,2}\,p_{3,1}) + \beta(1)\,(p_{2,1}\,p_{3,2} + p_{2,2}\,p_{3,1}) \\ & + \gamma(1)\,(p_{2,1}\,p_{12,2} + p_{2,2}\,p_{12,1}) + \rho(1)\,(p_{3,1}\,p_{12,2} + p_{3,2}\,p_{12,1}) \\ & + \eta(1)\,(p_{1,1}\,p_{12,2} + p_{1,2}\,p_{12,1}) + \upsilon(1)\,(p_{13,1}\,p_{13,2} + p_{13,2}\,p_{13,1})\end{aligned}$$

$$\begin{aligned}\partial^2 f^1_{\mu 0}(\mathbf{0}) / \partial x_2^2 = {} & \alpha(1)\,p_{1,2}\,p_{3,2} + \beta(1)\,p_{2,2}\,p_{3,2} + \gamma(1)\,p_{2,2}\,p_{12,2} \\ & + \rho(1)\,p_{3,2}\,p_{12,2} + \eta(1)p_{1,2}\,p_{12,2} + \upsilon(1)\,p_{13,2}\,p_{13,2}\end{aligned}$$

$$\partial^2 f^2_{\mu 0}(\mathbf{0}) / \partial x_1^2 = \alpha(2)\, p_{1,1}\, p_{3,1} + \beta(2)\, p_{2,1}\, p_{3,1} + \gamma(2)\, p_{2,1}\, p_{12,1} + \rho(2)\, p_{3,1}\, p_{12,1} + \eta(2) p_{1,1}\, p_{12,1} + \upsilon(2)\, p_{13,1}\, p_{13,1}$$

$$\partial^2 f^2_{\mu 0}(\mathbf{0}) / \partial x_1 \partial x_2 = \alpha(2)\,(p_{1,1}\, p_{3,2} + p_{1,2}\, p_{3,1}) + \beta(2)\,(p_{2,1}\, p_{3,2} + p_{2,2}\, p_{3,1}) + \gamma(2)\,(p_{2,1}\, p_{12,2} + p_{2,2}\, p_{12,1}) + \rho(2)\,(p_{3,1}\, p_{12,2} + p_{3,2}\, p_{12,1}) + \eta(2)\,(p_{1,1}\, p_{12,2} + p_{1,2}\, p_{12,1}) + \upsilon(2)\,(p_{13,1}\, p_{13,2} + p_{13,2}\, p_{13,1})$$

and

$$\partial^2 f^2_{\mu 0}(\mathbf{0}) / \partial x_2^2 = \alpha(2)\, p_{1,2}\, p_{3,2} + \beta(2)\, p_{2,2}\, p_{3,2} + \gamma(2)\, p_{2,2}\, p_{12,2} + \rho(2)\, p_{3,2}\, p_{12,2} + \eta(2) p_{1,2}\, p_{12,2} + \upsilon(2)\, p_{13,2}\, p_{13,2}$$

Now, the algorithms have been presented for obtaining all the terms in (3.5), and the coefficient d'''(0) follows.

Appendix C The Jacobian Matrix Along a Solution Path of (3.9)

$A(t) = [\, A_1(t)\ \ A_2(t)\ \ A_3(t)\,]$

where

$$A_1(t) = \begin{bmatrix}
\omega_b/Q_1\,(r_a+r)\,x_f & \omega_b/Q_1\,r_f\,x_{ad} & \omega_b/Q_1\,(-\,x_f\,x_t - x_f\,x_q\,\omega) & \omega_b/Q_1\,x_f & 0 & 0 \\
\omega_b/Q_1\,(r_a+r)x_{ad} & \omega_b/Q_1\,r_f(x_d + x_t) & \omega_b/Q_1\,(-\,x_{ad}\,x_t - x_q\,x_{ad}\,w) & \omega_b/Q_1\,x_{ad} & 0 & 0 \\
\omega_b/Q_2\,(x_t+x_d\,\omega) & \omega_b/Q_2\,(-x_{ad}\,\omega) & \omega_b/Q_2\,(r_a+r) & 0 & \omega_b/Q_2 & 0 \\
\omega_b\,\mu\,x_t & 0 & 0 & 0 & \omega_b & 0 \\
0 & 0 & \omega_b\,\mu\,x_t & -\omega_b & 0 & 0 \\
0 & 0 & 0 & 0 & 0 & -D_1/M_1 \\
0 & 0 & 0 & 0 & 0 & \omega_b \\
0 & 0 & 0 & 0 & 0 & 0 \\
0 & 0 & 0 & 0 & 0 & 0 \\
0 & 0 & 0 & 0 & 0 & 0 \\
0 & 0 & 0 & 0 & 0 & 0 \\
1/M_4\,(x_d-x_q)\,i_q & 1/M_4\,(-\,x_{ad}\,i_q) & 1/M_4\,[(x_d - x_q)\,i_d - x_{ad}\,i_f] & 0 & 0 & 0 \\
0 & 0 & 0 & 0 & 0 & 0 \\
0 & 0 & 0 & 0 & 0 & 0 \\
0 & 0 & 0 & 0 & 0 & 0
\end{bmatrix}$$

$$A_2(t) = \begin{bmatrix}
0 & 0 & 0 & 0 & 0 & w_b/Q_1 \, (- x_q \, x_f \, i_q) \\
0 & 0 & 0 & 0 & 0 & \omega_b/Q_1 \, (- x_{ad} \, x_q \, i_q) \\
0 & 0 & 0 & 0 & 0 & \omega_b/Q_2 \, (x_d \, i_d - x_{ad} \, i_f) \\
0 & 0 & 0 & 0 & 0 & 0 \\
0 & 0 & 0 & 0 & 0 & 0 \\
-K_{12}/M_1 & 0 & K_{12}/M_1 & 0 & 0 & 0 \\
0 & 0 & 0 & 0 & 0 & 0 \\
K_{12}/M_2 & -D_2/M_2 & -(K_{12} + K_{23})/M_2 & 0 & K_{23}/M_2 & 0 \\
0 & \omega_b & 0 & 0 & 0 & 0 \\
0 & 0 & K_{23}/M_3 & -D_3/M_3 & -(K_{23} + K_{34})/M_3 & 0 \\
0 & 0 & 0 & \omega_b & 0 & 0 \\
0 & 0 & 0 & 0 & K_{34}/M_4 & - D_4/M_4 \\
0 & 0 & 0 & 0 & 0 & \omega_b \\
0 & 0 & 0 & 0 & 0 & 0 \\
0 & 0 & 0 & 0 & 0 & 0
\end{bmatrix}$$

and

$$A_3(t) = \begin{bmatrix}
w_b/Q_1 \, x_f \, v_o \cos\delta & 0 & 0 \\
\omega_b/Q_1 \, x_{ad} \, v_o \cos\delta & 0 & 0 \\
\omega_b/Q_2 \, (- v_o \sin\delta) & 0 & 0 \\
0 & 0 & 0 \\
0 & 0 & 0 \\
0 & 0 & 0 \\
0 & 0 & 0 \\
0 & 0 & 0 \\
0 & 0 & 0 \\
K_{34}/M_3 & 0 & 0 \\
0 & 0 & 0 \\
- (K_{34} + K_{45})/M_4 & 0 & K_{45}/M_4 \\
0 & 0 & 0 \\
K_{45}/M_5 & -D_5/M_5 & - K_{45}/M_5 \\
0 & \omega_b & 0
\end{bmatrix}$$

Appendix D An EMTP Modelling of the TCSC

A detailed configuration and the parameters of the TCSC model is shown in Fig AD.1

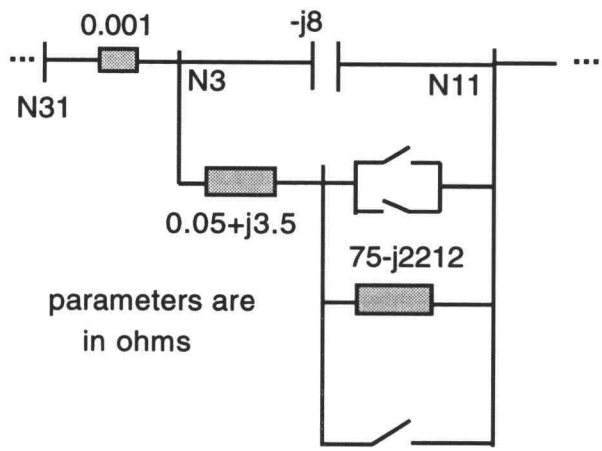

Fig.AD.1 The TCSC model

Modelling of the TCSC using the "MODELS" feature of EMTP is shown in the following:

```
MODELS
C ---------------------------
C  Getting the voltages of nodes N31 and N3 into MODELS for calculating
C  the current going through the TCSC. The current through N31 and N3
C  is same as that through the TCSC.
C ---------------------------
INPUT VN31A {v(N31A)}
INPUT VN3A {v(N3A)}
INPUT VN31B {v(N31B)}
INPUT VN3B {v(N3B)}
INPUT VN31C {v(N31C)}
INPUT VN3C {v(N3C)}
C ---------------------------
C  The following outputs control the switches simulating the
C  thyristors of the TCSC. For each phase, there is a pair of
C  switches for the TCSC.
C ---------------------------
OUTPUT GATE1A,GATE2A,GATE1B,GATE2B,GATE1C,GATE2C
MODEL TC1
 INPUT v1a,v2a,v1b,v2b,v1c,v2c
 VAR g1a,g2a,g1b,g2b,g1c,g2c,xc2
```

```
 VAR alpha,ONTIME
 VAR ilinea,ilineb,ilinec
 VAR ia,tt
 VAR rampa,compa,dcmpa,dcmp1a,comp1a
 VAR rampb,compb,dcmpb,dcmp1b,comp1b
 VAR rampc,compc,dcmpc,dcmp1c,comp1c
 VAR rampan,compan,dcmpan,dcmp1an,comp1an
 VAR rampbn,compbn,dcmpbn,dcmp1bn,comp1bn
 VAR rampcn,compcn,dcmpcn,dcmp1cn,comp1cn
 VAR vcontl1,vcontl
 OUTPUT g1a,g2a,g1b,g2b,g1c,g2c
 INIT
    rampa:=0.
    rampan:=0.
    rampb:=0.
    rampbn:=0.
    rampc:=0.
    rampcn:=0.
    tt:=0.
 ENDINIT
 EXEC
   tt:=tt+timestep
C ---------------------------
C  "ONTIME (in electrical degrees)" is an important variable, which determines
C  thyristor conduction interval per 180 electrical degrees.
C ---------------------------
   ONTIME:=100.
   alpha:=(180.-ontime)/2.
   vcontl:=1000.0*alpha/90.0
   vcontl1:=1000.0*(alpha+ontime)/90.0
C ---------------------------
C  A resistor with resistance 0.001 ohms is connected between N31 and N3.
C  Thus, by the following procedure, we can get the line current,
C  which is also the current through the TCSC.
C ---------------------------
   ilinea:=1000*(v1a-v2a)
   ilineb:=1000*(v1b-v2b)
   ilinec:=1000*(v1c-v2c)
   IF ilinea>=0.
     THEN
      rampa:=rampa+timestep*2.4e+5
      compa:=bool(rampa-vcontl)
      comp1a:=bool(rampa-vcontl1)
      dcmp1a:=nor(comp1a)
      g1a:=-0.5+and(dcmp1a,compa)
      g2a:=-0.5
     ELSE
      rampa:=0.
      g1a:=-0.5
   ENDIF
   IF ilinea<=0.
     THEN
      rampan:=rampan+timestep*2.4e+5
      compan:=bool(rampan-vcontl)
```

```
    comp1an:=bool(rampan-vcontl1)
    dcmp1an:=nor(comp1an)
    g2a:=-0.5+and(dcmp1an,compan)
    g1a:=-0.5
   ELSE
    g2a:=-0.5
    rampan:=0.
 ENDIF
IF ilineb>=0.
  THEN
   rampb:=rampb+timestep*2.4e+5
   compb:=bool(rampb-vcontl)
   comp1b:=bool(rampb-vcontl1)
   dcmp1b:=nor(comp1b)
   g1b:=-0.5+and(dcmp1b,compb)
   g2b:=-0.5
  ELSE
   rampb:=0.
   g1b:=-0.5
 ENDIF
IF ilineb<=0.
  THEN
   rampbn:=rampbn+timestep*2.4e+5
   compbn:=bool(rampbn-vcontl)
   comp1bn:=bool(rampbn-vcontl1)
   dcmp1bn:=nor(comp1bn)
   g2b:=-0.5+and(dcmp1bn,compbn)
   g1b:=-0.5
  ELSE
   g2b:=-0.5
   rampbn:=0.
 ENDIF
IF ilinec>=0.
  THEN
   rampc:=rampc+timestep*2.4e+5
   compc:=bool(rampc-vcontl)
   comp1c:=bool(rampc-vcontl1)
   dcmp1c:=nor(comp1c)
   g1c:=-0.5+and(dcmp1c,compc)
   g2c:=-0.5
  ELSE
   rampc:=0.
   g1c:=-0.5
 ENDIF
IF ilinec<=0.
  THEN
   rampcn:=rampcn+timestep*2.4e+5
   compcn:=bool(rampcn-vcontl)
   comp1cn:=bool(rampcn-vcontl1)
   dcmp1cn:=nor(comp1cn)
   g2c:=-0.5+and(dcmp1cn,compcn)
   g1c:=-0.5
  ELSE
   g2c:=-0.5
```

```
      rampcn:=0.
    ENDIF
C ---------------------------
C  following lines are for setting the initial switching time(if other than 0)
C  for the TCSC
C ---------------------------
C    IF tt<=0.0167
C     THEN
C      g1a:=-0.5
C      g2a:=-0.5
C      g1b:=-0.5
C      g2b:=-0.5
C      g1c:=-0.5
C      g2c:=-0.5
C    ENDIF
 ENDEXEC
ENDMODEL
USE tc1 AS tc1
 INPUT  v1a:=vn31a
       v2a:=vn3a
       v1b:=vn31b
       v2b:=vn3b
       v1c:=vn31c
       v2c:=vn3c
 OUTPUT  gate1a:=g1a
       gate2a:=g2a
       gate1b:=g1b
       gate2b:=g2b
       gate1c:=g1c
       gate2c:=g2c
ENDUSE
C ---------------------------
C  Following lines are for asking for outputs if needed
C ---------------------------
C  RECORD
C        tc1.g1a AS g1a
C        tc1.g2a AS g2a
C        tc1.g1b AS g1b
C        tc1.g2b AS g2b
C        tc1.g1c AS g1c
C        tc1.g2c AS g2c
C        tc1.ilinea as ia
C        tc1.ilineb as ib
C        tc1.ilinec as ic
C       tc1.vcontl as con
C       tc1.vcontl1 as con1
ENDMODELS
```